Title
Development of a Therapeutic CRISPR/Cas9 Platform for Duchenne Muscular Dystrophy

Author
Young, Courtney

Publication Date
2018

Peer reviewed|Thesis/dissertation

UNIVERSITY OF CALIFORNIA

Los Angeles

Development of a Therapeutic CRISPR/Cas9 Platform for Duchenne Muscular Dystrophy

A dissertation submitted in partial satisfaction of the requirements for the degree Doctor of Philosophy in Molecular Biology

by

Courtney Sarah Young

2018

ABSTRACT OF THE DISSERTATION

Development of a Therapeutic CRISPR/Cas9 Platform

for Duchenne Muscular Dystrophy

by

Courtney Sarah Young

Doctor of Philosophy in Molecular Biology

University of California, Los Angeles, 2018

Professor Melissa J. Spencer, Chair

Duchenne muscular dystrophy (DMD) is a progressive muscle wasting disorder with no cure. Patients with DMD typically have out-of-frame mutations in the *DMD* gene, which leads to lack of dystrophin protein. However, there is an allelic, milder disease, Becker muscular dystrophy (BMD), where in-frame mutations allow for some production of an internally deleted dystrophin, which is at least somewhat functional. Thus, a therapeutic strategy is to restore the *DMD* reading frame, thereby making a DMD mutation into a BMD mutation and likely leading to a milder clinical phenotype. Gene editing tools such as the clustered regularly interspaced short palindromic repeats (CRISPR)/CRISPR associated protein (Cas) 9 system would allow for permanent gene reframing. Here we describe development of a CRISPR/Cas9 gene editing platform which deletes *DMD* exons 45-55, creating an in-frame mutation associated with a very mild disease course in BMD patients. This region also encompasses a hotspot of approximately

half of all DMD patient mutations, meaning this single platform would be therapeutically relevant for a large percentage of patients.

We first demonstrate *in vitro* applicability of our CRISPR/Cas9 platform in DMD human induced pluripotent stem cells where we show restored dystrophin protein and function in cardiac and skeletal muscle cells *in vitro* and after engraftment *in vivo*. An alternative route of delivery besides cell therapy is direct delivery of CRISPR/Cas9 to muscle *in vivo.* To that end, we created a novel humanized dystrophic mouse model containing an out-of-frame *DMD* gene that we can target with our CRISPR/Cas9 platform, which is human sequence specific. We demonstrate restored dystrophin protein after application of our CRISPR/Cas9 platform through electroporation, viral delivery, and nanoparticle delivery *in vivo*. Although we have achieved highest efficiency of dystrophin generation using adeno-associated virus (AAV) as a delivery vehicle, this work also provides proof-of-principle development of novel nanoparticles as an alternative means to AAV to deliver gene editing platforms to muscle *in vivo.* Non-viral delivery strategies may be advantageous due to their potential to evade an immune response and achieve stem cell targeting. Future work will continue to improve both approaches for effective direct delivery of our CRISPR platform, which reframes the *DMD* gene for a large percentage of Duchenne patients.

The dissertation of Courtney Sarah Young is approved.

April Dawn Pyle

Rachelle Hope Watson

M. Carrie Miceli

Donald Barry Kohn

Melissa J. Spencer, Committee Chair

University of California, Los Angeles

2018

Dedication

To my cousin Christopher, whose diagnosis with Duchenne is what set me on this journey and inspires me every day.

To the rest of my family who has always supported me.

To my friends and colleagues who have made my time so much fun.

Table of Contents

List of Figures

List of Tables

Acknowledgements

I would like to thank my advisor, Dr. Melissa Spencer, and my (unofficial) co-advisor, Dr. April Pyle, for their unwavering support of me and this project, it wouldn't have been possible without them. A big thank you to the members of the Spencer, Pyle, and other collaborating labs, as well as my thesis committee, who assisted me with advice and research in the lab as well as making my time enjoyable. I am also highly thankful and appreciate of the whole Center for Duchenne Muscular Dystrophy at UCLA for being a fun, supportive environment, and all the trainees who have been part of the Bruin Allies for Duchenne student group, happy hours, weekly soccer games and more. Lastly, I would like to acknowledge my family, who encouraged and supported my interest in science, and my many previous mentors who helped mold me into a scientist, including Drs. Ryan Soderquist, Adam Moyer, Kathryn Wagner, Maaike van Putten, Annemieke Aartsma-Rus, Debbie Briggs, and Jenny Morgan.

Chapter 2 is adapted from Young CS, Hicks MR, Ermolova NV, Nakano H, Jan M, Younesi S, Karumbayaram S, Kumagai-Cresse C, Wang D, Zack JA, Kohn DB, Nakano A, Nelson SF, Miceli MC, Spencer MJ*, Pyle AD* (2016). "A Single CRISPR-Cas9 Deletion Strategy that Targets the Majority of DMD Patients Restores Dystrophin Function in hiPSC-Derived Muscle Cells." *Cell Stem Cell*. 18(4):533-540. DOI: 10.1016/j.stem.2016.01.021. We would like to thank Doug Black, Richard Wang, and Haibin Xi for suggestions and Diana Becerra and Jane Wen for technical assistance. The following cores were utilized: CDMD Muscle Phenotyping and Imaging Core, HTS and Cell Repository Core, and Bioinformatics and Genomics Core (supported by NIAMS-P30 AR057230), the UCLA Broad Stem Cell Research Center (BSCRC) Flow Cytometry Core Resource, the UCLA Jonsson Comprehensive Cancer Center (JCCC) and Center for AIDS Research (CFAR) Flow Cytometry Core Facility (supported

by NIH P30 CA016042, 5P30 AI028697), the UCLA Integrated Molecular Technologies Core (supported by CURE/P30 DK041301), the UCLA Humanized Mouse Core (supported by the JCCC, BSCRC, CFAR, NIH/NIAID AI028697), and the UCLA GenoSeq core. This material is based upon work supported by the National Science Foundation Graduate Research Fellowship Program under Grant No. DGE-1144087 (CSY). Funding was provided by NIAMS of the NIH (P30 AR057230-MJS, AN, ADP, R01AR064327-ADP) and the Eli & Edythe Broad Center of Regenerative Medicine and Stem Cell Research at UCLA (MJS, ADP) and Rose Hills Foundation Research Award (ADP). Author contributions were: Conceptualization, Methodology, Writing-Original Draft, Visualization, Project Administration - CSY, MJS, ADP; Validation- CSY, MRH, NVE; Formal Analysis- CSY; Investigation- CSY, MRH, NVE, HN, MJ, SY, SK CK-C, DW; Resources- AN, SFN, MCM, MJS, ADP; Writing- Review and Editing- CSY, MRH, NEV, SK, CK-C, DBK, AN, SFN, MCM, MJS, ADP; Supervision- JAZ, DBK, AN, MCM, MJS, ADP; Funding Acquisition- MJS, ADP.

Chapter 3 is adapted from Young CS, Mokhonova E, Quinonez M, Pyle AD, Spencer MJ (2017). “Creation of a novel humanized dystrophic mouse model of Duchenne muscular dystrophy and application of a CRISPR/Cas9 gene editing therapy.” *Journal of Neuromuscular Diseases*. 4:139-145. DOI: 10.3233/JND-170218. We would like to thank Diana Becerra, Joana Capote, Natalia Ermolova, Brandon Lippold, Chino Kumagai-Cresse, and Jane Wen for technical assistance. We are grateful for the technical support, products, and/or services provided to our research by the Mouse Biology Program at the University of California Davis and the Center for DMD at UCLA Muscle Phenotyping and Imaging Core. This material is based upon work supported by the National Science Foundation Graduate Research Fellowship Program under Grant No. DGE-1144087 (CSY). Additional funding was provided by a pilot and

feasibility seed grant from the Center for DMD at UCLA (NIH NIAMS 5P30AR05723UCLA and CTSI Grant #UL1TR000124), the Eli & Edythe Broad Center of Regenerative Medicine and Stem Cell Research at UCLA, the California Institute of Regenerative Medicine, Wellstone Cooperative Muscular Dystrophy Center (U54AR052646-Sweeney-PI, Spencer-Co-I) and NIAMS of the NIH (R01AR064327-ADP). Author contributions were: Conceptualization, Methodology, Writing- Review and Editing, Visualization, Project Administration - CSY, ADP, MJS; Writing-Original Draft- CSY, Validation, Formal Analysis- CSY, EM; Investigation- CSY, EM, MQ; Resources- ADP, MJS; Supervision- MJS; Funding Acquisition- ADP, MJS.

Chapter 4 is partly adapted from a manuscript in preparation. I would like to thank everyone who contributed to the work including Michael Emami, Ying Ji, Xiangsheng Liu, Ekaterina Mokhonova, Niclas Bengtsson, Jeffrey Chamberlain, April Pyle, Huan Meng, and Melissa Spencer. We would like to thank Diana Becerra, Catherine Li, Jesus Perez, Marbella Quinonez, and Jane Wen for technical assistance. We are grateful for the Center for DMD at UCLA Muscle Phenotyping and Imaging Core. Schematic in Figure 4-1C was courtesy of Drs. Jinhong Jiang and Xiangsheng Liu. This material is based upon work supported by the National Science Foundation Graduate Research Fellowship Program under Grant No. DGE-1144087 (CSY), a UCLA Graduate Division Dissertation Year Fellowship (CSY), and a CMB T32 Ruth L. Kirschstein NRSA GM007185 (MRE). Additional funding was provided by the California Institute of Regenerative Medicine, the Eli & Edythe Broad Center of Regenerative Medicine and Stem Cell Research at UCLA, the Wellstone Cooperative Muscular Dystrophy Center (JSC), and NIAMS of the NIH (R01AR064327-ADP; P30 AR057230). Author contributions were: Conceptualization, Methodology, Visualization, Project Administration - CSY, MRE, YJ, XL, ADP, HM, MJS; Validation, Formal Analysis, Investigation- CSY, MRE, YJ, XL, EM; Writing-

Original Draft- CSY; Writing- Review and Editing- CSY, ADP, MJS; Resources- NB, JSC, ADP, HM, MJS; Supervision- JSC, ADP, HM, MJS; Funding Acquisition- JSC, ADP, HM, MJS.

Biographical Sketch

Education

- 2012 – 2013: **University College London;** London, UK
  - *Master of Research in Biomedicine – with Distinction*
- 2009 – 2012: **Johns Hopkins University;** Baltimore, MD
  - *Bachelor of Science in Chemical and Biomolecular Engineering, GPA: 3.93*

Research Experience

- Sept 2013 – present: **University of California, Los Angeles**, Molecular Biology; Los Angeles, CA. *Graduate Student Researcher, Dr. Melissa Spencer laboratory, NSF GRFP.*
  - Thesis: Development of a therapeutic CRISPR/Cas9 platform for Duchenne muscular dystrophy.
- Sept 2012 – Sept 2013: **University College London**, Institute of Child Health; London, UK. *Graduate Student Researcher, Dr. Jennifer Morgan laboratory, Whitaker scholar.*
  - Thesis: Interaction of muscle stem (satellite) cells and stromal cells in skeletal muscle.
- June 2012 – Sept 2012: **Sarepta Therapeutics,** Biology Discovery Research; Bothell, WA. *Summer Intern*.
  - Completed various projects involving antisense oligonucleotide therapies.
- Sept 2010 – May 2012: **Kennedy Krieger Institute (JHMI),** Center for Genetic Muscle Disorders; Baltimore, MD. *Research Assistant, Dr. Kathryn Wagner's laboratory.*
  - Researched effect of sildenafil on muscle regeneration.
- June 2011 – Aug 2011: **Leiden University Medical Center,** DMD Genetic Therapy Group; Leiden, Netherlands. *Summer Research Intern, Dr. Annemieke Aartsma-Rus' laboratory, Vredenburg scholar.*
  - Determined minimum amount of dystrophin required for benefit in mouse model of muscular dystrophy.
- May 2010 – Aug 2010: **Covidien,** Tissue Engineering Research and Development; Boulder, CO. *Summer Intern.*
  - Completed project of testing medical devices to high seal count on animal tissue.
- Jan 2010 – May 2010: **Johns Hopkins Medicine,** McKusick-Nathans Institute of Genetic Medicine; Baltimore, MD. *Research Assistant, Dr. Ronald Cohn's laboratory.*
  - Researched cause/effect of nNOS on muscular dystrophies.
- June 2008 – Feb 2009: **University of Colorado,** Chemical and Biological Engineering Department; Boulder, CO. *Research Assistant, Dr. Melissa Mahoney's laboratory.*
  - Researched IL-10 delivery for reducing back pain and inflammation.

Leadership and Volunteering Experience

- Oct 2013 – present: **UCLA Bruin Allies for Duchenne;** Los Angeles, CA
  - *Volunteer, fundraise, and promote awareness for Duchenne muscular dystrophy.*
- Oct 2013 – present: **Volunteer for Reading to Kids;** Los Angeles, CA
- Sept 2014 – present: **UCLA Advancing Women in Science and Engineering (AWISE)**; Los Angeles, CA
- July 2016: **ASCB KGI Managing Science in the Biotech Industry**; Claremont, CA

Selected Awards & Fellowships

- UCLA Dissertation Year Fellowship, 2017-present
- Charles E. and Sue K. Young Graduate Student Award, 2017

- UCLA Jules Brenner Award, 2017
- UCLA Molecular Biology Interdepartmental Program Dissertation Year Award, 2017
- UCLA Molecular Biology Institute Retreat Poster Award, 2017
- National Science Foundation Graduate Research Fellowship, 2014-2017
- World Muscle Society Elsevier WMS Membership Award, 2016 and 2017
- UCLA Grad Slam, 3rd place and Audience Choice Award, 2016
- ASGCT meritorious abstract travel award, 2015
- UCLA Graduate Dean's Scholar Award, 2013-2015

Publications

1. Hicks M, Hiserodt J, Paras K, Fujiwara W, Eskin A, Jan M, Xi H, **Young CS**, Evseenko D, Nelson S, Spencer MJ, Van Handel B, Pyle AD (2018). "ERBB3 and NGFR mark a distinct skeletal muscle progenitor cell in human development and hPSCs." *Nature Cell Biology*. 20:46-57. PMID: 29255171.
2. **Young CS**, Mokhonova E, Quinonez M, Pyle AD, Spencer MJ (2017). "Creation of a novel humanized dystrophic mouse model of Duchenne muscular dystrophy and application of a CRISPR/Cas9 gene editing therapy." *Journal of Neuromuscular Diseases*. 4:139-145. PMID: 28505980.
3. **Young CS**, Pyle AD (2016). "Bench to Bedside: Exon Skipping Therapy." *Cell*. 167(5): 1144.
4. Hoban MD, Lumaquin D, Kuo CY, Romero Z, Long J, Ho M, **Young CS**, Mojadidi M, Fitz-Gibbon S, Cooper AR, Lill GR, Urbinati F, Campo-Fernandez B, Bjurstrom CF, Pellegrini M, Hollis RP, Kohn DB (2016). "CRISPR/Cas9-mediated correction of the sickle mutation in human CD34+ cells." *Molecular Therapy.* 24(9):1561-9. PMID: 27406980.
5. **Young CS,** Hicks MR, Ermolova NV, Nakano H, Jan M, Younesi S, Karumbayaram S, Kumagai-Cresse C, Wang D, Zack JA, Kohn DB, Nakano A, Nelson SF, Miceli MC, Spencer MJ*, Pyle AD* (2016). "A Single CRISPR-Cas9 Deletion Strategy that Targets the Majority of DMD Patients Restores Dystrophin Function in hiPSC-Derived Muscle Cells." *Cell Stem Cell*. 18(4):533-540. PMID: 26877224.
6. van Putten M, **Young C**, van der Berg S, Pronk A, Hulsker M, Karnaoukh T, Vermue R, de Kimpe S, van Dijk K, van Deutekom, Aartsma-Rus A (2014). "Preclinical studies on intestinal administration of antisense oligonucleotides as a model for oral delivery for treatment of Duchenne muscular dystrophy." *Molecular Therapy Nucleic Acids.* 3:e211. PMID: 25405468.
7. van Putten M, Hulsker M, **Young C**, Nadarajah VD, Heemskerk H, van der Weerd L, 't Hoen PA, van Ommen GJ, Aartsma-Rus AM (2013). "Low dystrophin levels increase survival and improve muscle pathology and function in dystrophin/utrophin double-knockout mice." *FASEB J*. 27(6):2484-95. PMCID: PMC3659351.
8. Soderquist RG, Sloane EM, Loram LC, Harrison JA, Dengler EC, Johnson SM, Amer LD, **Young CS**, Lewis MT, Poole S, Frank MG, Watkins LR, Milligan ED, Mahoney MJ (2010). "Release of Plasmid DNA-Encoding IL-10 from PLGA Microparticles Facilitates Long-Term Reversal of Neuropathic Pain Following a Single Intrathecal Administration." *Pharmaceutical Research*. 27(5):841-54. PMCID: PMC3583569.

Patents

1. Pyle AD, **Young CS**, Spencer MJ. 2017. Methods and compositions for modifying a mutant dystrophin gene in a cell's genome. PCT/US17/17255, filed February 9, 2017.

Chapter 1 - Introduction

Duchenne and Becker muscular dystrophy

Duchenne muscular dystrophy (DMD) is one of the most common fatal genetic diseases of childhood. It is an X-linked disorder that affects approximately 1 in 3500-5000 live male births[1]. DMD presents in childhood as a severe, progressive muscle degenerative disease, typically resulting in loss of ambulation in the teens and premature death by the third decade of life. Although skeletal muscle regeneration occurs in young patients and can help compensate for muscle degeneration, over time the muscle stem (satellite) cells become exhausted and muscle degeneration and weakness leads to loss of muscle function[2–5]. Eventually respiratory system failure and/or cardiomyopathy develops. Corticosteroid use and improvements in care have slightly improved muscle strength, walking ability and lifespan, but there is currently no cure for DMD[6,7].

An allelic disease, Becker muscular dystrophy (BMD), presents a milder phenotype, by definition, BMD patients remain ambulatory until age 16 or older[8]. The difference in phenotype is due to the 'reading frame hypothesis'; DMD is most often caused by frame shifting mutations, whereas the reading frame is typically maintained in BMD. In Duchenne, the out-of-frame mutations in the *DMD* gene prevent expression of dystrophin protein while in-frame BMD mutations result in production of an internally deleted but partially functional dystrophin[9].

Dystrophin in muscle

The dystrophin protein normally functions as a shock absorber at the muscle cell sarcolemma connecting the actin cytoskeleton to the extracellular matrix via the dystrophin glycoprotein complex (DGC). Dystrophin also anchors the DGC to the membrane, loss of

dystrophin results in mislocalization of the complex and membrane instability. Progressive contraction-induced injury of muscle fibers causes calcium influx, reactive oxygen species (ROS) production, and increased membrane permeability, including leakage of creatine kinase (CK) into the serum, which is commonly observed with muscle injury and can be used as a diagnostic tool for DMD. Eventually the damaged muscle cells die and become replaced with fat and fibrotic tissue[10,11].

Dystrophin is a 427kDa protein containing an actin binding domain at the N-terminus, a central rod domain composed of 24 triple-helical spectrin-like repeats with 4 hinge regions and containing a second actin binding domain and a neuronal nitric oxide synthase (nNOS) binding site, a cysteine rich region which binds β-dystroglycan, and a C-terminus where dystrobrevin and syntrophins bind[12] (**Figure 1-1**). There are 4 shorter isoforms of dystrophin expressed in other tissues. Importantly it has been demonstrated that the entire dystrophin protein is not required for its function in muscle; for example, portions of the rod domain are somewhat redundant[13] and the C-terminus is not required[14]. Studies testing mini- and micro-dystrophin constructs *in vivo* have demonstrated up to 70% of the gene can be deleted and dystrophin will still retain many of its functional properties[15–18]. Recent work in mice used a micro-dystrophin construct containing just 5 repeats which restored almost normal force *in vivo*[19] and a construct containing just 4 repeats in dogs improved gait and clinical score[20].

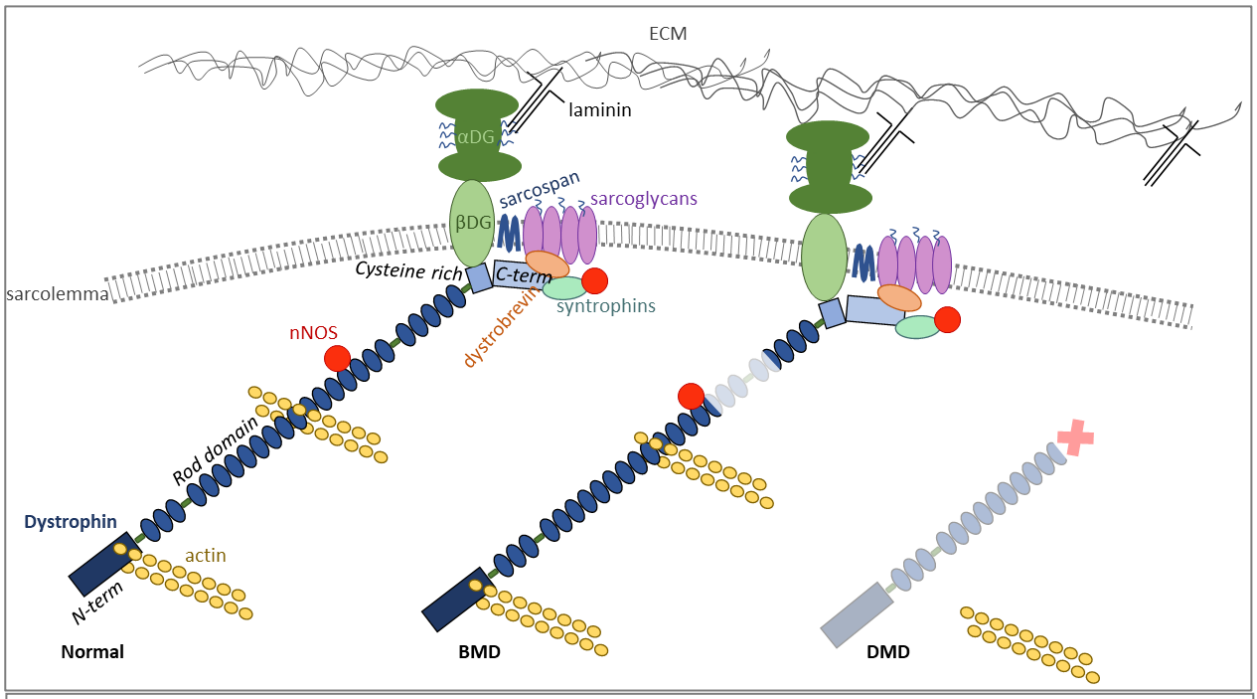

Figure 1-1: Schematic of dystrophin and the dystrophin glycoprotein complex (DGC) in normal, BMD, and DMD muscle.
Wild type dystrophin binds to actin at the N-terminus (term) to connect it to the extracellular matrix (ECM) via the DGC which binds at the cysteine rich region and C-terminus. In skeletal muscle, the DGC is composed of dystrophin, α- and β-dystroglycan (DG), α-, β-, γ-, and δ-sarcoglycans, sarcospan, syntrophins, dystrobrevin and neuronal nitric oxide synthase (nNOS). In-frame BMD mutations (shown by the white box) may not affect DGC localization (although there could be reduced expression) whereas DMD mutations resulting in a lack of dystrophin completely prevent DGC assembly and sarcolemmal localization.

Additionally, one of the mildest BMD mutations is an in-frame exon 45-55 deletion in the rod domain (spectrin-like repeats 17-22). Modeling of the repeat structure by eDystrophin software[21] supports that an exon 45-55 deletion can preserve near normal repeat structure (**Figure 1-2**). Phenotyping studies from multiple groups have independently found patients with this deletion that maintain walking ability and/or are asymptomatic until a late age (i.e. in their 60s). ~90% of patients with this deletion have been classified as mild BMD or asymptomatic[22–26]. This offers further support that internally deleted dystrophin proteins can be extremely functional in muscle *in vivo*.

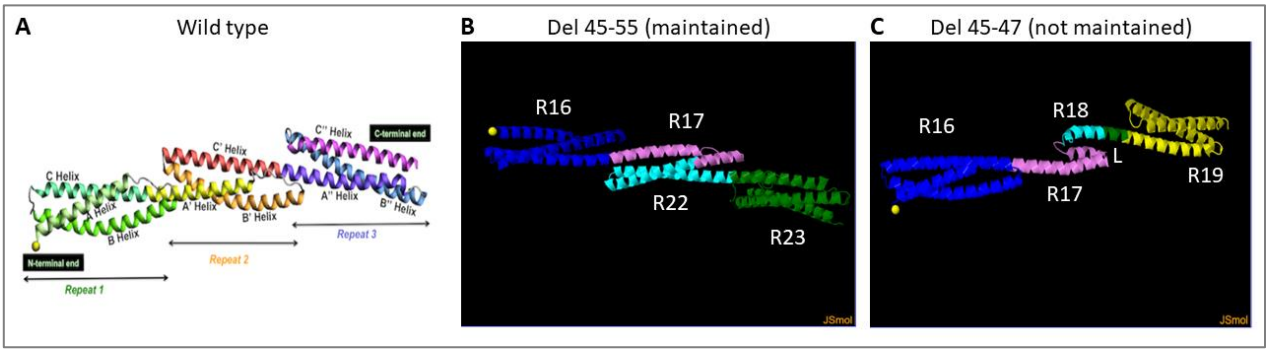

Figure 1-2: Modeling of an exon 45-55 deletion in dystrophin.
eDystrophin software[21] was used to model the repeat structure of dystrophin.
A) An example of a wild type dystrophin repeat structure.
B) Model of a *DMD* exon 45-55 deletion (del) where repeat 17 (R17) joins with repeat 22 (R22). The repeat structure is predicted to be maintained.
C) Example of a smaller deletion, *DMD* exon 45-47, where the repeat structure is not maintained.

Therapeutic strategies for DMD

Therapies being developed for DMD either focus on restoring dystrophin/membrane stability or treating downstream effects such as inflammation or fibrosis, which will not be discussed here. Some strategies to produce dystrophin aim to restore the reading frame, typically turning a DMD mutation into a BMD mutation. Exon skipping uses antisense oligonucleotides to affect splicing and cause skipping of an exon next to the patient's deletion to put the mRNA back in-frame. This technique is transient and thus needs to be administered repeatedly, over the entire lifetime of the patient. Currently only a single exon can be skipped at a time and the most prevalent exon 51 skipping is only applicable for ~13% of patients[27]. One of these drugs, EXONDYS 51, was recently granted accelerated approval from the FDA by demonstrating an increase of ~1% dystrophin by Western blot[28]. Importantly, other mouse studies have shown that low levels of dystrophin can have functional benefit[29–32].

Other potential treatments that are in clinical trials include gene therapy of a mini- or micro-dystrophin using adeno-associated virus (AAV) to deliver the dystrophin construct

systemically to muscle[33], and compounds that allow readthrough of premature stop codons, applicable for ~13% of DMD patient mutations[34]. Upregulation of a compensatory protein, utrophin, is also being developed for DMD as it has been shown that utrophin is a homolog and can functionally replace dystrophin in muscle[35]. Preclinical work includes stem cell therapy and gene editing (discussed below).

Gene editing and CRISPR/Cas9

One way in which the dystrophin gene could be modified is with the clustered regularly interspaced short palindromic repeats (CRISPR) and CRISPR associated protein (Cas) system. CRISPR/Cas was originally discovered as part of the bacterial adaptive immune response. It consists of a guide RNA strand (CRISPR (cr) RNA complexed with trans-activation CRISPR (tracr) RNA) which targets a Cas protein to cut DNA[36–38]. The CRISPR/Cas system was recently adapted for use in specific gene editing in mammalian cells[39–41]. In this system, a 20bp guide sequence complementary to the target site in the DNA is added into the guide RNA (gRNA) which then targets a Cas protein, for example the commonly used type II *Streptococcus pyogenes* (Sp) Cas9, to create a double stranded break (DSB) in the DNA 3bp upstream of the protospacer adjacent motif (PAM, typically an NGG for SpCas9)[42]. The double stranded break can be repaired through two main mechanisms, either the cell's endogenous repair machinery by non-homologous end joining (NHEJ), which can result in small insertions or deletions, or incorporation of new DNA through homology directed repair (HDR) by addition of an exogenous template (**Figure 1-3**). HDR will only occur during late S/G2 phase of the cell cycle[43].

Other techniques for gene editing, including meganucleases, zinc finger nucleases, and transcription activator-like effector nucleases (TALENs), have been around for more than 20 years, however CRISPR/Cas has revolutionized the field due to its ease of use and increased efficiency. One of the commonly used applications of CRISPR has been in generating novel mouse models faster and easier but it has extremely wide-ranging potential uses[44]. Therapeutically, CRISPR can be used to remove, edit, or add to a cells genome *in vitro* or *in vivo* for countless diseases. CRISPR/Cas editing in blood cells *ex vivo* is the first clinical application for humans. Clinical trials were initiated in 2016 in China[45] and are expected to start this year in the USA[46,47], mostly using CRISPR-edited cells to fight cancer. Chinese scientists also plan to start a trial for *in vivo* gene editing in humans by applying a gel containing CRISPR/Cas to the cervix to destroy human papillomavirus (HPV)[48].

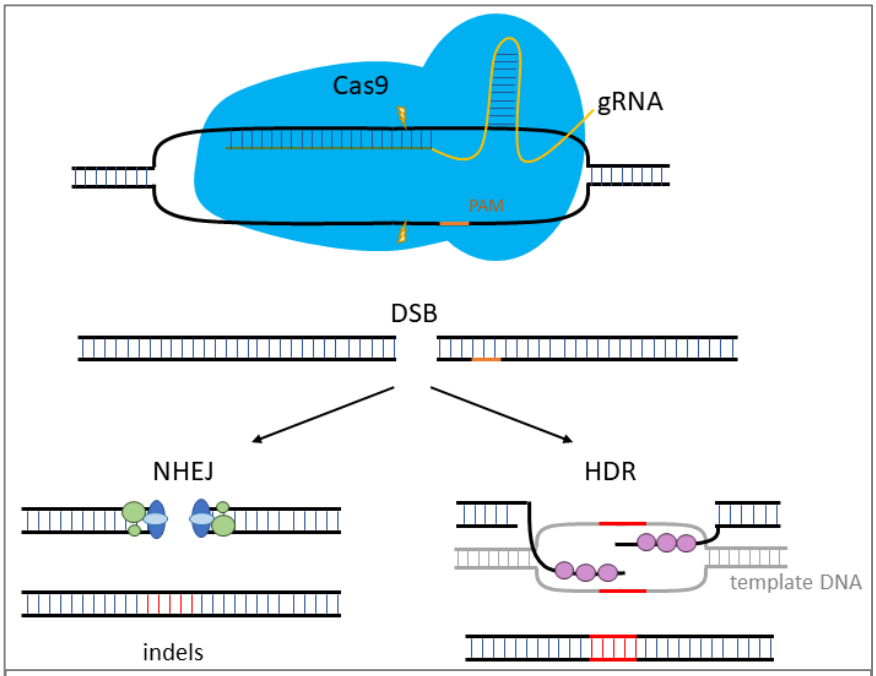

Figure 1-3: The CRISPR/Cas system for gene editing. The CRISPR/Cas9 gene editing system consists of two components, the Cas9 endonuclease (shown in blue) and a guide RNA (gRNA) which is composed of a target spacer region for DNA binding (shown in green) and a scaffold region for binding to Cas9 (in yellow). The gRNA spacer sequence is designed to be homologous to a target site in the genome which must have a 3′ protospacer adjacent motif (PAM) sequence. gRNA targeting results in Cas9 creating a double stranded break (DSB) in the DNA 3bp upstream of the PAM. The DSB can be repaired either through the cells endogenous repair, nonhomologous end joining (NHEJ) which can sometimes result in small insertions or deletions (indels), or through homology directed repair (HDR) to incorporate new DNA by addition of template DNA containing homology arms.

For Duchenne, CRISPR/Cas has been tested *in vitro* to restore the *DMD* reading frame by creating exon or duplication deletion(s), frameshifts, or exon insertion(s) in patient myoblasts or pluripotent stem cells[49–58]. *In vivo*, CRISPR has been used in mdx mice, the most commonly used mouse model of DMD which contains a premature stop codon in exon 23, or mdx4CV mice, to restore the reading frame by point mutation correction or exon deletion[59–66]. These studies offer a variety of strategies of how CRISPR/Cas can be applied to potentially treat DMD.

Pluripotent stem cells

Pluripotent stem cells (PSCs) have the ability to self-renew indefinitely and differentiate into any cell type of the three germ layers. PSCs are either obtained from the inner cell mass of blastocysts (embryonic stem cells) or by reprogramming somatic cells, such as fibroblasts, to a pluripotent cell state using transcription factors (called induced pluripotent stem cells (iPSCs)). Human iPSCs have enormous potential for patient specific disease modeling and for autologous cell therapy.

To use hiPSCs as a cell therapy for DMD, the main challenges are to correct the patient's mutation *in vitro* and to derive skeletal muscle progenitor cells that would be able to engraft across multiple muscles in the body. Recent work has demonstrated improved derivation of skeletal muscle cells *in vitro* without using overexpression[67–70] but the systemic engraftment and long-term potential of these cells is still unknown. CRISPR/Cas offers potential as an easy and efficient strategy to correct the patient's mutation *in vitro* as discussed above.

AAV as a delivery vehicle for CRISPR

In vivo delivery is a major challenge for getting therapeutics to muscle in DMD. Skeletal muscle makes up to 30-40% of body mass and is present throughout the entire body. Preclinical work suggests AAV can systemically deliver mini/micro-dystrophin constructs to muscle in mice and dogs[71] and CRISPR/Cas9 in mice[60–63], however AAV presents some additional concerns for CRISPR delivery. 1) It is not believed that AAV can efficiently target muscle stem cells *in vivo*[72], which would be a requirement for long term correction to be sustained in skeletal muscle. 2) Pre-existing antibodies to AAV preclude treatment[73]. 3) Antibodies made against the AAV capsid after a single injection would prevent readministration if high immune suppression or other techniques are not used. 4) AAV DNA may last 5-10 years in post-mitotic muscle, which means Cas9 would be expressed for an extended amount of time, potentially increasing off-target risks, and would eventually be lost through cell death or division. 5) The immune response to the AAV capsid could act as an adjuvant to Cas9, a bacterial protein that is expected to induce an immune response[74]. 6) AAV has a small carrying capacity (~4.7kb), which is not quite large enough to contain SpCas9 and multiple gRNAs in the same vector. Some of these concerns will be able to be overcome with future studies.

Nanoparticle delivery to muscle

Nanoparticles offer an alternative means for delivery to muscle. These are nano-scale particles made of inorganic or organic material which can be loaded with specific cargo. Nanoparticles can be modified to be non-immunogenic, some are biodegradable, can be modified to be targeted (for example, to muscle stem cells) and can be readministered[75]. There are over 50 approved nanomedicines and more than 75 in clinical trials, mostly for cancer[76].

Recent studies have adapted nanoparticles for carrying CRISPR/Cas components. The CRISPR/Cas system can be delivered as DNA, RNA, or ribonucleoprotein (RNP) complexes and each type of platform may require a different nanoparticle formulation. To date, published nano-CRISPR studies have consisted of liposomes carrying Cas9 and gRNA as RNA or RNPs, and DNA particles (called nanoclews), gold nanoparticles, or cationic polymer nanoparticles carrying CRISPR RNPs[77–90]. In mice, these particles have been used to target the liver, lung, kidneys, tumors, the inner ear, brain, and muscle *in vivo*[77–80,83–85,87–90]. Most *in vivo* studies are via local delivery, although the liver, lung, and tumors have been targeted by systemic delivery[77,79,84,87,89,90]. The one published study of nano-CRISPR in skeletal muscle was delivered through intramuscular injection and utilized HDR, which is expected to be inefficient in post-mitotic muscle[43,63], thus no studies have yet addressed systemic muscle targeting of nanoparticles carrying an efficient CRISPR platform.

Other nanoparticles that have been utilized for delivery to muscle have included different nano-formulations such as liposomes, polymeric nanoparticles, perfluorocarbon nanoparticles, and atelocollagen. These have been used to delivery antisense oligonucleotides, rapamycin, siRNA or other genes[91–100]. However, these have been fairly limited, proof-of-concept studies without much disease specific optimization. Thus, in general, the nano-muscle field is relatively unexplored and could offer enormous potential for non-viral delivery to skeletal muscle.

Significance

Duchenne muscular dystrophy is a devastating disorder with a clear unmet need. Therapeutic strategies to restore or replace dystrophin offer the most promise for treating the

underlying cause of the disease. CRISPR/Cas is a powerful tool that has potential to reverse DMD mutations and can be applied for larger groups of patients by targeting hotspot regions.

The aim of this research was to develop a therapeutic CRISPR/Cas9 gene editing strategy to restore the reading frame for a large percentage of DMD patients. Our platform creates an exon 45-55 deletion in the DNA using CRISPR/Cas9, thereby generating an in-frame deletion associated with one of the mildest BMD phenotypes. We applied this deletion to hiPSCs from DMD patients *in vitro* and demonstrated restoration of dystrophin protein and function in muscle cells derived from reframed hiPSCs. In order to have a relevant *in vivo* model to test our CRISPR/Cas9 platform on the human *DMD* gene, we created a novel humanized dystrophic mouse model. We generated an out-of-frame mutation (deletion of exon 45 using CRISPR/Cas9) in the hDMD mouse, which contains the entire human *DMD* gene. We then utilized AAV and nanoparticles to directly deliver our CRISPR/Cas9 platform to muscle *in vitro* and *in vivo.* This work offers a potential therapeutic strategy to permanently restore the reading frame for half of all DMD patients and allow for an internally deleted but functional dystrophin to be produced.

Chapter 2 - A Single CRISPR-Cas9 Deletion Strategy that Targets the Majority of DMD Patients Restores Dystrophin Function in hiPSC-Derived Muscle Cells

Abstract

Mutations in *DMD* disrupt the reading frame, prevent dystrophin translation, and cause Duchenne muscular dystrophy (DMD). Here we describe a CRISPR/Cas9 platform applicable to 60% of DMD patient deletion mutations. We applied the platform to DMD-derived hiPSCs where successful deletion and non-homologous end joining of up to 725kb reframed the *DMD* gene. This is the largest CRISPR/Cas9-mediated deletion shown to date in *DMD*. Use of hiPSCs allowed for evaluation of dystrophin in disease relevant cell types. Cardiomyocytes and skeletal muscle myotubes derived from reframed hiPSC clonal lines had restored dystrophin protein. The internally deleted dystrophin was functional as demonstrated by improved membrane integrity and restoration of the dystrophin glycoprotein complex *in vitro* and *in vivo*. Furthermore, miR31 was reduced upon reframing, similar to observations in Becker muscular dystrophy. This work demonstrates the feasibility of using a single CRISPR pair to correct the reading frame for most DMD patients.

Introduction

Duchenne muscular dystrophy (DMD) is the most common fatal genetic disease of childhood, affecting ~1 in 3500-5000 boys. In DMD, progressive muscle degeneration generally leads to death in the twenties, and there are currently no highly effective therapies. DMD is often caused by frameshifting exonic deletions in *DMD*, which encodes dystrophin. Dystrophin stabilizes the dystrophin glycoprotein complex (DGC) at the sarcolemma; loss of functional

dystrophin leads to the degradation of DGC components which results in muscle membrane fragility and leakage of creatine kinase (CK)[101]. Approximately 60% of deletion mutations, or 50% of all mutations, causing Duchenne occur between *DMD* exons 45-55[24,26]. Multiple independent clinical reports in patients and dystrophic mice have revealed that in-frame deletions of exons 45-55 produce an internally deleted dystrophin protein and are associated with a very mild Becker muscular dystrophy (BMD) disease course, with some patients still asymptomatic in their 60s[22–24,102]. Thus, genetic manipulation to create a large deletion of exons 45-55 is a therapeutic strategy to restore the reading frame for DMD patients with mutations in this region.

One promising approach to induce genetic correction of *DMD* is through the use of the bacterially acquired immune surveillance system known as clustered regularly interspaced short palindromic repeats (CRISPR) and CRISPR-associated nuclease (Cas) 9. In this system a short guide RNA (gRNA), which is complimentary to a specific site in the genome, is used to target the Cas9 nuclease and induce double stranded breaks (DSBs)[40,41]. The DSB can be repaired through non-homologous end joining (NHEJ) or homology directed repair.

Previous work has shown that CRISPR/Cas9 components can modify the *DMD* gene[49,51,52,59–62,64]. In this investigation, we describe a therapeutically relevant CRISPR/Cas9 platform that we designed to modify *DMD*. Our platform involves excision of exons 45-55 and NHEJ to reframe dystrophin through creation of an internally deleted protein that is stable and functional. The internally deleted protein mimics the naturally occurring exon 45-55 deletion observed in mild BMD patients and encompasses most DMD patient mutations.

For the first time, we demonstrate CRISPR/Cas9-mediated deletion and NHEJ of up to 725kb of the *DMD* gene in human induced pluripotent stem cell (hiPSC) lines. We show that CRISPR/Cas9 reframed hiPSC-derived skeletal and cardiac muscle cells express stable

dystrophin that improves membrane stability and restores a DGC member, β-dystroglycan. We also demonstrate reduced microRNA 31 (miR31) levels after the reading frame is restored, consistent with the observations made in BMD patients[103]. Furthermore, we show restoration of dystrophin and β-dystroglycan *in vivo* after engraftment of reframed hiPSC-derived skeletal muscle cells into a mouse model of DMD. This work sets the stage for use of reframed DMD hiPSC-derived cells or *in vivo* correction strategies using CRISPR/Cas9 for direct translation to patients with DMD.

Materials and Methods

Mice

All animal work was conducted under protocols approved by the UCLA Animal Research Committee in the Office of Animal Research Oversight. Mice used for engraftment experiments were generated by crossing mdx *scid* (Jackson Laboratory) with NOD *scid* IL2Rgamma (Jackson Laboratory) mice. Briefly, female B10ScSn.Cg-*Prkdc*^{scid}Dmd^{mdx}/J were crossed with male NOD.Cg-*Prkdc*^{scid}Il2rg^{tm1Wjl}/SzJ. Then the F1 females from that cross were crossed with male mdx-*scid*. The F3 males were screened for dystrophin and gamma mutations and the mutants were then backcrossed again with mdx-*scid* females. F4 females were crossed with F3 mutant males which generated homozygous NSG-mdx mice. Genotyping was performed through TransnetYX.

Cloning of gRNAs

Five guide RNAs were designed to target *DMD* introns 44 and 55 using the Zhang lab CRISPR design tool (crispr.mit.edu) and cloned into the SpCas9 plasmids pX330 or pX459 from

Feng Zhang (Addgene #42230, #48139 respectively) adapted from [104]. In brief, oligos complementary to each other containing the gRNA sequence and BbsI restriction enzyme site were obtained from Integrated DNA Technologies and annealed. The annealed oligos and plasmid were simultaneously digested with BbsI (New England Biotechnologies) and ligated with T4 DNA ligase (Life Technologies).

gRNA sequences and oligos used for cloning

Name	Sequence	Sense oligo	Antisense oligo
44C1	GTGGTGTCCTTTGAATATGCAGG	CACCGTGGTGTCCTTTGAATATGC	AAACGCATATTCAAAGGACACCAC
44C2	AGATTGTCCAGGATATAATTTGG	CACCGAGATTGTCCAGGATATAATT	AAACAATTATATCCTGGACAATCTC
44C3	TTAGCAACCAAATTATATCCTGG	CACCGTTAGCAACCAAATTATATCC	AAACGGATATAATTTGGTTGCTAAC
44C4	GTTGAAATTAAACTACACACTGG	CACCGTTGAAATTAAACTACACAC	AAACGTGTGTAGTTTAATTTCAAC
44C5	ATCTTTACCTGCATATTCAAAGG	CACCGATCTTTACCTGCATATTCAA	AAACTTGAATATGCAGGTAAAGATC
55C1	TACACATTTTTAGGCTTGACAGG	CACCGTACACATTTTTAGGCTTGAC	AAACGTCAAGCCTAAAAATGTGTAC
55C2	CATTCCTGGGAGTCTGTCATGGG	CACCGCATTCCTGGGAGTCTGTCAT	AAACATGACAGACTCCCAGGAATGC
55C3	TGTATGATGCTATAATACCAAGG	CACCGTGTATGATGCTATAATACCA	AAACTGGTATTATAGCATCATACAC
55C4	GTGGAAAGTACATAGGACCTTGG	CACCGTGGAAAGTACATAGGACCT	AAACAGGTCCTATGTACTTTCCAC
55C5	TCTTATCATAACTCTTACCAAGG	CACCGTCTTATCATAACTCTTACCA	AAACTGGTAAGAGTTATGATAAGAC

Red text is NGG PAM sequence

Cell culture

Human embryonic kidney (HEK) 293FT cells (Life Technologies) were grown in standard conditions with growth medium consisting of DMEM (high glucose) with 10% fetal bovine serum (FBS, Life Technologies), 0.1mM non-essential amino acids (NEAA, Life Technologies), 6mM L-glutamine (Life Technologies).

Human skeletal muscle myoblasts (HSMM, Lonza) were maintained according to the manufacturer's instructions with SkGM-2 medium (Lonza). For terminal differentiation, they were cultured on Matrigel (Corning) until at least 80% confluent and then switched to N2 differentiation medium (DMEM/F12 with 1% N2 supplement (Life Technologies) and 1% insulin-transferrin-selenium (ITS, Life Technologies)) for 7 days.

Human induced pluripotent stem cells (hiPSCs) were reprogrammed from skin fibroblasts with the STEMCCA cassette as previously described[105]. They were grown on hESC qualified Matrigel (Corning), fed daily with mTeSR1 medium (Stem Cell Technologies) and passaged with 0.5mM EDTA every 5-7 days. Karyotype and FISH analyses were performed by Cell Line Genetics®.

Teratoma injections

To prepare hiPSCs for injection, 1-2 confluent wells were collected using 1mg/ml of collagenase type IV or 0.5mM EDTA. Colonies were dissociated using a 5ml pipette and centrifuged at 1000rpm. Cell pellets were resuspended in 40µl of Hank's Balanced Salt Solution (HBSS) and injected into the testes of 6–8 week-old SCID BEIGE mice (Charles River) as described previously[106]. After 4-8 weeks, teratomas were isolated and fixed in 4% paraformaldehyde (PFA) for 24 hours, then 70% ethanol. Fixed teratomas were embedded and processed by the Tissue Procurement Core Laboratory, Department of Pathology and Laboratory Medicine, David Geffen School of Medicine at UCLA. If teratomas were large, four to six quadrants were isolated and fixed in PFA as described above. Tumors were stained with hematoxylin and eosin and imaged with an Olympus BX51 microscope.

Transfection and nucleofection of gRNAs

$3x10^5$ HEK293FT cells were seeded per 12 well and transfected in duplicate the following day with 1µg DNA using 3µl TransIT293 (Mirus Bio) according to the manufacturer's instructions.

Amaxa 4D (Lonza) nucleofection of hiPSCs was performed according to the manufacturer's instructions. In brief, hiPSCs were pre-treated with 10µM ROCK inhibitor Y-27632 (ROCKi, Tocris Bioscience) for 1hr and trysinized into a single cell suspension with TryplE (Life Technologies). $8x10^5$ hiPSCs were nucleofected per 100µl cuvette using solution P3, 2µg or 3.5µg total DNA, and program CA-137 (Lonza). pMAX GFP (Lonza) was used as a transfection control. After nucleofection, cells were immediately plated in mTeSR1 with ROCKi. For selection, 0.35µg/ml of puromycin in mTeSR1 was added to the cells for 24hrs the day after nucleofection.

Generation of clonal hiPSC lines

For generation of clonal lines, the day following nucleofection of gRNAs 44C4 and 55C3 (in pX459) cells were selected with 0.35µg/ml of puromycin in mTeSR1 for one day. The cells were expanded for 7-9 days in mTeSR1 and then either single cell sorted in ROCKi using a FACSAria sorter (BD) into individual 96 wells or plated at low densities of $3x10^5$-$5x10^5$ cells per 10cm dish in mTeSR1 plus ROCKi. After 2 weeks, individual colonies were scrapped into a corresponding 48 well and a subset of the colony was manually dissected and screened using the deletion genotyping PCR below.

Deletion genotyping PCR

For determining if the exon 45-55 deletion occurred, either individual PCR reactions or a multiplex PCR containing both sets of primers was performed with AccuPrime Taq High Fidelity (Life Technologies). One primer pair flanked the deleted region (del) and one pair was within the deleted region (undel). PCR products were run on a 1.2% agarose gel and visualized with ethidium bromide staining.

Primer sequences for PCR

Primer name, *purpose*	Sequence
44_F, *forward primer for del genotyping*	CTGGACGGAGCTGGTTTATCT
55surv2_R, *reverse primer for del genotyping*	CCCTTTTCTTGGCGTATTGCC
55undel1_F, *forward primer for undel genotyping*	GCCTGGGTCTCTGCTATCAA
55undel1_R, *reverse primer for undel genotyping*	GCCACTTTGTACTCCGCACT

Analysis of the rejoining sequence after an exon 45-55 deletion was performed by blunt cloning the deleted PCR products into the Zero Blunt TOPO backbone (Life Technologies), according to the manufacturer's instructions, and sequencing of the insert by Laragen Inc.

Differentiation of hiPSC-derived skeletal muscle

hiPSCs were differentiated into skeletal muscle cells by overexpression of MyoD, adapted from [107]. Cells were trypsinized with TryplE and plated as single cells on Matrigel in SMC4 (basal medium: DMEM/F-12 with 20% knock-out serum replacement (KOSR, Life Technologies), 1% NEAA, 1% Glutamax (Life Technologies), 100µM beta-mercaptoethanol, 10ng/mL basic fibroblast growth factor (bFGF, Life Technologies); SMC4: basal media with daily addition of 5µM ROCKi, 0.4µM PD0325901 (Sigma-Aldrich), 2µM SB431542 (Tocris Bioscience), 1µM CHIR99021 (Tocris Bioscience)) at $3.5x10^5$ cells/ 6 well. When they reached approximately 60-80% confluent they were infected with 0.06µg/mL of a tamoxifen inducible

MyoD-ERT lentivirus (adapted from [108]) with 4µg/mL protamine sulfate per well and spun inoculated at 1250rpm for 90mins at 32°C. After a day of recovery they were selected with 2µg/ml puromycin in SMC4 for 2 days. The cells were then split and plated on Matrigel in basal medium without bFGF plus 10µM ROCKi at approximately $1x10^5$ cells/cm^2 and induced in DMEM with 15% FBS and 5µM tamoxifen for 4 days. Following induction, the cells were differentiated in low glucose DMEM with 5% horse serum and 1µM tamoxifen for 5-7 days. Medium was changed daily.

An alternative protocol for MyoD overexpression was used for engraftment. Cells were single cell plated at $2.5x10^4$ cells/cm^2 on Matrigel in mTeSR1 with ROCKi. Beginning the following day, they were treated with 3µM CHIR99021 in DMEM/F12 with 1% ITS for 2 days. The cells were split to approximately $6x10^4$ cells/cm^2 in DMEM with 10% FBS and 1% NEAA and infected with the MyoD-ERT lentivirus as above. After a day of recovery, the cells were selected with 1µg/ml puromycin for 4 days followed by induction in IMDM containing 15% FBS, 10% horse serum (HS), 1% chick embryo extract, 50µg/ml ascorbic acid, 4.5mM monothioglycerol, 5ng/ml bFGF with 5µM tamoxifen for 2 days and used for engraftment as described below.

A directed differentiation protocol for hiPSCs adapted from [69] was also used to obtain SMPCs. Cells were single cell plated in mTeSR1 with 10µM ROCKi at $3.75x10^5$ cells/6 well. The following day, 10µM of CHIR99021 was added in Essential 6 medium (E6, Stem Cell Technologies) for 2 days and the cells were allowed to differentiate until day 12 in E6. StemPro (Gibco) containing 20ng/ml bFGF was added between days 12 to 20. E6 was then added until day 35 when the cells were switched to N2 medium in order to terminally differentiate. At day 50, cells were fluorescently activated cell sorted to remove neural crest cells with $HNK1^-$ (1:300,

Sigma-Aldrich) and enrich for SMPCs with BV650-NCAM$^+$ (1:25, BD Bioscience). The SMPCs were cultured in expansion media (20% FBS, 5% HS, 1% chick embryo extract, 0.5% penicillin/streptomycin) until confluent when they were changed to N2 medium for 7 days to induce terminal differentiation.

Differentiation of hiPSC-derived cardiomyocytes

Confluent hiPSCs were enzymatically dissociated to form aggregates and differentiated into the cardiomyocyte lineage as previously described[109,110]. The medium was changed every 2 days up to day 15, and every 5 days up to day 30. At day 30, cardiomyocytes were harvested for analysis or subjected to the hypoosmotic stress assay.

Surveyor assay

For testing the activity of different gRNAs, genomic DNA (gDNA) was extracted on day 3 or 4 after transfection/nucleofection using the Quick gDNA mini prep kit (Zymo Research) or Quick Extract DNA Extraction Solution 1.0 (Epicenter) according to the manufacturer's instructions. PCR for use in Surveyor assay was performed with AccuPrime Taq High Fidelity with primers flanking the target region.

The Surveyor assay (Integrated DNA Technologies) was performed according to the manufacturer's instructions. In brief, approximately 300ng of PCR product in 1x AccuPrime buffer up to 20µl was denatured and reannealed by heating at 95°C for 10min and slowly step-wise cooling to 4°C. Then 2µl $MgCl_2$, 1µl Surveyor enhancer, and 1.2µl Surveyor enzyme were added and incubated at 42°C for 1hr. The G/C plasmids provided in the Surveyor kit were used as a positive control for every gel. The products were run on a 6% or 4-20% TBE

polyacrylamide gel (Bio-Rad) and visualized with ethidium bromide staining. The percent of cutting was determined using ImageJ[111].

Primer sequences for PCR

Primer name, *purpose*	Sequence
44surv_F *forward primer for intron 44 surveyor*	GAGAGTTTGCCTGGACGGA
44surv_R, *reverse primer for intron 44 surveyor*	CCTCTCTATACAAATGCCAACGC
55surv2_F, *forward primer for intron 55 surveyor*	TCCAGGCCTCCTCTCTTTGA
55surv2_R, *reverse primer for intron 55 surveyor*	CCCTTTTCTTGGCGTATTGCC

Hypoosmotic stress CK release assay

Hypoosmolar salt solutions ranging from 66-240mosmol were made by adding varying amounts of sucrose (~25-175mM) to a basic salt solution consisting of 5mM HEPES, 5mM KCl, 1mM $MgCl_2$, 5mM NaCl, 1.2mM $CaCl_2$, 1mM glucose. Osmolarities were measured with a Wescor Vapro 5520 osmometer.

Differentiated MyoD OE skeletal myotubes and cardiomyocytes were plated in a 384 or 96 well plate in duplicate per condition tested. 100µl (or 30µl for 384 well plates) of the hypoosmolar solution was added to each well and the cells were incubated at 37°C for 20mins. The solution (supernatant) was then removed and stored at -80°C until CK analysis. The cells were trypsinzed and lysed in 100µl dI water by repeated freeze/thawing three times. The lysate was stored at -80°C until CK analysis. CK was measured in triplicate with 2µl or 8µl of undiluted sample using the Creatine Kinase-SL kit (Sekisui Diagnostics) according to the manufacturer's instructions. Any negative readings were forced to be 0 and outliers were discounted from the analysis. The percent of CK release into the supernatant was determined and the standard error was propagated throughout all calculations.

RNA extraction, cDNA, and PCR

RNA was extracted from differentiated cardiomyocytes using the RNeasy Micro Kit (Qiagen) according to the manufacturer's instructions. cDNA synthesis was performed on 50-250ng of RNA using the iScript Reverse Transfection Supermix for RT-qPCR (Bio-Rad). Two PCR reactions were done on all samples, one with primers internal to the deletion and one with primers flanking the deletion for 40 cycles using AccuPrime Taq. PCR products were cloned using the TOPO-TA cloning kit (Life Technologies) according to the manufacturer's instructions and sequenced at the UCLA GenoSeq Core.

Primer sequences for PCR

Primer name, *purpose*	Sequence
DMD_E43-44_F, *forward primer for cDNA, deleted*	CCGACAAGGGCGATTTGACA
DMD_E57_R, *reverse primer for cDNA, deleted*	AAGTCGCCTCCAATAGGTGC
DMD_E52_F, *forward primer for cDNA, undeleted*	ACTCATTACCGCTGCCCAAA
DMD_E55_R, *reverse primer for cDNA, undeleted*	TCTTCCAAAGCAGCCTCTCG

miRNA extraction, cDNA, and ddPCR

miRNA was isolated from fused myotubes obtained by MyoD OE using a microRNA purification kit (Norgen Biotek Corp) according to the manufacturer's instructions. cDNA synthesis was performed on 5µl of miRNA with TaqMan microRNA reverse transcription kit (Applied Biosystems) using a TaqMan MicroRNA Assay (Applied Biosystems) for hsa-miR-31 (assay ID 002279) and U6 snRNA (assay ID 001973) with specific RT primers. PCR reactions were prepared in a premix of 22µl with 1.46µl of cDNA (either diluted 1:30 for U6 or undiluted for miR31) in ddPCR supermix for probes (without UTP) (Bio-Rad) and 1.1µl 20x TaqMan assay probes for each sample in duplicate. 20µl of the PCR reaction premix was used to generate droplets according to the manufacturer's protocol. Briefly, PCR premix was added to a droplet generator cartridge with 70µl of oil and droplets were generated with the QX200 droplet

generator (Bio-Rad). 40µl of this reaction mix was transferred to a PCR plate and run on at T100 thermal cycler (Bio-Rad) at 95°C for 10mins, 40 cycles of 95°C 15sec, 60°C for 60sec, followed by 98°C for 10mins. A no template control was included for each PCR reaction. FAM fluorescence was evaluated using the QX200 droplet reader and QuantaSoft software (Bio-Rad). The percent of positive droplets for miR31 was normalized to the percent of positive droplets for U6. Standard deviation error was propagated through all calculations. All lines were normalized to CDMD 1002 wild type.

Engraftment into immunodeficient mice

NOD *scid* IL2Rgamma (NSG) immunodeficient mice (Jackson Laboratory) were crossed to mdx *scid* mice (Jackson Laboratory) to generate NSG-mdx mice, see above. 24hrs prior to engraftment, the right tibialis anterior (TA) of 5-7 week-old NSG-mdx mice was pretreated with 50µl of 10µM cardiotoxin (Sigma-Aldrich). For MyoD OE cells, 100µL of 5mg/ml tamoxifen (Sigma-Aldrich) was also IP injected for 5 days with tamoxifen pretreatment starting the day before engraftment[112]. $1x10^6$ cells obtained from MyoD OE after induction were pelleted and resuspended in 5µL HBSS and injected intramuscularly into the TA. Tissue was harvested after 30 days and analyzed as described below. Engraftment was considered successful when we identified human cells that were both lamin A/C and spectrin positive. Successful engraftment was seen in the following: CDMD 1002 N=4/4 engrafted successfully; CDMD 1003 N=1/1 engrafted successfully; and CDMD 1003-49 N=1/2 engrafted successfully.

Immunostaining

hiPSCs were fixed in 4% PFA for 20mins, permeabilized with 0.3% Triton X for 10mins and blocked in 10% goat serum for 1hr. Primary antibodies to SOX2 (1:200, Cell Signaling) and NANOG (1:800, Cell Signaling) were added in 1% goat serum and 0.1% Triton X overnight at 4°C followed by secondary antibodies for 2hrs the following day.

Differentiated skeletal myotubes obtained from MyoD overexpression were fixed in 80% acetone for 7mins at -20°C, blocked with 10% goat serum for 1hr and stained with dystrophin (1:300, Abcam) and myosin heavy chain (1.9µg/ml, MF20, DHSB) as above. Differentiated cardiomyocytes and skeletal myotubes obtained from the 50 day directed differentiation protocol were fixed in 4% PFA for 20mins, permeabilized with 0.3% Triton X for 10mins, blocked in 10% goat serum for 1hr and stained with dystrophin (1:5, MANDYS106, MDA Monoclonal Antibody Resource, [113]) or beta-dystroglycan (1:100, Leica Biosystems) and myosin heavy chain (1.9µg/ml, MF20, DHSB). Images were obtained with the Axio Observer Z1 microscope (Zeiss).

Harvested TA muscles were flash frozen in isopentane. 10µm cryosections were obtained at intervals throughout the entire muscle and stored at -20°C. For staining, they were blocked in 0.25% gelatin, 0.1% Tween, 3% bovine serum albumin for 1hr. The M.O.M. blocking kit (Vector Laboratories) was applied according to the manufacturer's instructions. Primary antibodies consisting of human lamin A/C (1:125, Vector Laboratories), human spectrin (1:75, Leica Biosystems), human dystrophin (1:5, MANDYS106), laminin (1:200, Sigma-Aldrich), dystrophin (1:75, Abcam), and beta-dystroglycan (1:50, Leica Biosystems) were applied overnight at 4°C. The following day secondary antibodies were incubated for 1hr and the slides were mounted with VECTASHIELD containing DAPI (Vector Laboratories) and imaged on the Axio Observer Z1 microscope.

Western blot analysis

Terminally differentiated skeletal muscle cells and cardiomyocytes were trypsinized, pelleted, and flash frozen in liquid nitrogen. Cell pellets were stored in liquid nitrogen until lysis. For Western blotting, samples were prepared as described in [114] with slight modifications. In brief, cells were solubilized in 500 µl of lysis buffer (10mM Tris-HCl (pH 7.4), 1% Triton X-100, 10% glycerol, 150mM NaCl, 5mM EDTA, and HALT protease and phosphatase inhibitor cocktail (ThermoScientific) per a 10cm culture dish, followed by incubation at 4℃ for 30 min with gentle rotation. Then lysates were mixed with 100µl of 6× RSB and passed several times through a syringe needle to reduce viscosity. Afterwards samples were boiled for 3 min, cooled on ice, passed through a syringe needle again and centrifuged for 5 min at 13,000*g*. Clarified lysates were transferred to new tubes, aliquoted and stored at -80^{o}C till use. To evaluate dystrophin and MyHC content, cell lysates were subjected to 6% polyacrylamide gel electrophoresis (PAGE) for 3 hours at constant current (10mA per gel); followed by blotting to nitrocellulose membrane at constant voltage (100V) for 2.5 hours on ice. 0.1% sodium dodecyl sulfate (SDS) and 10mM dithiothreitol was added to the transfer buffer to facilitate blotting of high molecular proteins. Immunoblot assay was carried out with mouse anti-MyHC (1:1,000; MF20, DHSB), and mouse anti-dystrophin (1:500; Mandys8, Sigma-Aldrich) antibodies. Secondary antibodies used were anti-mouse peroxidase conjugates from Sigma-Aldrich (1:10,000). Blots were developed using ChemiGlow West chemiluminescent detection kit (ProteinSimple). Signals were registered by the FluorChem FC2 digital imaging system (Alpha Innotech).

For β-dystroglycan, a 7.5% PAGE gel was run for 1.5hrs at 100V. Transfer was performed in Tris/Glycine with 20% MetOH for 1hr 15min at 100V. Immunoblotting was

performed with mouse anti-β-dystroglycan (1:200, MANDAG2(7D11), DHSB) and MyHC antibody as above.

Off-target analysis

The top 10 unique off-target sites for each gRNA used (44C4 and 55C3) were determined with COSMID[115] using the following criteria: NRG PAM, 3 mismatches with no indels, and 2 mismatches with 1-base deletions or insertions. Access Array primers corresponding to the potential off-target locations were designed, manufactured and validated by Fluidigm. gDNA extracted from the parental and deleted clonal lines was run on an Access Array (Fluidigm) and sequenced with MiSeq in the UCLA GenoSeq Core. Reads were trimmed with Trimmomatic and aligned to the genome using BWA. A base quality score recalibration and indel realignment was performed using GATK and SNP calling was done using two separate programs, GATK and LoFreq on the 20bp gRNA homologous region. A true induced mutation was considered possible if the fraction of reads with a given variant was substantially higher than error rate of base calling.

Top potential off-target sites as determined by COSMID

Name	Genomic location (hg19)
44C4_OT1	Chr11:87808333-87808355
44C4_OT2	Chr3:160301263-160301285
44C4_OT3	Chr4:168882168-168882190
44C4_OT4	Chr11:12974242-12974264
44C4_OT5	Chr11:28401278-28401300
44C4_OT6	Chr11:96681660-96681682
44C4_OT7	ChrX:44266358-44266380
44C4_OT8	Chr6:75606852-75606874
44C4_OT9	Chr1:91110525-91110547
44C4_OT10	Chr3:145258890-145258912
55C3_OT1	Chr18:31956684-31956706
55C3_OT2	Chr2:28730131-28730153
55C3_OT3	Chr10:4923833-4923855
55C3_OT4	Chr13:68797419-68797440
55C3_OT5	Chr13:70672235-70672256

55C3_OT6	Chr4:101494350-101494372
55C3_OT7	Chr3:81046407-81046428
55C3_OT8	Chr11:45856883-45856904
55C3_OT9	Chr1:171162826-171162847
55C3_OT10	Chr3:108717117-108717140

Statistical analysis

Statistical analyses were performed using a two-tailed t-test on two groups of data. First an F-test was used to determine if the variances were equal or unequal, then the corresponding t-test was used. Significance was determined by a p-value less than 0.05.

Results

DMD hiPSC lines are pluripotent and genetically stable

We have developed several xenobiotic-free hiPSC lines derived from wild type and DMD patient fibroblasts using current good manufacturing practice protocols. Each DMD hiPSC line harbors a unique frame-shifting *DMD* mutation within the exon 45-55 hotspot region. All hiPSC lines (Center for Duchenne Muscular Dystrophy (CDMD) 1003, 1006 and 1008) express pluripotency markers (NANOG and SOX2) and are karyotypically normal (**Figures 2-1A** and **2-1B**). CDMD hiPSCs maintain pluripotency, as they form teratomas *in vivo* that represent all three germ layers (**Figure 2-1C**), and each harbor unique mutations (**Figure 2-1D**).

CRISPR/Cas9-mediated deletion and NHEJ of up to 725kb in the DMD gene

In order to delete exons 45-55 of *DMD*, gRNAs were designed to target introns 44 and 55. gRNA sites were chosen to only retain ~500bp of the intron next to each of the flanking exons (44 and 56). The rationale for this design is to develop gRNAs applicable to as many patient mutations as possible and to ensure a small functional chimeric intron is generated.

During NHEJ, the 3′ end of intron 44 and the 5′ end of intron 55 join to create a ~1kb chimeric intron (**Figure 2-2A**). We expect introns generated in this manner are functional and splice correctly to create an in-frame transcript, with exon 44 joined with exon 56.

Since hiPSCs are challenging to genetically manipulate, human embryonic kidney (HEK) 293FT cells were used to screen five gRNAs at each intronic region. All gRNAs demonstrated individual cutting activity on Surveyor assay up to 34% (**Figures 2-2B** and **2-2C**). Using multiplex PCR, gRNAs transfected in pairs were shown to effectively delete the entire 708kb region encompassing exons 45-55 (**Figures 2-2D**).

In order to assess the feasibility of an exon 45-55 deletion across different patient mutations, we applied our gRNAs to three DMD hiPSC lines. The lines (CDMD 1003, 1006, 1008) require ~530kb, 670kb, or 725kb for successful deletion and NHEJ of *DMD* respectively. The gRNAs used were shown to be active in all three lines and effectively deleted exons 45-55 (**Figures 2-3** and **2-4**). Transient puromycin selection of cells nucleofected with the CRISPR plasmids improved the efficiency of deletion in CDMD 1003 and 1006 hiPSCs (**Figure 2-4D**).

Clonal reframed DMD hiPSC lines contain no off-target activity at candidate sites

Stably deleted DMD hiPSC lines were generated from CDMD 1003 and 1006 by clonal selection after nucleofection with the gRNA pair 44C4 and 55C3 (**Figure 2-5**) and are pluripotent (**Figures 2-5C** and **2-6A**). All reframed lines were karyotypically normal (**Figure 2-6B**) except for one clone (CDMD 1003-81), which was found to contain a 1q32 amplification confirmed via FISH analysis, also observed in the original parental line and in all daughter clones after post-hoc analysis. The 1q32 amplification is common in hPSCs after extended propagation in culture[116], and thus was not a result of CRISPR-mediated off-target activity. To

determine off-target activity of our gRNAs, the top 10 homologous sites per guide were determined by COSMID[115] and sequenced in all clonal and parental lines. No off-target mutations were observed at any site (**Table 2-2**). All variants, besides a heterozygous SNP in chromosome 11, were detected in less than 1% of reads which is consistent with error in the sequencing method.

Dystrophin ($DYS^{\Delta 45\text{-}55}$) expression is restored in reframed DMD hiPSC-derived cardiomyocytes and skeletal myotubes

CRISPR/Cas9-mediated deletion of *DMD* should result in an internally deleted dystrophin protein lacking exons 45-55 (hereafter referred to as $DYS^{\Delta 45\text{-}55}$). As hiPSCs do not express dystrophin, we differentiated the reframed DMD hiPSC clonal lines to two disease-relevant cell types, cardiomyocytes and skeletal muscle myotubes, using directed differentiation or overexpression of MyoD to evaluate rescue of $DYS^{\Delta 45\text{-}55}$. PCR and sequencing of the exon 44/56 boundary in cDNA from the reframed cardiomyocyte clones demonstrated correct splicing of the dystrophin transcript (**Figures 2-7A** and **2-7B**). Additionally, both the reframed cardiac and skeletal muscle cell lines restored dystrophin expression as assayed by immunocytochemistry and Western blot (**Figures 2-7C-E**). Compared to wild type CDMD 1002 or human skeletal muscle myotubes (HSMM), the band was truncated by ~66kDa as expected.

$DYS^{\Delta 45\text{-}55}$ protein restores membrane functionality to cardiomyocytes and skeletal myotubes in vitro

Cardiomyocytes or skeletal myotubes lacking dystrophin demonstrate membrane fragility *in vitro* and respond to osmotic stress by releasing elevated levels of CK[117,118], as is seen in

human patients[101]. To determine whether $DYS^{\Delta 45\text{-}55}$ could restore stability to dystrophic plasma membranes, we subjected differentiated cardiomyocytes and skeletal muscle myotubes derived from reframed and out-of-frame hiPSCs to hypoosmotic conditions. Cells were stressed by incubation in hypoosmolar solutions (66-240mosmol) and CK release into the supernatant was measured to show functional improvement after dystrophin restoration. Both the reframed CDMD 1003-49 cardiomyocytes and skeletal muscle cells demonstrated reduced CK release, similar to wild type (CDMD 1002), versus the out-of-frame CDMD 1003 cells, indicating that $DYS^{\Delta 45\text{-}55}$ was capable of reducing membrane fragility (**Figure 2-8A** and **2-8B**). The same trend was also observed with CDMD 1006/1006-1 cardiomyocytes (**Figure 2-8C**). After normalizing and pooling all experiments, we observed that significantly less CK was released at 93, 135, and 240mosmol in the reframed and wild type cells compared to out-of-frame (**Figure 2-8D**).

CRISPR/Cas9 reframing correlates with miR31 levels in skeletal myotubes in vitro

Elevated levels of miR31 have been observed in DMD patient biopsies compared to wild type or BMD[103]. We measured levels of miR31 using droplet digital PCR (ddPCR) after differentiation of out-of-frame and reframed CDMD hiPSCs to skeletal myotubes. Reframing *DMD* reduced levels of miR31 (similar to wild type cells), compared to out-of-frame *DMD,* as is observed in human dystrophinopathies (**Figure 2-9A**). Thus, reframing the *DMD* gene normalizes miR31 levels similar to BMD, demonstrating functional rescue of the dystrophic phenotype to a BMD phenotype.

DYS$^{\Delta 45\text{-}55}$ protein restores the DGC in vitro and in vivo

As a third assay of DYS$^{\Delta 45\text{-}55}$ functionality, we evaluated its ability to restore the DGC *in vitro* and *in vivo*. The DGC member, β-dystroglycan, was restored and detected at the membrane of reframed hiPSCs, but not out-of-frame hiPSCs, after directed differentiation to skeletal muscle *in vitro* by immunostaining and Western blot (**Figure 2-9B** and **2-9C**). Additionally, skeletal muscle cells derived from a wild type (CDMD 1002), out-of-frame (CDMD 1003), or reframed (CDMD 1003-49) hiPSC line were injected into the tibialis anterior of NSG-mdx mice. Correctly localized dystrophin and β-dystroglycan was only observed in engrafted human cells (demarked by human lamin A/C and spectrin) from the reframed or wild type lines (**Figure 2-9D** and **2-9E**). These studies taken together with the hypoosmotic stress assays demonstrate the ability of DYS$^{\Delta 45\text{-}55}$ to functionally reassemble the DGC and restore membrane stability *in vitro* and *in vivo.*

Discussion

Using CRISPR/Cas9 gene editing, we have induced the largest deletion accomplished to date in DMD hiPSCs and restored a functional dystrophin protein. Deletion of *DMD* exons 45-55 has the potential to be therapeutically relevant to at least half of all Duchenne patients. Since this internal deletion has been associated with a very mild disease course in multiple independent Becker patients, a therapy utilizing this approach should create a highly functional dystrophin. We showed successful deletion of exons 45-55 using a single gRNA pair and did not identify any off-target activity at the top 10 homologous sites, however a more comprehensive and unbiased approach should be undertaken such as whole genome sequencing. Importantly, removal of exons 45-55 resulted in stable dystrophin protein (DYS$^{\Delta 45\text{-}55}$) in both cardiomyocytes and

skeletal myotubes *in vitro*. Functionality of DYS$^{\Delta 45\text{-}55}$ was tested in cardiomyocytes and skeletal muscle derived from reframed DMD hiPSCs and demonstrated improved membrane stability by a physiologically relevant measure of CK release, similar to wild type. The ability to evaluate cardiomyocyte functionality is an advantage of using hiPSCs, as some current preclinical and clinical studies for DMD therapies do not efficiently target the heart (e.g. exon skipping[119]). Additionally, we demonstrated a normalization in miR31 levels, a microRNA that inhibits dystrophin, after reading frame restoration similar to what is observed in human BMD patients[103]. Finally, we show restored DGC localization *in vitro* and *in vivo*, which further validates the functionality of DYS$^{\Delta 45\text{-}55}$ (**Figure 2-10**).

Previous work by Ousterout et al. demonstrated that multiplexed gRNAs can restore the *DMD* reading frame in primary myoblasts[49]. However, myoblasts do not provide a renewable source of stem cells, which is a requirement for long-term therapeutic efficacy[120]. In contrast, we used hiPSCs which offer the opportunity to evaluate the internally deleted dystrophin protein in multiple cell types that are affected in DMD, and in future studies, may provide a renewal source of corrected progenitor cells. Our work is further distinguished from previous studies as we are the only group to show restoration of dystrophin function on membrane integrity, miR31 expression, and the DGC in cardiac and skeletal muscle cells following CRISPR-mediated gene editing.

An advantage of our CRISPR platform is the therapeutic potential of a single pair of gRNAs to treat around half of all DMD patients. By designing gRNAs that accomplish a deletion that encompasses a large percentage of DMD mutations, this approach is optimized for future clinical studies. It would be unreasonable to design, validate, and evaluate off-targets for every new CRISPR pair tailored for each individual patient. Additionally, CRISPR/Cas9 is

advantageous over exon skipping, as it results in permanent restoration of reading frame as opposed to transient effects on RNA splicing. Previously, Li et al. used CRISPR/Cas9 to induce exon skipping, frameshifting, or exon knockin to restore dystrophin in a DMD hiPSC line with an exon 44 deletion[51]; however, their platform is only applicable to 3-9% of DMD patients[121], and two of their strategies relied on creation of indels which would be difficult to apply consistently to each patient. While Ousterout et al. deleted exons 45-55, they removed significantly less of the intervening region (336kb) and thus their approach would cover fewer patient mutations within the hotspot region. This is because many mutations extend into the intronic region, thus by designing gRNAs that encompass more of the intron, our platform is applicable to more patients.

Another benefit of using this platform to delete a large portion of *DMD*, as opposed to single exons, is the known correlation of $DYS^{\Delta 45\text{-}55}$ with a mild BMD phenotype. Large deletions in the rod domain of dystrophin often produce a more functional (more like wild type) protein, than even very small deletions[15]. Larger deletions, which remove hinge III (exons 50-51), are believed to lead to a milder BMD phenotype than smaller deletions, or those which retain hinge III[122]. Thus, in many cases larger deletions are more therapeutically beneficial than smaller ones, due to the way they affect the secondary structure of the protein.

In summary, we have developed a potentially therapeutic gene editing platform for DMD to permanently restore dystrophin reading frame in multiple patient-derived hiPSCs. Our approach using CRISPR/Cas9 and NHEJ deletes up to 725kb of *DMD* encompassing exons 45-55 and restores dystrophin protein function in both cardiomyocytes and skeletal muscle cells derived from reframed hiPSCs. A current limitation of this platform is that clinical protocols still need to be developed that allow for rapid clonal line derivation, and the utilization of hiPSC-

derived cardiac and skeletal muscle progenitors combined with gene correction. Alternatively, CRISPR/Cas9 to restore the reading frame in DMD mouse models has been delivered directly *in vivo*[123–125]. Thus, applications of this platform in the future will allow for the development of an *in situ* gene correction strategy or *ex vivo* gene correction followed by autologous cell transplantation, either of which offers tremendous potential for DMD.

Acknowledgements

We would like to thank Doug Black, Richard Wang, and Haibin Xi for suggestions and Diana Becerra and Jane Wen for technical assistance. The following cores were utilized: CDMD Muscle Phenotyping and Imaging Core, HTS and Cell Repository Core, and Bioinformatics and Genomics Core (supported by NIAMS-P30 AR057230), the UCLA Broad Stem Cell Research Center (BSCRC) Flow Cytometry Core Resource, the UCLA Jonsson Comprehensive Cancer Center (JCCC) and Center for AIDS Research (CFAR) Flow Cytometry Core Facility (supported by NIH P30 CA016042, 5P30 AI028697), the UCLA Integrated Molecular Technologies Core (supported by CURE/P30 DK041301), the UCLA Humanized Mouse Core (supported by the JCCC, BSCRC, CFAR, NIH/NIAID AI028697), and the UCLA GenoSeq core. This material is based upon work supported by the National Science Foundation Graduate Research Fellowship Program under Grant No. DGE-1144087 (CSY). Funding was provided by NIAMS of the NIH (P30 AR057230-MJS, AN, ADP, R01AR064327-ADP) and the Eli & Edythe Broad Center of Regenerative Medicine and Stem Cell Research at UCLA (MJS, ADP) and Rose Hills Foundation Research Award (ADP).

Author contributions

Conceptualization, Methodology, Writing-Original Draft, Visualization, Project Administration - CSY, MJS, ADP; Validation- CSY, MRH, NVE; Formal Analysis- CSY; Investigation- CSY, MRH, NVE, HN, MJ, SY, SK CK-C, DW; Resources- AN, SFN, MCM, MJS, ADP; Writing- Review and Editing- CSY, MRH, NEV, SK, CK-C, DBK, AN, SFN, MCM, MJS, ADP; Supervision- JAZ, DBK, AN, MCM, MJS, ADP; Funding Acquisition- MJS, ADP.

Figures

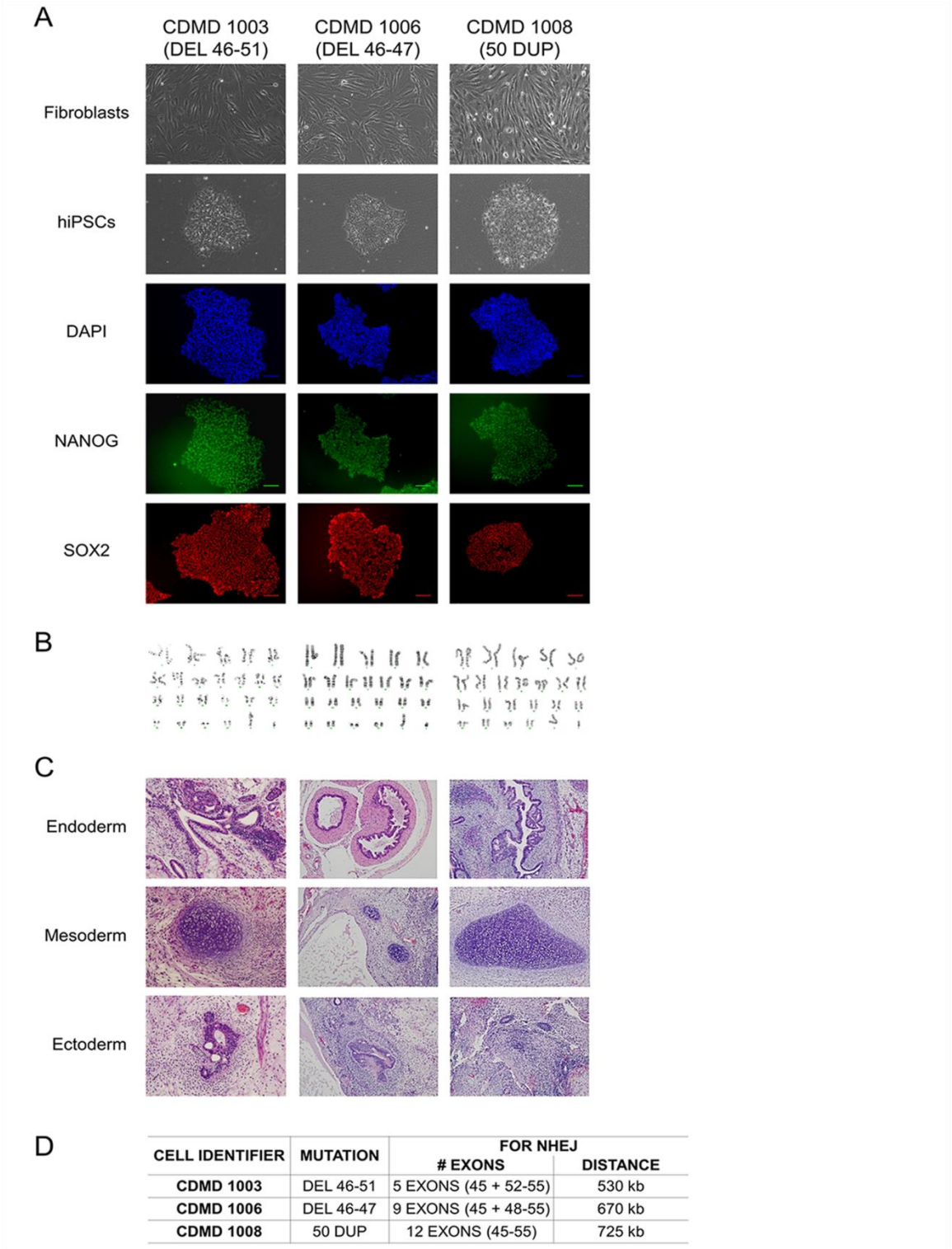

D

CELL IDENTIFIER	MUTATION	FOR NHEJ	
		# EXONS	DISTANCE
CDMD 1003	DEL 46-51	5 EXONS (45 + 52-55)	530 kb
CDMD 1006	DEL 46-47	9 EXONS (45 + 48-55)	670 kb
CDMD 1008	50 DUP	12 EXONS (45-55)	725 kb

Figure 2-1: CDMD hiPSCs are pluripotent and genetically stable.
A) CDMD hiPSCs were generated from DMD fibroblasts. Brightfield images depict fibroblasts before and after reprogramming to hiPSCs. Immunocytochemical staining reveals that cells express pluripotency markers NANOG (green) and SOX2 (red). Scale bar 100µm.
B) Karyotyping of all lines is shown.
C) CDMD hiPSCs were injected into mice to test teratoma formation *in vivo*. Representative hematoxylin and eosin stainings of the three germ layers (endoderm, mesoderm, and ectoderm) are shown.
D) Patient mutations for each CDMD hiPSC line are shown. In addition, the number of exons and the approximate distance necessary for successful NHEJ is indicated, based on comparative genomic hybridization data for the patient's underlying mutation size.

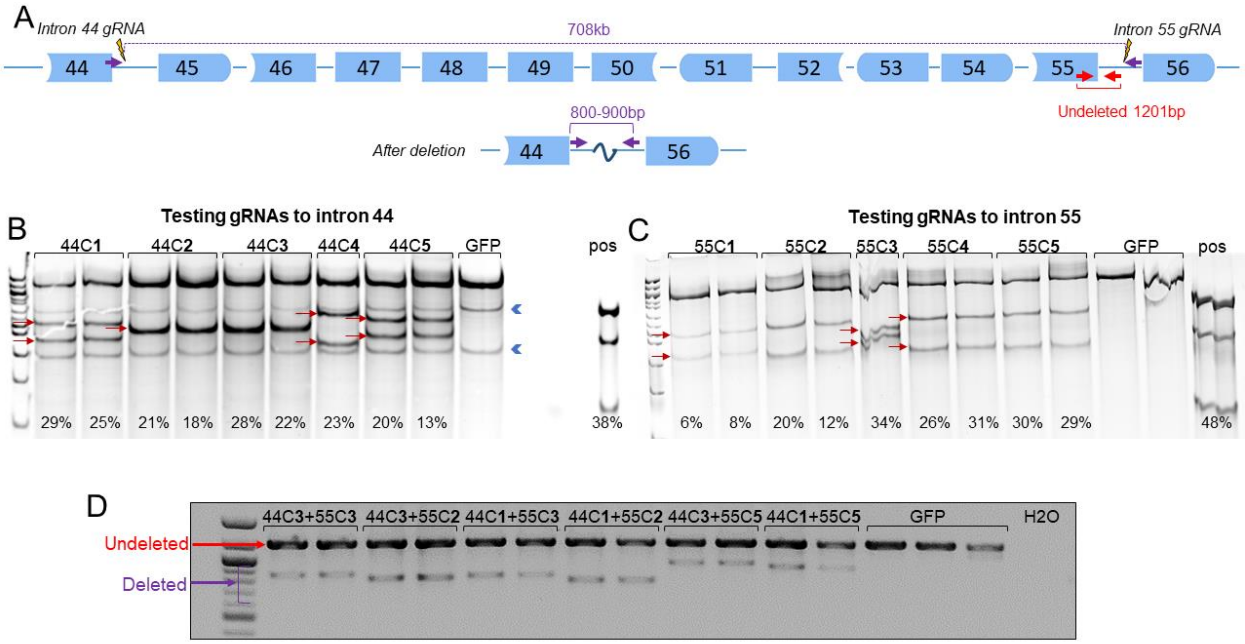

Figure 2-2: gRNA activity and exon 45-55 deletion in 293FT cells.
A) A cartoon (not to scale) highlighting the region of DNA targeted by CRISPR pairs and indicating primers used for PCR. CRISPR gRNA sites are shown by lightning bolts. When pairs of gRNAs targeted to introns 44 and 55 are co-transfected, an exon 45-55 deletion (~708kb) results after NHEJ. This deletion is measured using multiplex PCR where the primer pair shown in red will amplify the undeleted product while the purple primer pair flanking the deleted region only gives a product when successful rejoining has occurred.
B)-C) Five gRNAs targeted to introns 44 and 55 respectively, show activity on Surveyor assay in HEK293FT cells. Red arrows denote expected cleavage product bands (sizes in **Table 2-1**). Note in A, the bands highlighted by the blue arrowheads are likely non-specific PCR products and were discounted from the analysis. The estimated percent of cutting is shown below each lane. The positive control (pos) is provided with the Surveyor kit. A 100bp ladder was used.
D) Example of a multiplex PCR, using the primers indicated in A, in which effective deletion of exons 45-55 was achieved with all gRNA pairs tested in 293FT cells. A 100bp ladder was used.

Table 2-1: Expected cleavage product sizes from Surveyor assay.

gRNA	Expected sizes (bp)
44C1	423, 480
44C2	445, 458
44C3	449, 454
44C4	387, 516
44C5	419, 484
55C1	379, 490
55C2	364, 505
55C3	411, 458
55C4	357, 512
55C5	351, 518

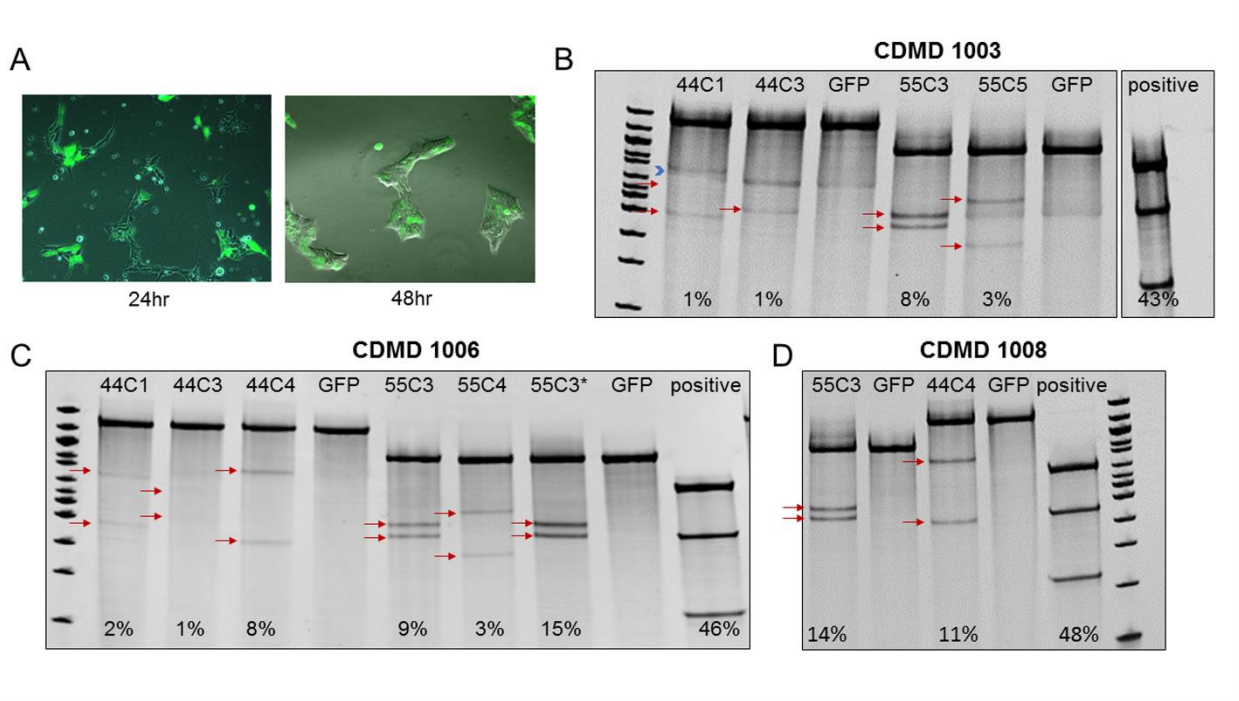

Figure 2-3: gRNAs show cutting by Surveyor assay in CDMD hiPSCs.
A) CDMD 1006 hiPSCs nucleofected with GFP serve as an untreated control and demonstrate ~40% transfection efficiency.
B)-D) gRNAs demonstrate activity on Surveyor assay in CDMD 1003, 1006 and 1008 lines respectively. *3x the amount of 55C3 DNA was added during nucleofection. Red arrows denote expected cleavage product bands (sizes in **Table 2-1**). Note the band in B highlighted by the blue arrow head is likely a non-specific PCR product and was discounted from analysis. The estimated percent of cutting is shown below each lane. A 100bp ladder was used.

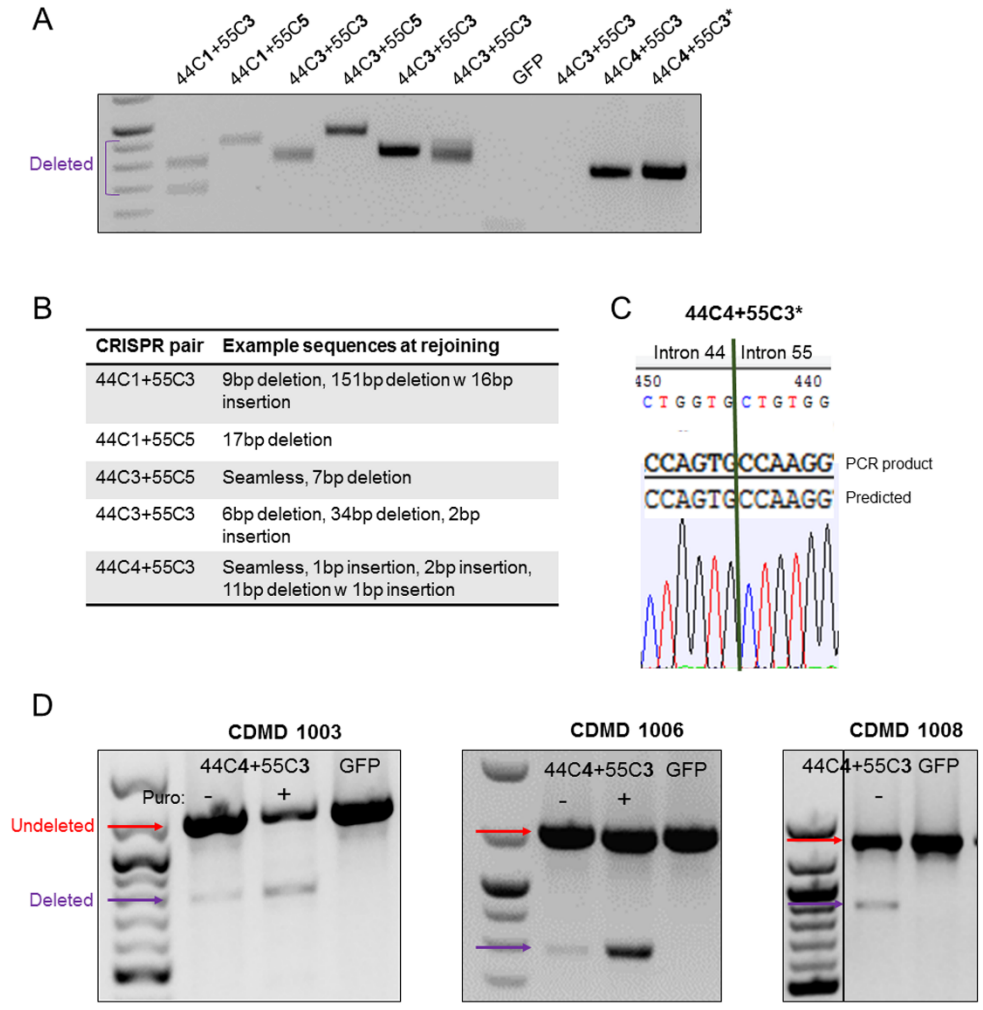

CRISPR pair	Example sequences at rejoining
44C1+55C3	9bp deletion, 151bp deletion w 16bp insertion
44C1+55C5	17bp deletion
44C3+55C5	Seamless, 7bp deletion
44C3+55C3	6bp deletion, 34bp deletion, 2bp insertion
44C4+55C3	Seamless, 1bp insertion, 2bp insertion, 11bp deletion w 1bp insertion

Figure 2-4: Nucleofection of paired gRNAs results in an exon 45-55 deletion in CDMD hiPSCs.

A) PCR using primers flanking the deleted region show bands for successful deletion and rejoining after nucleofection of a variety of CRISPR pairs in hiPSC CDMD 1006. A 100bp ladder was used.

B) Examples of the types of different rejoined products identified after sequencing.

C) The sequencing for 44C4 + 55C3* seamless rejoining is shown. *3x the amount of DNA was added during nucleofection.

D) Multiplex PCR shows an exon 45-55 deletion product in all lines nucleofected with 44C4 and 55C3 gRNAs. A significant increase in the efficiency of deletion in CDMD 1006 and 1003 after selection with 0.35µg/ml puromycin for one day is shown. A 100bp ladder was used.

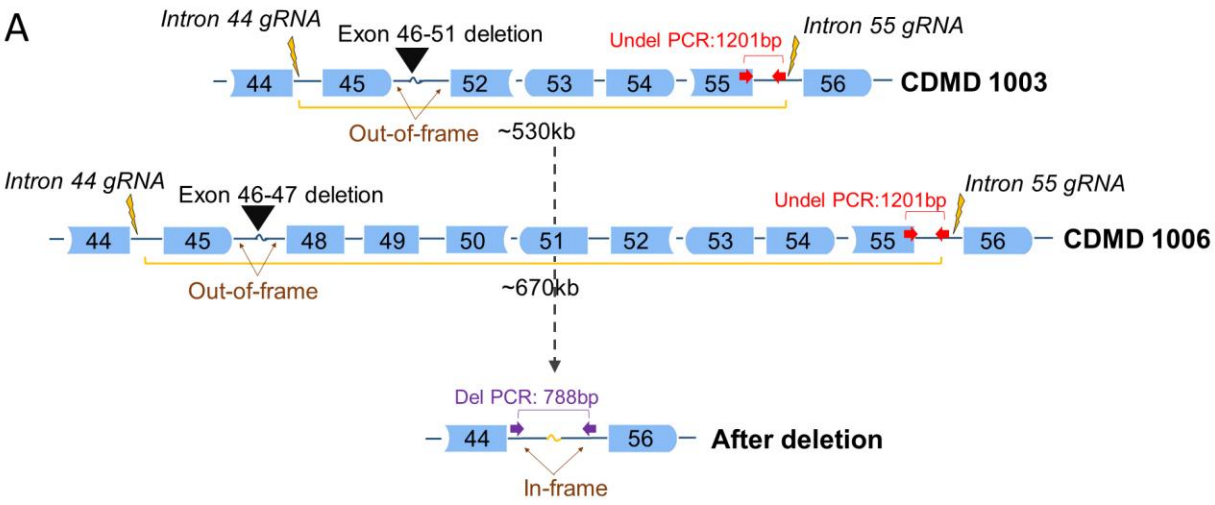
A
Intron 44 gRNA
Exon 46-51 deletion
Undel PCR:1201bp
Intron 55 gRNA
44
45
52
53
54
55
56
CDMD 1003
Out-of-frame
~530kb
Intron 44 gRNA
Exon 46-47 deletion
Undel PCR:1201bp
Intron 55 gRNA
44
45
48
49
50
51
52
53
54
55
56
CDMD 1006
Out-of-frame
~670kb
Del PCR: 788bp
44
56
After deletion
In-frame

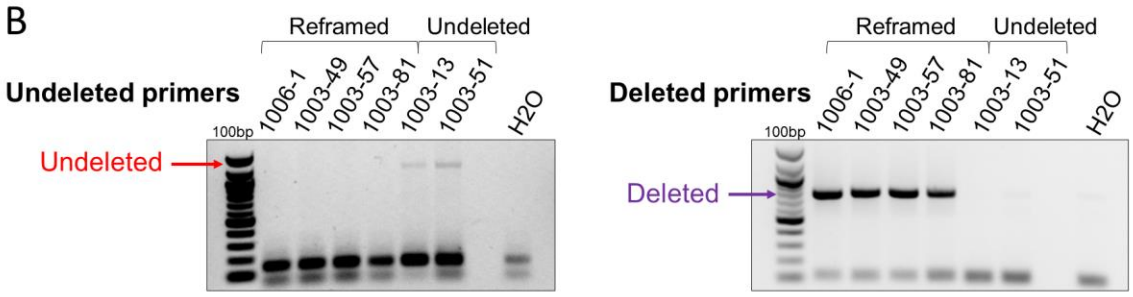
B
Reframed
Undeleted
Undeleted primers
1006-1
1003-49
1003-57
1003-81
1003-13
1003-51
H2O
100bp
Undeleted
Reframed
Undeleted
Deleted primers
1006-1
1003-49
1003-57
1003-81
1003-13
1003-51
H2O
100bp
Deleted

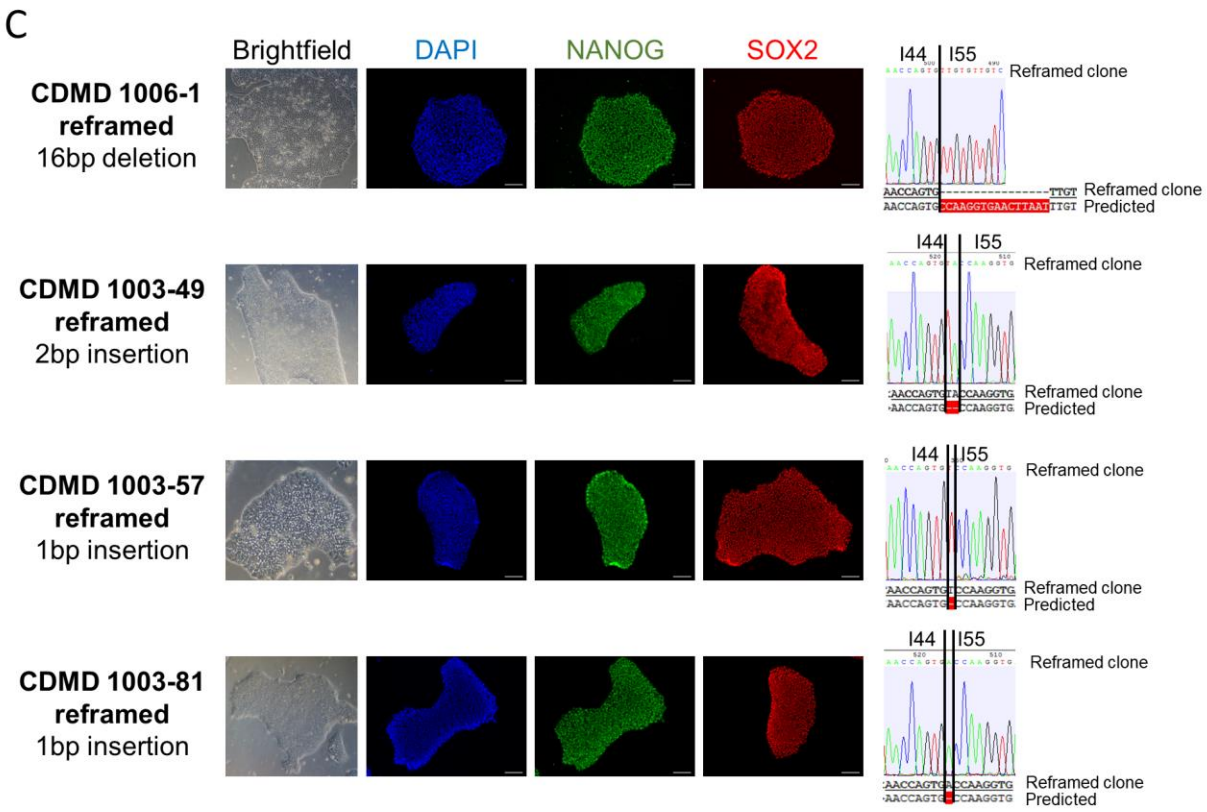
C
Brightfield
DAPI
NANOG
SOX2
CDMD 1006-1
reframed
16bp deletion
I44
I55
Reframed clone
Reframed clone
Predicted
CDMD 1003-49
reframed
2bp insertion
I44
I55
Reframed clone
Reframed clone
Predicted
CDMD 1003-57
reframed
1bp insertion
I44
I55
Reframed clone
Reframed clone
Predicted
CDMD 1003-81
reframed
1bp insertion
I44
I55
Reframed clone
Reframed clone
Predicted

Figure 2-5: Generation of stable, pluripotent CDMD hiPSC lines with an exon 45-55 deletion.
A) Shown is a cartoon (not to scale) of the region of *DMD* targeted for CRISPR/Cas9-mediated deletion in CDMD hiPSCs using gRNAs specific to introns 44 and 55 (lightning bolts). Successful NHEJ deletes exons 45-55 and restores the reading frame for DMD mutations within this region. Different deletion sizes are required depending on the patient's underlying mutation (black arrow heads).
B) PCR genotyping of 117 and 109 single cell clones from parental lines CDMD 1006 and 1003, respectively, was carried out on cells nucleofected with gRNAs 44C4 and 55C3. One clone from CDMD 1006 (CDMD 1006-1) and three from CDMD 1003 (CDMD 1003-49, 1003-57, 1003-81) were identified as stably deleted. Deletion PCR genotyping results for 6 hiPSC clonal lines is shown. One pair of primers (red arrows in A) was located internal to the deletion and only produced a 1201bp band in the undeleted clones CDMD 1003-13 and 1003-51. Another primer set (purple arrows in A) flanked the deletion region and produced a 788bp band only when the deletion and NHEJ occurred successfully, as in the reframed clones CDMD 1006-1, 1003-49, 1003-57, 1003-81.
C) Each clonal line maintained normal morphology (brightfield) and expressed NANOG (green) and SOX2 (red) by immunocytochemistry. Scale bar 100µm. Shown to the right is the sequence of the gDNA at the rejoining site between introns 44 (I44) and 55 (I55). Sequencing revealed a 16bp deletion in CDMD 1006-1, a 2bp insertion in CDMD 1003-49, and 1bp insertions in CDMD 1003-57 and CDMD 1003-81.

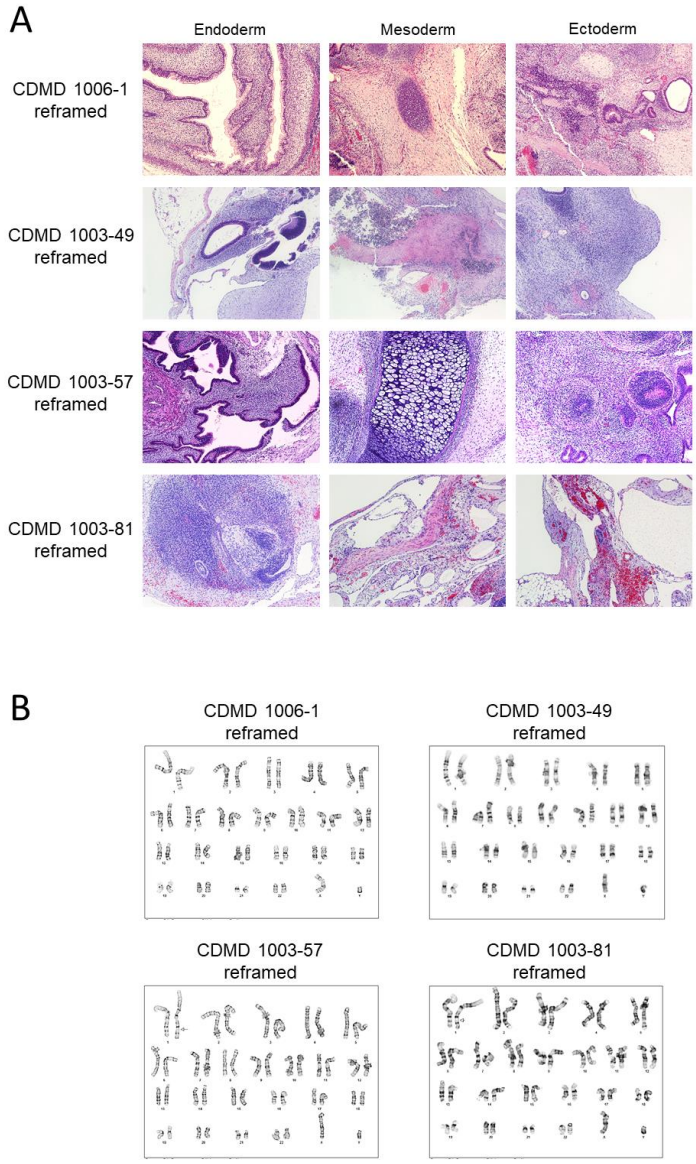

Figure 2-6: Additional characterization of reframed lines.
A) Reframed lines CDMD 1006-1, 1003-49, 1003-57, and 1003-81 formed teratomas consisting of the three germ layers *in vivo*.
B) All reframed lines were determined to be karyotypically normal except for CDMD 1003-81, which was found to contain a 1q32 amplification via FISH analysis. Upon retrospective analysis, the 1q32 amplification was determined to have existed in the parent line (CDMD 1003 line at 22%) and was found in all daughter lines (CDMD 1003-57 and 1003-49 at 82.5%) and was not a result of CRISPR activity.

Table 2-2: Sequencing results from off-target analysis.
See excel file under Supplemental Information at http://www.cell.com/cell-stem-cell/fulltext/S1934-5909(16)00022-9.

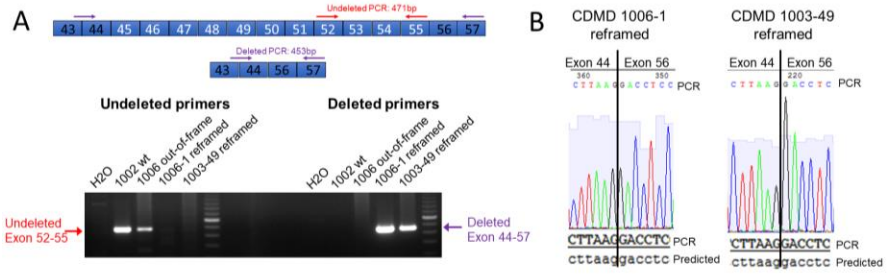
A
Undeleted PCR: 471bp
43 44 45 46 47 48 49 50 51 52 53 54 55 56 57
Deleted PCR: 453bp
43 44 56 57
Undeleted primers
Deleted primers
H2O
1002 wt
1006 out-of-frame
1006-1 reframed
1003-49 reframed
Undeleted Exon 52-55
Deleted Exon 44-57
B
CDMD 1006-1 reframed
CDMD 1003-49 reframed
Exon 44
Exon 56
PCR
CTTAAGGACCTC
cttaaggacctc
Predicted

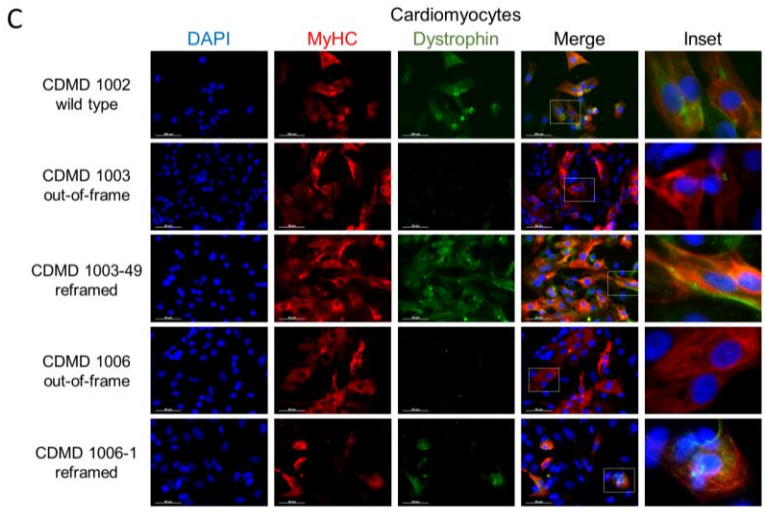
C
Cardiomyocytes
DAPI
MyHC
Dystrophin
Merge
Inset
CDMD 1002 wild type
CDMD 1003 out-of-frame
CDMD 1003-49 reframed
CDMD 1006 out-of-frame
CDMD 1006-1 reframed

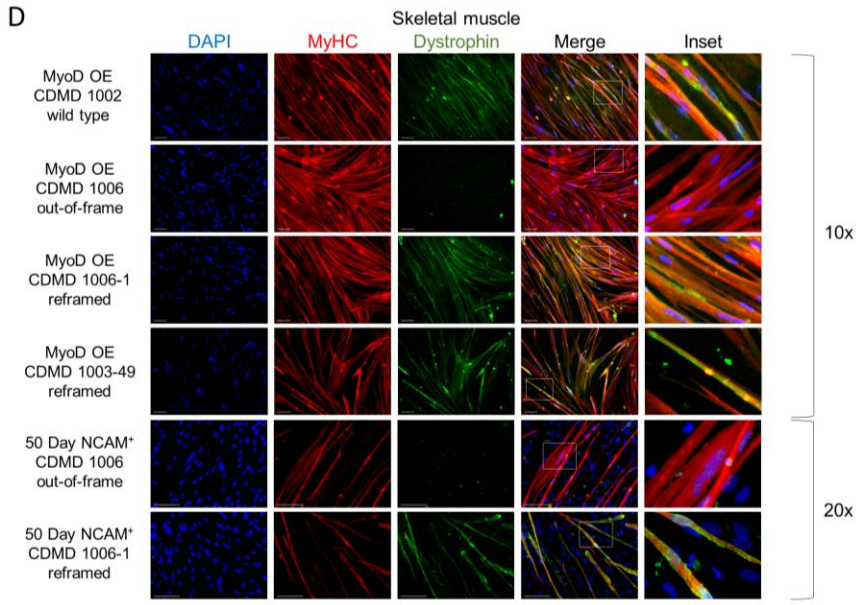
D
Skeletal muscle
DAPI
MyHC
Dystrophin
Merge
Inset
MyoD OE CDMD 1002 wild type
MyoD OE CDMD 1006 out-of-frame
MyoD OE CDMD 1006-1 reframed
MyoD OE CDMD 1003-49 reframed
50 Day NCAM+ CDMD 1006 out-of-frame
50 Day NCAM+ CDMD 1006-1 reframed
10x
20x

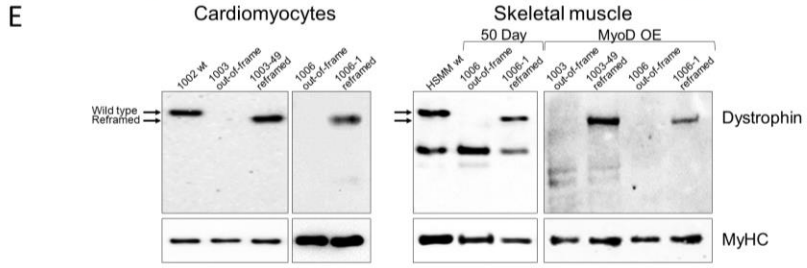
E
Cardiomyocytes
Skeletal muscle
50 Day
MyoD OE
1002 wt
1003 out-of-frame
1003-49 reframed
1006 out-of-frame
1006-1 reframed
HSMM wt
Wild type
Reframed
Dystrophin
MyHC

Figure 2-7: Reframed CDMD hiPSC-derived skeletal muscle and cardiomyocytes restore dystrophin expression.
A) Analysis of the mRNA from reframed lines. PCR using primers within the deleted region (red arrows) or flanking the deleted region (purple arrows) on dystrophin cDNA from hiPSC-derived cardiomyocytes shows undeleted bands in both CDMD 1002 and 1006 and deleted bands in both CDMD 1006-1 and 1003-49. A 100bp ladder was used.
B) Sequencing confirms exon 44 and 56 rejoining in reframed CDMD 1006-1 and 1003-49 mRNA.
C) Immunocytochemical staining of human myosin heavy chain (MyHC, red) and dystrophin (green) of wild type (CDMD 1002), out-of-frame (CDMD 1003, 1006) or reframed (CDMD 1003-49, 1006-1) cardiomyocytes derived from hiPSCs by directed differentiation. Inset depicts zoomed in region defined by the white box. Scale bar 50µm.
D) Immunocytochemical staining of MyHC (red) and dystrophin (green) of wild type (CDMD 1002), out-of-frame (CDMD 1006) or reframed (CDMD 1006-1, 1003-49) skeletal muscle myotubes derived from hiPSCs. Myotubes were fused after MyoD overexpression (OE) or from sorted $NCAM^+$ cells after an adapted directed differentiation 50-day protocol. Inset depicts zoomed in region defined by the white box. Scale bar 100µm.
E) Western blots of cell extracts probed with anti-dystrophin. Extracts were from out-of-frame and reframed cardiomyocytes (left) and skeletal muscle myotubes (right), derived from CDMD hiPSCs. Wild type (wt) hiPSCs (CDMD 1002) or human skeletal muscle myotubes (HSMM) were used as a control for dystrophin. The molecular weight shift caused by the exon 45-55 deletion (1779bp, ~66kDa) is evident in reframed vs. wild type dystrophin (arrows). A non-specific band around 220kDa was seen in some samples. Samples were also probed with anti-MyHC as a loading control (bottom panels).

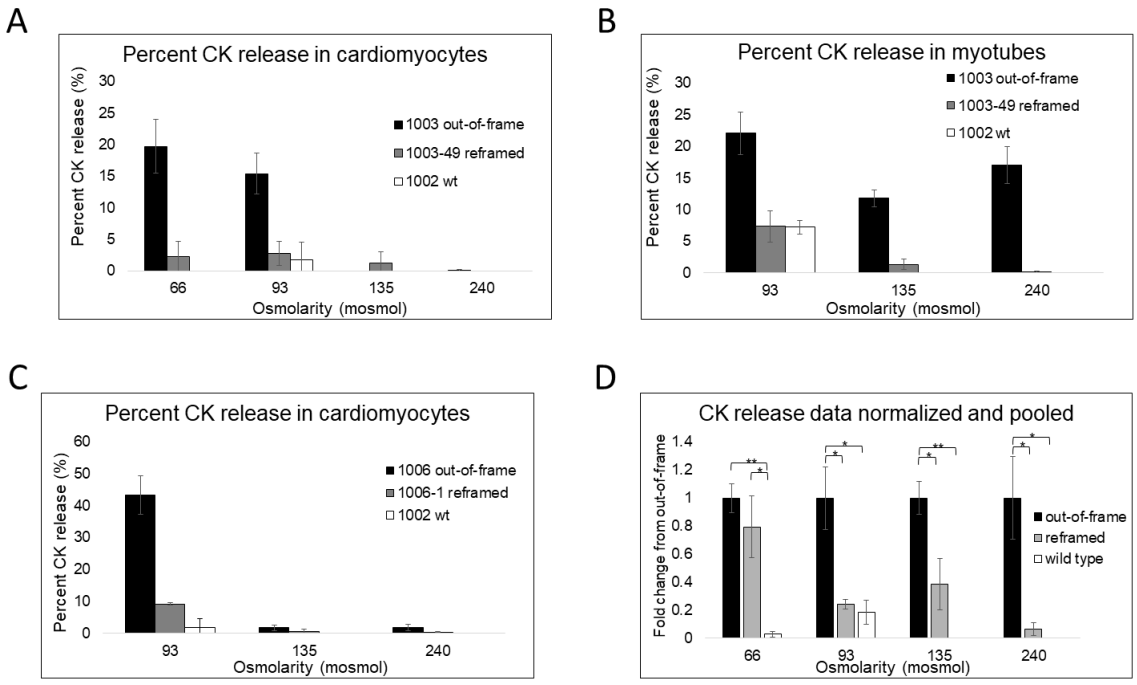

Figure 2-8: Reframed hiPSC-derived cardiomyocytes and skeletal muscle cells demonstrate restored membrane stability *in vitro*.

A)-C) Representative graphs of CK release assays from cells exposed to hypoosmotic conditions. Cardiomyocytes and skeletal muscle myotubes derived from hiPSCs were subjected to a range of osmolarities below 240mosmol and CK release to the supernatant was measured as an indication of membrane fragility. Data are presented as average ± standard error.

D) CK release assay data normalized to out-of-frame cells and pooled from all experiments shown (n=6 for out-of-frame and reframed (except n=5 for reframed 135mosmol), n=4 for wild type). Data are presented as average ± standard error. *$p<0.05$, **$p<0.01$.

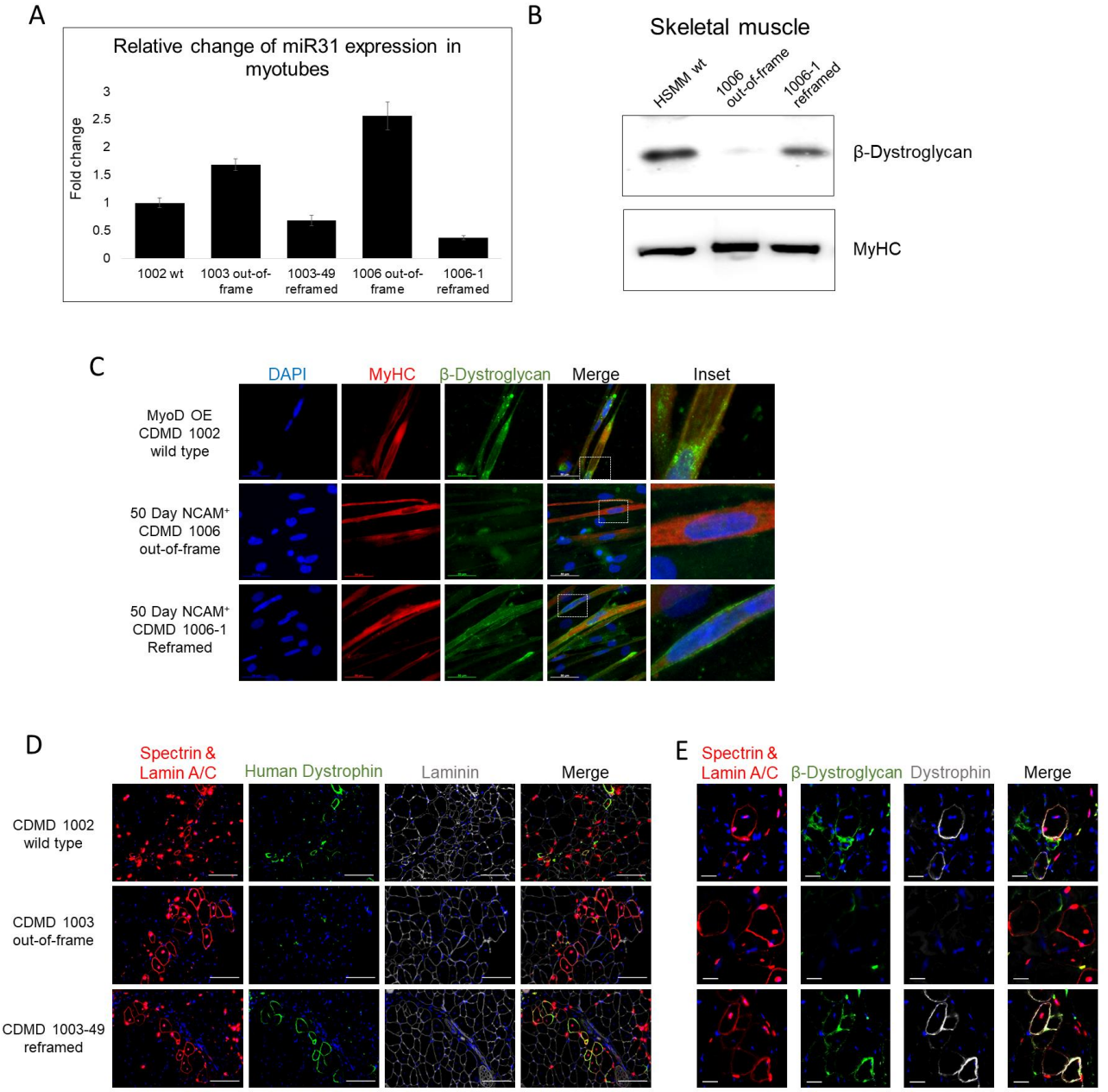

Figure 2-9: Reframed hiPSC-derived cardiomyocytes and skeletal muscle cells demonstrate restored function *in vitro* and *in vivo*.

A) Fold change in expression of miR31 measured by ddPCR in myotubes derived from out-of-frame or reframed hiPSCs by MyoD OE, normalized to wild type (CDMD 1002). Data are presented as average ± standard deviation.

B) Western blots of cell extracts probed with anti-β-dystroglycan, a component of the DGC. Extracts were from out-of-frame and reframed skeletal muscle myotubes derived by MyoD OE. HSMM was used as a positive control. Samples were also probed with anti-MyHC as a loading control (bottom panel).

C) Immunocytochemical staining of MyHC (red) and β-dystroglycan (green) in wild type (CDMD 1002), out-of-frame (CDMD 1006) or reframed (CDMD 1006-1) skeletal muscle myotubes. Inset depicts zoomed in region defined by the white box. Scale bar 50μm.
D) Assessment of human dystrophin restoration in wild type (CDMD 1002), out-of-frame (CDMD 1003), and reframed (CDMD 1003-49) MyoD OE cells engrafted into the TA of NSG-mdx mice. Engrafted human cells were identified by co-immunostaining for human spectrin and lamin A/C (shown in red). Positive staining for human dystrophin is shown in green and all fibers are shown using laminin (grey). All sections were stained with DAPI (blue) to identify nuclei. Scale bar 100μm.
E) Assessment of β-dystroglycan restoration in human fibers from wild type (CDMD 1002), out-of-frame (CDMD 1003), and reframed (CDMD 1003-49) MyoD OE cells engrafted into the TA of NSG-mdx mice. Engrafted human cells were identified by co-immunostaining for human spectrin and lamin A/C (shown in red). Positive staining for dystrophin is shown in grey and β-dystroglycan is shown in green. All sections were stained with DAPI (blue) to identify nuclei. Cell order is same as noted in D. Scale bar 20μm.

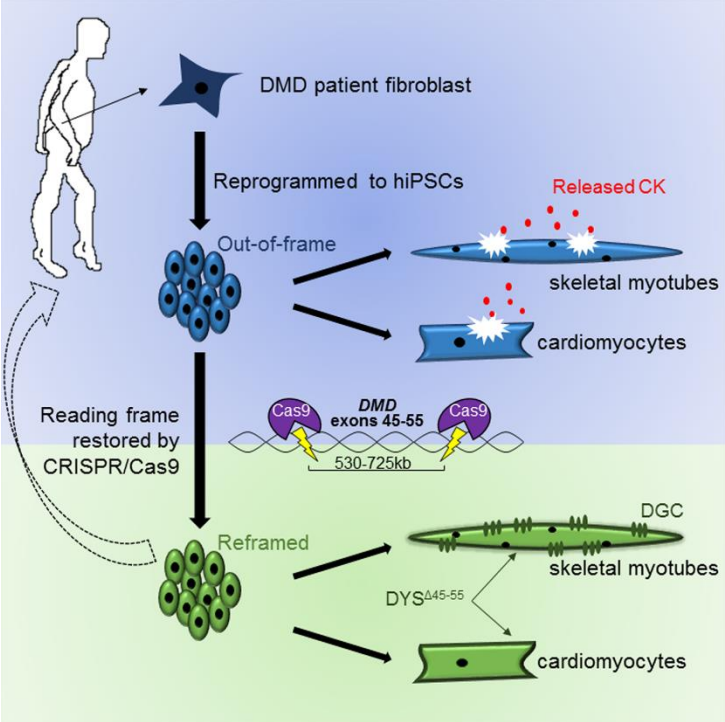

Figure 2-10: Summary of CRISPR/Cas9 mediated reframing of the *DMD* gene in DMD hiPSCs.

DMD patient fibroblasts were reprogrammed into hiPSCs, which were differentiated to disease relevant cell types of skeletal and cardiac muscle. The out-of-frame muscle cells demonstrated a lack of dystrophin and β-dystroglycan and reduced membrane stability seen by leakage of CK. Stable hiPSC reframed lines were obtained using CRISPR/Cas9 to delete *DMD* exons 45-55. Reframed hiPSC derived muscle cells had restored dystrophin and β-dystroglycan and improved membrane stability.

Chapter 3 - Creation of a Novel Humanized Dystrophic Mouse Model of Duchenne Muscular Dystrophy and Application of a CRISPR/Cas9 Gene Editing Therapy

Abstract

Duchenne muscular dystrophy is caused by mutations in *DMD* which disrupt the reading frame. Therapeutic strategies that restore *DMD*'s reading frame, such as exon skipping and CRISPR/Cas9, need to be tested in the context of the human *DMD* sequence *in vivo*. We have developed a novel dystrophic mouse model by using CRISPR/Cas9 to delete exon 45 in the human *DMD* gene in hDMD mice, which places *DMD* out-of-frame. We have utilized this model to demonstrate that our clinically-relevant CRISPR/Cas9 platform, which targets deletion of human *DMD* exons 45-55, can be directly applied *in vivo* to restore dystrophin.

Introduction

Duchenne muscular dystrophy (DMD) is a progressive muscle degenerative disease, affecting about 1 in 5000 male births[126]. It is most often caused by out-of-frame mutations in the *DMD* gene, which prevent expression of dystrophin protein. Dystrophin normally stabilizes and assembles the dystrophin glycoprotein complex (DGC) at the muscle fiber sarcolemma to connect the actin cytoskeleton to the extracellular matrix. Lack of dystrophin and the DGC leads to muscle fiber damage and progressive degeneration, resulting in fibro-adipogenic accumulation in the muscle. Potential therapeutic strategies, such as exon skipping, or clustered, regularly interspaced, short palindromic repeats (CRISPR) and -associated protein (Cas) 9 (CRISPR/Cas9), aim to restore the *DMD* reading frame, which will lead to the milder, allelic disease Becker muscular dystrophy[127]. Exon skipping therapies use antisense oligonucleotides to

target a specific sequence in the dystrophin mRNA and alter the splicing pattern to reframe the transcript[128]. CRISPR/Cas9-based therapies use guide RNAs (gRNAs) and the Cas9 nuclease to target specific sequences of genomic DNA for deletion or editing[39–41]. Currently, there are no mouse models that allow for testing of such therapies on the human *DMD* sequence in a dystrophic context *in vivo*.

A humanized mouse (hDMD) was previously generated in which the entire human *DMD* sequence was integrated into mouse chromosome 5[129]. However, this mouse expresses the wild type human *DMD* transcript and does not present a dystrophic phenotype, even if crossed to the mdx mouse which lacks murine dystrophin, since human dystrophin can functionally replace the mouse protein. Since the CRISPR/Cas9 system has shown much promise in quickly and easily generating novel mouse models, we used CRISPR/Cas9 to make an out-of-frame mutation by deleting exon 45 of the human *DMD* gene in hDMD mouse zygotes (hereafter referred to as hDMD del45 mice). We have crossed this mouse to both the mdx and mdxD2 backgrounds, both of which have a premature stop codon in the mouse *Dmd* gene. MdxD2 mice are on the DBA2 background and have a more severe phenotype than mdx mice on the C57BL/10 background, primarily due to two modifier genes, *Ltbp4* and *Anxa6*[130–132]. Here we describe the initial characterization of the hDMD del45 model. We show that muscles of hDMD del45 mdxD2 mice contain a mutated human *DMD* gene lacking exon 45 and are dystrophic. We also show proof-of-principle *in vivo* application of our CRISPR/Cas9 gene editing platform which targets human *DMD* exons 45-55 for deletion to restore the reading frame for about half of all Duchenne patients[57].

Materials and Methods

Mice

All animal work was conducted under protocols approved by the UCLA Animal Research Committee in the Office of Animal Research Oversight. hDMD (Tg(DMD)72Thoen/J, 018900), C57BL/10 mdx (001801), and mdxD2 (D1.B10-Dmdmdx/J, 013141) mice were obtained from Jackson Laboratories.

Generation of hDMD del45 mice

CRISPR/Cas9 injection into hDMD zygotes was performed by the University of California, Davis, Mouse Biology Program. 100ng/µl mRNA Cas9 was mixed with 20ng/µl of each of 44C1, 44C2, 45C2, 45C3 gRNAs (sequences below) produced via *in vitro* transcription. 2-4pL (0.2-0.4pg Cas9 and 0.04-0.08pg each gRNA) was injected into the nucleus with excess positive flow into the cytoplasm. Pups were PCR screened for the deletion and the sequence confirmed via Sanger sequencing.

Mice genotyping

An hDMD genotyping protocol was adapted from Jackson Laboratories for use with GeneMate Taq (BioExpress). Mdx genotyping was performed using ARMS PCR and confirmed by sequencing. Genotyping for the *Ltbp4* allele was done using primers flanking the deletion with GeneMate Taq. The *Anxa6* mutation was checked by sequencing. Genotyping for hDMD del45 mice was performed using GeneMate Taq. Per 12.5µl reaction, 1.25µl NH4 buffer, 1µl 50mM $MgCl_2$, 0.5µl DMSO, 0.6µl hDMD 45 del2 F primer, 0.6µl hDMD 45 del2 R primer, 0.1µl 25mM dNTP, 0.3µl Taq, 7.15µl H_2O, and 1µl tail DNA was mixed. The PCR was run at

95°C 2min, then 35 cycles of 95°C 30s, 56.5°C 30s, 72°C 1:30min, then 72°C 10min. PCR products were run on a 2% gel. No deletion produced a 1254bp band and an exon 45 deletion produced a 550-715bp band. Primer sequences below. Sanger sequencing of PCR products was performed by Laragen Inc.

Primer sequences for PCR

Primer name, *purpose*	Sequence
Ltbp4 21991 F, *genotyping for LTBP4 allele*	AACCGCTACCCAAACCTTCA
Ltbp4 22379 R, *genotyping for LTBP4 allele*	AGGCTTTCTGCCTACTCGTC
hDMD45del2 F, *genotyping for hDMD del45 mice*	TGGCTCAAGTTCCCCTTCAA
hDMD45del2 R, *genotyping for hDMD del45 mice*	TGGGATGCTCCTGAAAGCAA
hdmdseq44F, *Surveyor for I44 and for 293FT deletion PCR*	AGGTGGGCAAAGACAACTGA
hdmdseq44R, *Surveyor for I44*	TGGGAAGCCTGAATCTGCG
hdmdseq45F, *Surveyor for I45*	TCTGACAACAGTTTGCCGC
hdmdseq45R, *Surveyor for I45 and for 293FT deletion PCR*	TGACATAAGGATTTGAGTCATTCAG
44_F, *PCR for exon 45-55 deletion*[57]	CTGGACGGAGCTGGTTTATCT
55surv2_R, *PCR for exon 45-55 deletion*[57]	CCCTTTTCTTGGCGTATTGCC
55undelF, *PCR for undeleted exon 45-55 allele*[57]	GCCTGGGTCTCTGCTATCAA
55undelR, *PCR for undeleted exon 45-55 allele*[57]	GCCACTTTGTACTCCGCACT

CRISPR/Cas9 gRNA generation and screening

gRNAs targeting *DMD* introns 44 and 45 were designed using crispr.mit.edu and cloned into px330 (Addgene 42230, Feng Zhang [40]) as previously described[57]. Sequences below. Each gRNA was screened individually or in pairs in human embryonic kidney (HEK) 293FT cells using TransIT 293 (Mirus Bio) according to the manufacturer's instructions and as described[57]. Surveyor assay (IDT) was performed to assess single gRNA cutting ability as described[57]. The exon 45 deletion was assessed by Accuprime Taq HiFi (Thermo Fisher Scientific) PCR using primers flanking the deleted region (primer sequences in table above) where a 2037bp undeleted or 1329-1521bp deleted product was produced.

gRNAs for the exon 45-55 deletion (44C4, 55C3) from [57] were cloned into px333 (Addgene 64073, Andrea Ventura [133]) in tandem using BbsI and BsaI.

gRNA sequences and oligos for cloning

Name	Sequence	Sense oligo	Antisense oligo
44C1	ATATACTTGTGGCTAGTTAG**TGG**	CACCGATATACTTG TGGCTAGTTAG	AAACCTAACTAGCC ACAAGTATATC
44C2	ATTCACCTTGAAGCAATCAT**GGG**	CACCGATTCACCTT GAAGCAATCAT	AAACATGATTGCTT CAAGGTGAATC
44C4	TCTTTACTGCTGTTGATTAA**TGG**	CACCGTCTTTACTG CTGTTGATTAA	AAACTTAATCAACA GCAGTAAAGAC
45C1	AAAAACTGGAGCTAACCGAG**AGG**	CACCGAAAAACTG GAGCTAACCGAG	AAACCTCGGTTAGC TCCAGTTTTTC
45C2	TGTCCTACAAATCAATTAGT**TGG**	CACCGTGTCCTACA AATCAATTAGT	AAACACTAATTGAT TTGTAGGACAC
45C3	CAGGGAAAAAAGCACCCTCT**CGG**	CACCGCAGGGAAA AAAGCACCCTCT	AAACAGAGGGTGCT TTTTTCCCTGC

Green is NGG PAM

In vivo electroporation

hDMD del45 mdx and hDMD del45 mdxD2 mice were electroporated as described[134] with 20µg of px333 plasmid DNA (Addgene 64073, Andrea Ventura [133]) containing CRISPR guides 44C4 and 55C3 (from [57]) or pmaxGFP as a control for hDMD del45 mdxD2 mice. In brief, 5µl hyaluronidase was injected into the flexor digitorum brevis (FDB) muscle and 1hr later the DNA was injected and electroporated 20 times for 20ms at 1Hz.

hDMD del45 mdx mice were harvested 22 or 33 days later and genomic DNA was extracted by digesting the muscles with proteinase K then using the Quick-gDNA™ Miniprep Kit (Zymo Research). PCR for an exon 45-55 deletion was performed as described using Accuprime Taq HiFi (Thermo Fisher Scientific) or Herculase II Fusion Polymerase (Agilent Genomics)[57]. Sequencing of blunt cloned PCR products from Zero Blunt® TOPO® (Life Technologies) was done by Laragen Inc.

hDMD del45 mdxD2 mice were harvested 24 days post-electroporation. The interosseous (IO) and FDB were flash frozen and samples of 10µm cryosections taken throughout the whole muscle. Intervening sections as well as the lumbricalis were used for genomic DNA extraction and PCR as above.

Immunostaining and H&E staining

Harvested muscles were flash frozen in isopentane and cryosectioned at 10µm thickness. Blocking and staining was done as previously described[57]. Primary antibodies consisting of anti-human dystrophin (1:5, MANDYS106, MDA Monoclonal Antibody Resource, [113]) and anti-laminin (1:200, Sigma-Aldrich), were applied overnight at 4°C. The following day secondary antibodies were incubated for 1hr and the slides were mounted with VECTASHIELD containing DAPI (Vector Laboratories) and imaged on the Axio Observer Z1 microscope (Zeiss).

Muscle sections were also stained with hematoxylin and eosin and imaged on an Axio Imager M1 microscope (Zeiss).

Muscle sections from the electroporation experiment were fixed in cold acetone for 1 min then blocked with PBS containing 0.05% Tween-20 and 5% horse serum for 1-1.5hrs. The M.O.M. blocking kit (Vector Laboratories) was applied according to the manufacturer's instructions then primary antibodies of anti-laminin, human dystrophin (1:55, MANDYS106, Millipore-Sigma), dystrophin E48/50 (1:10, MANEX4850, MDA Monoclonal Antibody Resource, [113]) were added in PBS with 0.05% Tween-20, 5% FBS at 4°C overnight. The rest of the procedure was the same as described above. Control and treated slides were imaged at the same exposure and the contrast adjusted the same.

Western blotting

100µg of frozen tissues were solubilized in 50mM tris-HCl (pH 7.4), 7M urea, 2M thiourea, 4% CHAPS, 2% SDS, 50mM β-mercaptoethanol. Lysates were incubated at 4°C for 60 min with gentle rotation, and centrifuged for 5 min at 13,000*g.* Clarified lysates were transferred into new tubes, aliquoted and stored at -80°C until use. Protein concentration was determined

using 2-D Quant Kit (GE Healthcare Life Sciences). 20µg of hDMD del45 mdxD2 or hDMD del45 mdx gastrocnemius, TA, diaphragm and heart muscle lysates, 20µg of mdxD2 gastrocnemius lysate and 5-20µg of hDMD (wt) mdxD2 or hDMD (wt) mdx gastrocnemius muscle lysate were subjected to electrophoresis in a 6% polyacrylamide gel (PAAG), transferred to a nitrocellulose membrane and blotted with anti-human dystrophin antibody MANDYS106 (1:100 in PBSAT, Millipore Sigma) and stained with Ponceau S (Sigma-Aldrich).

For titration blots, lysates were prepared as described[135]. Briefly, muscle tissue was homogenized for 1min in 1mL of ice-cold Mito buffer [0.2mM EDTA, 0.25mM sucrose, 10mM tris-HCl (pH 7.4)] with protease/phosphatase inhibitor cocktail (Pierce) and deoxyribonuclease/ribonuclease and subjected to low-speed (1500*g*) centrifugation for 10 min at 4°C. The supernatant was centrifuged at 100,000*g* for 30min for isolation of membrane fraction. Isolated membranes and pellet after low-speed centrifugation were combined and resuspended in 300µl extraction buffer [50mM tris-HCl (pH 7.4), 7M urea, 2M thiourea, 4% CHAPS, 2% SDS, 50mM β-mercaptoethanol] followed by centrifugation for 5min at 13,000*g*. Various amounts of hDMD (wt) mdxD2 and hDMD del45 mdxD2 gastrocnemius lysates were subjected to 6% SDS-PAAG electrophoresis, blotted onto nitrocellulose membranes and probed with anti-human dystrophin antibody MANDYS106, anti-dystrophin MANDYS8 (1:400, Sigma-Aldrich), anti-dystrophin (1:300, Abcam Ab15277) or anti-vinculin (1:5000, Sigma-Aldrich) overnight at 4°C.

Secondary antibodies used were anti-mouse and anti-rabbit peroxidase conjugates (1:10000 in 5% milk/PBST, Sigma-Aldrich). Blots were developed using ChemiGlow West chemiluminescent detection kit (Protein Simple). Signals were registered by the Azure C300 (Azure Biosystems).

Results

We sought to generate a mouse model that expresses a mutated human *DMD* gene in mice lacking murine dystrophin. To this end, we designed gRNAs targeting *DMD* introns 44 and 45 to cause deletion of exon 45 via non-homologous end joining (NHEJ) of the human *DMD* gene in hDMD mice. The gRNAs were screened individually and in pairs in HEK293FT cells, and their ability to cause Cas9 cutting (**Figure 3-1A**) or an exon 45 deletion (**Figure 3-1B**), respectively, was assessed. Two pairs that had the highest deletion efficacy were chosen and in combination, microinjected into hDMD zygotes to make an out-of-frame *DMD* mutation (**Figure 3-2A**). 15 pups were screened and one female heterozygous pup and one male compound heterozygous pup were obtained (data not shown), hereafter referred to as hDMD del45 mice. Upon crossing, both founder mice were shown to have germline transmission of the exon 45 deletion (**Figure 3-2B**), which was confirmed by sequencing of the intron 44/45 rejoining site (**Figure 3-2C**).

hDMD del45 mice were crossed to mdxD2 and then mdx mice to generate fully dystrophic models. As a control, wild type hDMD mice were also crossed to mdx and mdxD2 mice, so these mice expressed human dystrophin but lacked the murine equivalent. The resulting hDMD del45 mdxD2 mice and hDMD del45 mdx mice (from the first or second cross) lacked human dystrophin by Western blot (**Figures 3-2D, 3-3A** and **3-4A**) and immunostaining (**Figures 3-2E, 3-3B** and **3-4B**). Occasionally, a few revertant dystrophin+ fibers were seen (see asterisks in **Figure 3-2E** or heart in **Figures 3-3B** and **3-4B**) but these events were infrequent. The muscle pathology of hDMD del45 mdxD2 mice was dystrophic, with features of fibrosis, inflammation, and calcium deposits, compared to the hDMD mdxD2 mice which express the wild type *DMD* gene that rescues the dystrophic phenotype (**Figures 3-2F** and **3-3C**).

To demonstrate the *in vivo* utility of this mouse, we applied our therapeutic CRISPR/Cas9 gene editing platform that targets human *DMD* exons 45-55 for deletion. Treatment with the CRISPR/Cas9 platform will restore the reading frame for out-of-frame mutations in this region, such as an exon 45 deletion (**Figure 3-5A**). We electroporated a plasmid containing one gRNA targeted to intron 44 and one to intron 55[57] in tandem with Cas9 into the FDB muscle of 12 week old hDMD del45 mdx mice and 18.5 week old hDMD del45 mdxD2 mice. After 22-33 days, an exon 45-55 deletion in the FDB, IO, and/or lumbricalis (Lum) muscles was observed by genomic DNA PCR (**Figure 3-5B**) and sequencing of the intron 44/55 rejoining site (**Figure 3-5C**) in the electroporated mice. Dystrophin restoration was observed by immunostaining in the IO and FDB of the electroporated hDMD del45 mdxD2 mice (**Figure 3-5D**). Thus, our novel humanized dystrophic hDMD del45 mouse model demonstrates proof-of-principle that a human targeted CRISPR/Cas9 platform is functional *in vivo*. This mouse model will be a useful resource for testing different CRISPR/Cas9 strategies and other therapies that target the human *DMD* gene.

Discussion

Here we describe a novel humanized mouse model of Duchenne muscular dystrophy. We have created an out-of-frame human *DMD* exon 45 deletion in the hDMD mouse (referred to as hDMD del45) and have crossed it to mdx and mdxD2 backgrounds so that the mice completely lack dystrophin. We have validated that this model lacks human dystrophin and presents with a dystrophic muscle pathology in multiple muscles across the body. Lastly, we have shown one utility of this mouse by applying our CRISPR/Cas9 platform which targets human *DMD* exons 45-55 for deletion. After delivering the CRISPR/Cas9 platform via electroporation *in vivo* we

have demonstrated a restored *DMD* reading frame and dystrophin expression in the hDMD del45 mdx and mdxD2 mouse.

This mouse has a wide range of uses. The model will be useful for testing a variety of antisense oligonucleotides against a mutated human sequence *in vivo* since the reading frame can be restored using an exon 44 or 46 single skip, a 46/47 double skip, or a 43/44/46 or 46/47/48 triple skip. For CRISPR/Cas9-based therapies, the model can be used for testing various human targeted gRNAs around this region. Additionally, the hDMD del45 model is a relevant negative control for western blotting of human dystrophin protein from the hDMD wild type mouse. Lastly, it presents a unique model in which to study endogenous skipping of the human *DMD* gene, which is a phenomenon known to occur at a low level in human patients with an exon 45 deletion[136]. The ability to study the human protein and/or test potential therapeutics in a dystrophic context *in vivo* on the human *DMD* gene rather than just in human cells offers obvious advantages and will allow for faster translation of human specific therapies.

Acknowledgements

We would like to thank Diana Becerra, Joana Capote, Natalia Ermolova, Brandon Lippold, Chino Kumagai-Cresse, and Jane Wen for technical assistance. We are grateful for the technical support, products, and/or services provided to our research by the Mouse Biology Program at the University of California Davis and the Center for DMD at UCLA Muscle Phenotyping and Imaging Core. This material is based upon work supported by the National Science Foundation Graduate Research Fellowship Program under Grant No. DGE-1144087 (CSY). Additional funding was provided by a pilot and feasibility seed grant from the Center for DMD at UCLA (NIH NIAMS 5P30AR05723UCLA and CTSI Grant #UL1TR000124), the Eli & Edythe Broad Center of Regenerative Medicine and Stem Cell Research at UCLA, the California Institute of Regenerative Medicine, Wellstone Cooperative Muscular Dystrophy Center (U54AR052646-Sweeney-PI, Spencer-Co-I) and NIAMS of the NIH (R01AR064327-ADP).

Author contributions

Author contributions were: Conceptualization, Methodology, Writing- Review and Editing, Visualization, Project Administration - CSY, ADP, MJS; Writing-Original Draft- CSY, Validation, Formal Analysis- CSY, EM; Investigation- CSY, EM, MQ; Resources- ADP, MJS; Supervision- MJS; Funding Acquisition- ADP, MJS.

Figures

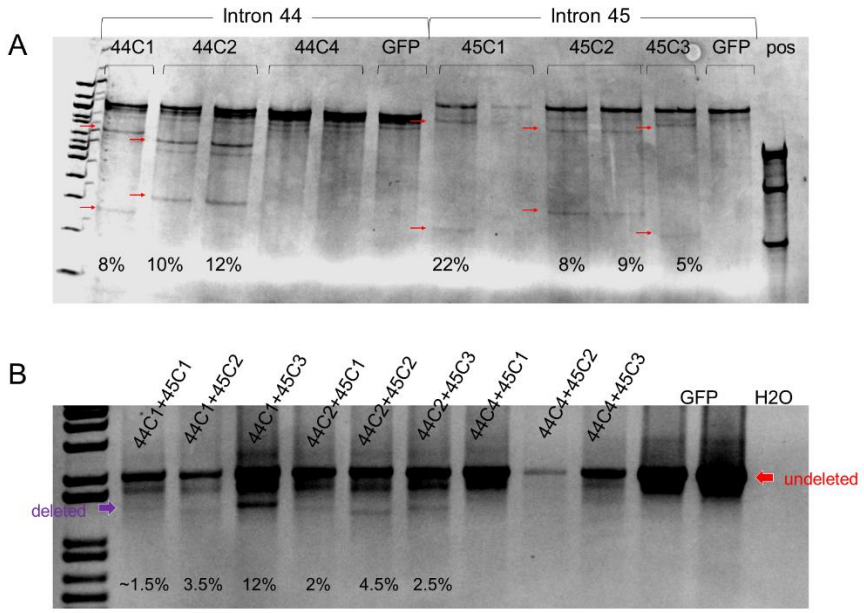

Figure 3-1: Testing of gRNAs for exon 45 deletion.
A) Surveyor assay of individual gRNA screening in HEK293FT cells. Three gRNAs for each intron 44 and intron 45 were designed and their cutting ability assessed in 293FT cells. Expected Surveyor assay cleavage products are shown with the red arrows (sizes in **Table 3-1**) and the estimated percent cutting is shown below. GFP plasmid was used as a negative control. A 100bp ladder was used.
B) Genomic DNA PCR for the exon 45 deletion after paired gRNAs were transfected in HEK293FT cells. The red arrow shows the 2037bp undeleted band and the purple arrow shows the 1329-1521bp deleted band. The estimated percent deletion is shown below. A 1kb ladder was used.

Table 3-1: Expected cleavage product sizes from Surveyor assay.

gRNA	Expected sizes (bp)
44C1	257, 700
44C2	309, 648
44C4	190, 767
45C1	257, 750
45C2	326, 681
45C3	253, 754

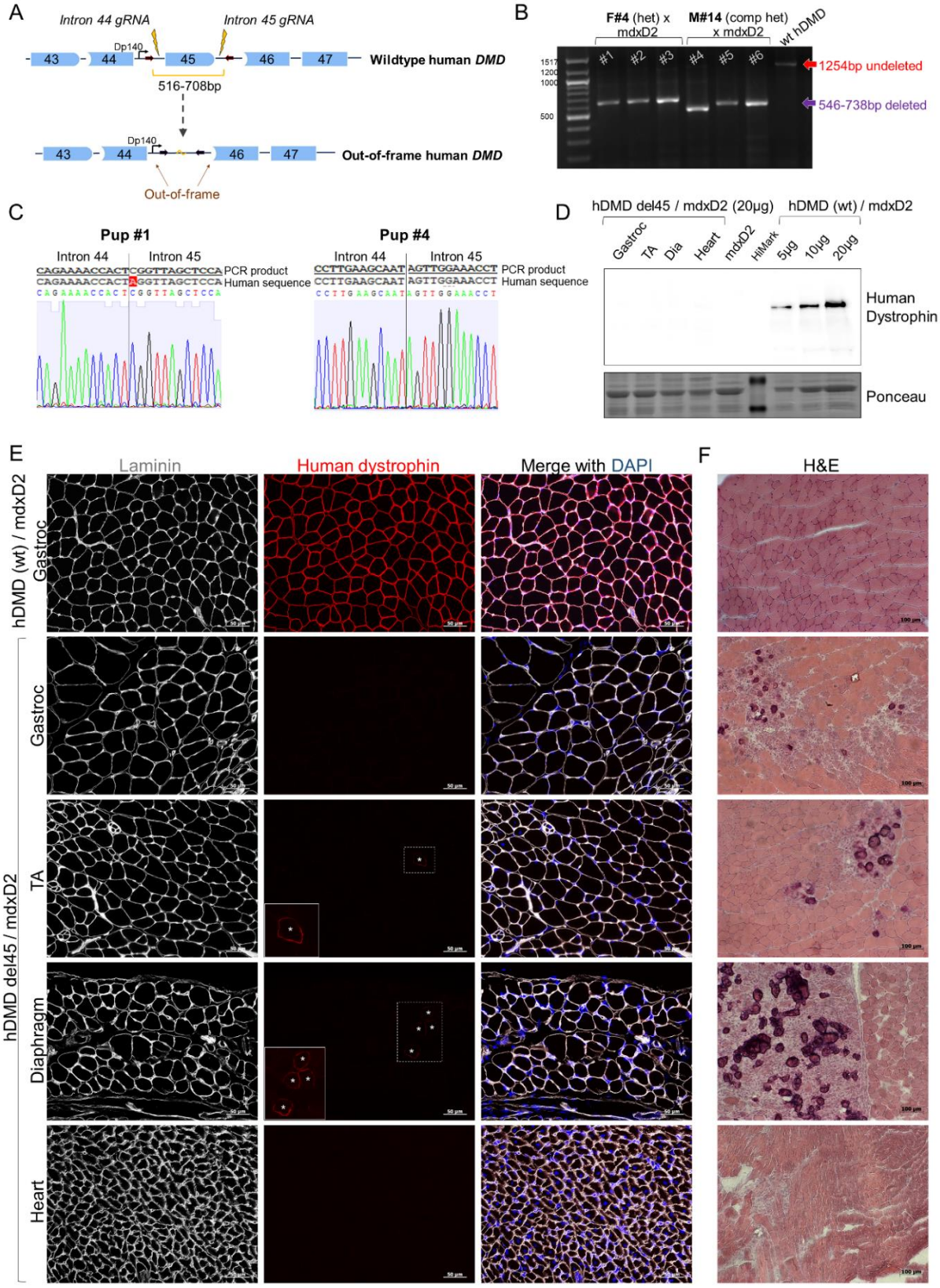
A
Intron 44 gRNA
Intron 45 gRNA
Dp140
43
44
45
46
47
Wildtype human DMD
516-708bp
Out-of-frame human DMD
Out-of-frame
B
F#4 (het) x mdxD2
M#14 (comp het) x mdxD2
wt hDMD
#1
#2
#3
#4
#5
#6
1517
1200
1000
500
1254bp undeleted
546-738bp deleted
C
Pup #1
Pup #4
Intron 44
Intron 45
PCR product
Human sequence
D
hDMD del45 / mdxD2 (20µg)
hDMD (wt) / mdxD2
Gastroc
TA
Dia
Heart
mdxD2
HiMark
5µg
10µg
20µg
Human Dystrophin
Ponceau
E
Laminin
Human dystrophin
Merge with DAPI
hDMD (wt) / mdxD2
hDMD del45 / mdxD2
Gastroc
TA
Diaphragm
Heart
F
H&E

Figure 3-2: Generation and characterization of hDMD del45 mice.
A) Cartoon showing the region of the human *DMD* gene targeted for mutation in hDMD mice. Guide RNAs (represented as lightning bolts) flank exon 45 to cause an exon 45 deletion by NHEJ, which puts the gene out-of-frame. The Dp140 isoform promoter is shown (arrow).
B) Genotyping PCR of genomic DNA from pups (labeled #1-6) from the founder mice F#4 and M#14 crossed to mdxD2 mice showing germline transmission of the deletion. The red arrow highlights the undeleted band seen in wild type (wt) hDMD mice and the purple arrow depicts the exon 45 deletion seen in the pups. Primers are depicted as arrows in A. Since two pairs of gRNAs were injected together, different deletion sizes occurred due to the various target sites.
C) Sequencing of the introns 44 and 45 rejoining site in two pups shows an exon 45 deletion.
D) Western blot of whole muscle extracts probed with human dystrophin. Ponceau stain is shown to demonstrate loading. The gastrocnemius (gastroc), tibialis anterior (TA), diaphragm (dia), and heart from an hDMD del45 / mdxD2 mouse (second backcross, 6wks old) show lack of dystrophin compared to an hDMD (wt) / mdxD2 mouse (third backcross, 6.5wks old) gastroc muscle.
E) Immunohistochemistry of muscle sections stained with anti-laminin (white) and human dystrophin (red). Laminin was used to delineate muscle fibers. hDMD del45 / mdxD2 muscles (second backcross, 6wks old) show a lack of dystrophin staining with a few faint revertant fibers (* and inset at higher contrast). Scale bar 50µm.
F) Hematoxylin and eosin (H&E) staining of muscle sections show dystrophic pathology in muscles of hDMD del45 / mdxD2 mice (second backcross, 6wks old). Scale bar 100µm. Similar analyses from another hDMD del45 / mdxD2 mouse is shown in Figure 3-3 (representative of n=4 mice analyzed).

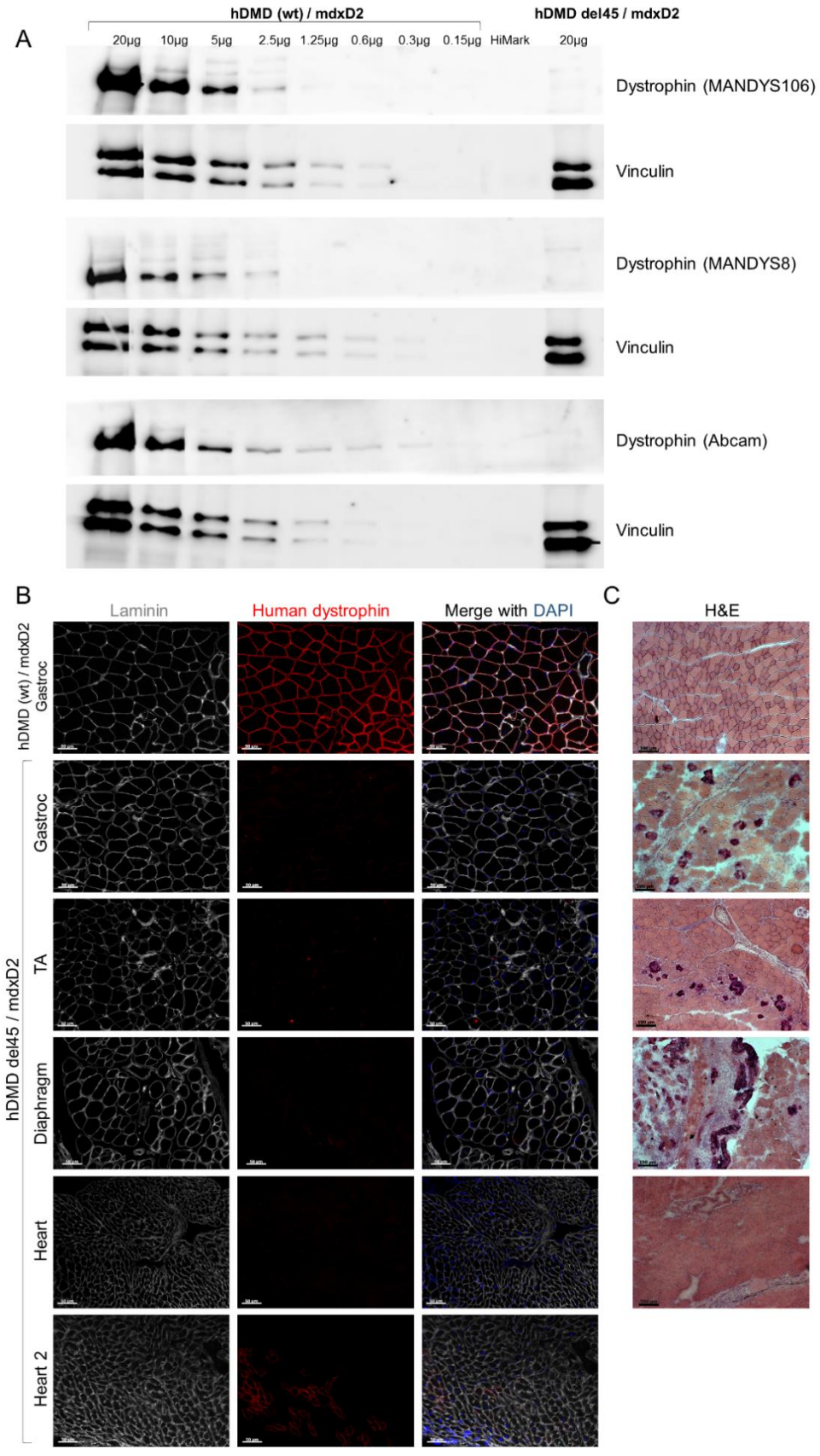
A
hDMD (wt) / mdxD2
hDMD del45 / mdxD2
20µg
10µg
5µg
2.5µg
1.25µg
0.6µg
0.3µg
0.15µg
HiMark
20µg
Dystrophin (MANDYS106)
Vinculin
Dystrophin (MANDYS8)
Vinculin
Dystrophin (Abcam)
Vinculin
B
Laminin
Human dystrophin
Merge with DAPI
hDMD (wt) / mdxD2
Gastroc
hDMD del45 / mdxD2
Gastroc
TA
Diaphragm
Heart
Heart 2
C
H&E

Figure 3-3: Characterization of hDMD del45 mdxD2 mice.
A) Western blotting titration of dystrophin from the gastrocnemius muscle of an hDMD (wt) / mdxD2 mouse (third backcross, 6.5wks old) and lack of dystrophin in the gastrocnemius muscle of an hDMD del45 / mdxD2 mouse (first cross, 4.5wks old). Three different dystrophin antibodies were used. Vinculin is shown as a loading control.
B) Immunohistochemistry of muscle sections stained with laminin (white) and human dystrophin (red). Laminin was used to delineate muscle fibers. hDMD del45 / mdxD2 muscles (first cross, 4.5wks old) show a lack of dystrophin staining. A few revertant fibers were seen in a second area of the heart. Scale bar 50µm.
C) Hematoxylin and eosin staining of muscle sections show dystrophic pathology in muscles of hDMD del45 / mdxD2 mice (first cross, 4.5wks old). Scale bar 100µm.

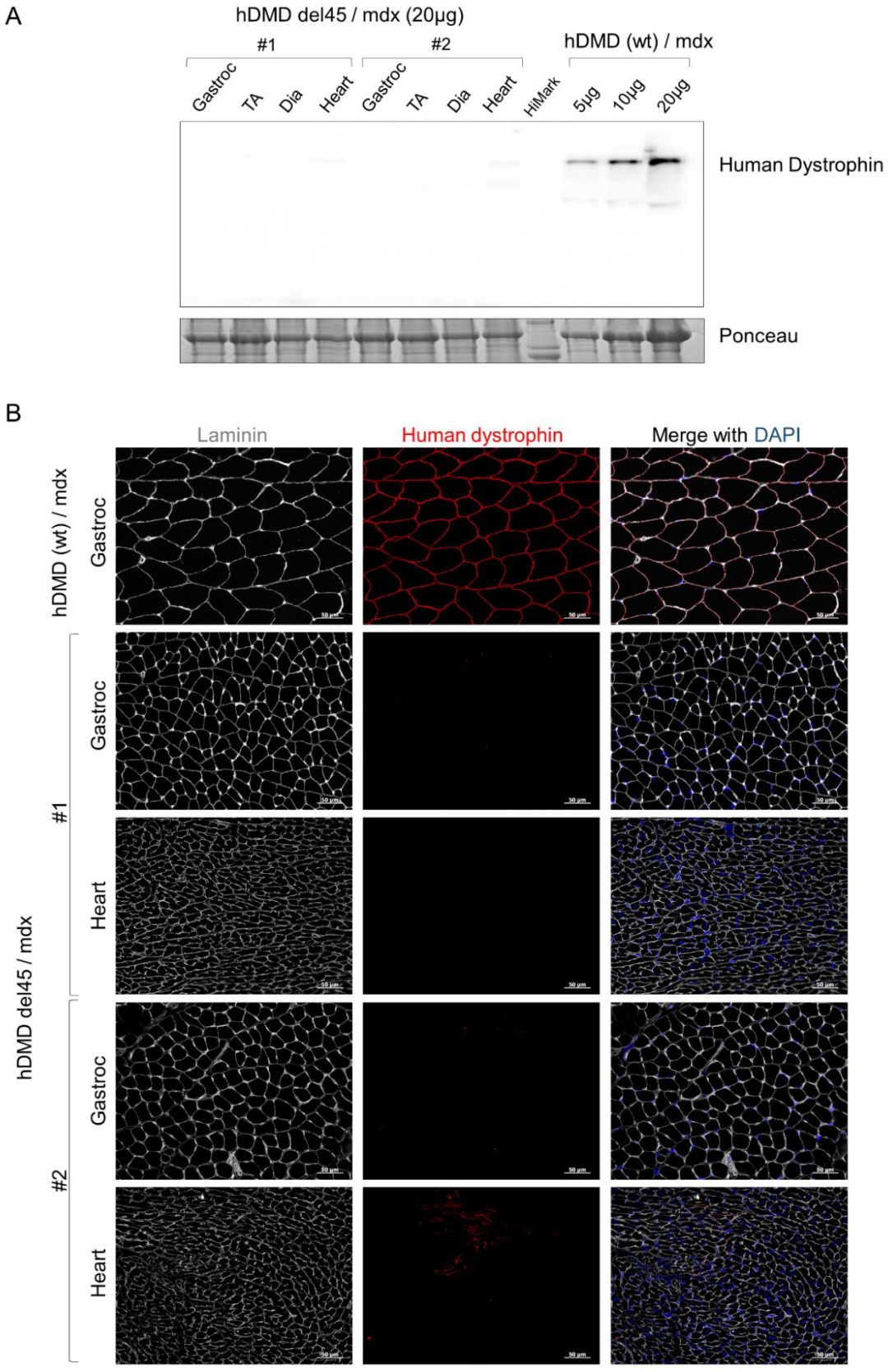
A
hDMD del45 / mdx (20µg)
#1
#2
hDMD (wt) / mdx
Gastroc
TA
Dia
Heart
Gastroc
TA
Dia
Heart
HiMark
5µg
10µg
20µg
Human Dystrophin
Ponceau
B
Laminin
Human dystrophin
Merge with DAPI
hDMD (wt) / mdx
Gastroc
hDMD del45 / mdx
#1
Gastroc
Heart
#2
Gastroc
Heart

Figure 3-4: Characterization of hDMD del45 mdx mice.
A) Western blot of whole muscle extracts probed with human dystrophin. Ponceau stain is shown to demonstrate loading. The gastrocnemius (gastroc), tibialis anterior (TA), diaphragm (dia), and heart from two hDMD del45 / mdx mice (#1 and #2, first cross, 2.5wks old) show lack of dystrophin compared to an hDMD (wt) / mdx mouse (third backcross, 8.5wks old) gastroc muscle.
B) Immunohistochemistry of muscle sections stained with anti-laminin (white) and human dystrophin (red). Laminin was used to delineate muscle fibers. hDMD del45 / mdx muscles from two mice (first cross, 2.5wks old) show a lack of dystrophin staining with a few revertant fibers seen in the heart of mouse #2. Scale bar 50μm.

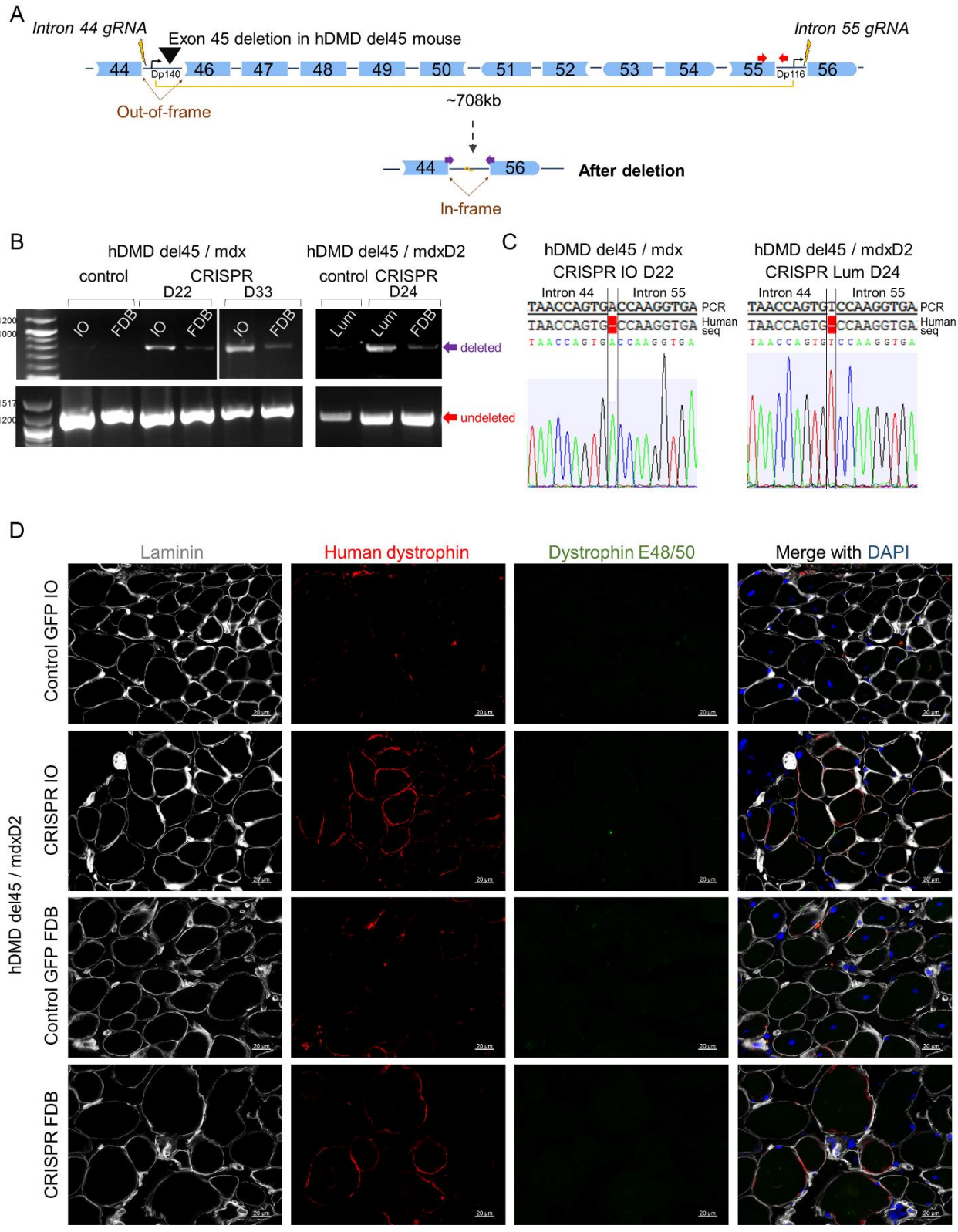
A
Intron 44 gRNA
Exon 45 deletion in hDMD del45 mouse
Intron 55 gRNA
44
Dp140
46
47
48
49
50
51
52
53
54
55
Dp116
56
Out-of-frame
~708kb
44
56
After deletion
In-frame
B
hDMD del45 / mdx
hDMD del45 / mdxD2
control
CRISPR
D22
D33
control
CRISPR
D24
IO
FDB
IO
FDB
IO
FDB
Lum
Lum
FDB
1200
1000
1517
1200
deleted
undeleted
C
hDMD del45 / mdx
CRISPR IO D22
hDMD del45 / mdxD2
CRISPR Lum D24
Intron 44
Intron 55
TAACCAGTGACCAAGGTGA
PCR
TAACCAGTGCCAAGGTGA
Human seq
D
Laminin
Human dystrophin
Dystrophin E48/50
Merge with DAPI
Control GFP IO
CRISPR IO
Control GFP FDB
CRISPR FDB
hDMD del45 / mdxD2

Figure 3-5: CRISPR/Cas9 deletion of *DMD* exons 45-55 to restore the reading frame in hDMD del45 mdx mice.
A) Cartoon showing our therapeutically relevant CRISPR/Cas9 platform that was electroporated into the FDB of hDMD del45 mdx and hDMD del45 mdxD2 mice. This platform consists of guide RNAs (represented as lightning bolts) in introns 44 and 55 that cause deletion of exons 45-55 through NHEJ to restore the reading frame for the out-of-frame exon 45 deletion in hDMD del45 mice. The Dp140 and Dp116 isoform promoters are shown (arrows).
B) Genomic DNA PCR using primers for the undeleted allele (red, 1201bp, bottom) or the deletion (purple, 788bp, top). An exon 45-55 deletion was observed in the FDB, IO and/or Lum muscles 22, 24, and 33 days (D22, D24, and D33) after *in vivo* electroporation of the CRISPR/Cas9 platform compared to the control mice.
C) Sequencing of the intron 44/55 rejoining site from the IO and Lum muscles of the CRISPR electroporated mice, which showed 1bp insertions.
D) Immunohistochemistry of hDMD del45 / mdxD2 IO and FDB muscles stained with anti-laminin (grey), human dystrophin (red), and dystrophin targeting exons 48/50 (E48/50, green). Laminin was used to delineate muscle fibers. Dystrophin E48/50 was used to exclude revertant fibers from the analysis, since after CRISPR/Cas9 application exons 45-55 will be deleted. Dystrophin positive fibers can be seen in the CRISPR electroporated sample compared to the GFP electroporated control. Scale bar 20µm.

Chapter 4 - Delivery of CRISPR/Cas9 via Viral and Non-Viral Methods to Reframe the *DMD* Gene in a Humanized Mouse Model of Duchenne Muscular Dystrophy

Abstract

Duchenne muscular dystrophy (DMD) is a progressive muscle wasting disorder caused by out-of-frame mutations in *DMD,* which prevent dystrophin production. Some therapeutic strategies are designed to reframe the *DMD* gene, thereby turning Duchenne into the clinically milder allelic disease, Becker muscular dystrophy. We have developed a CRISPR/Cas9 platform to reframe *DMD* using a single pair of guide RNAs to delete exons 45-55, which is associated with one of the mildest Becker phenotypes. This region also encompasses a hotspot of ~50% of all DMD patient mutations. Here we apply this platform *in vivo* to our novel humanized dystrophic mouse model, which contains an out-of-frame mutation in a transgenic human *DMD* gene. Through this work, we have systematically developed the first polyrotaxane (PRX) nanoparticle platform for delivery of a CRISPR/Cas9 plasmid to muscle *in vitro* and *in vivo.* We then compared the ability of PRXs or adeno-associated virus (AAV) 6 to deliver our CRISPR/Cas9 platform to muscle *in vivo*. Both AAV and PRXs restored dystrophin protein in muscle after local and systemic injections. Higher efficiency of dystrophin generation was observed following AAV-mediated delivery. Future studies will focus on increasing PRX efficiency and improving their delivery and trafficking in muscle *in vivo.* This work demonstrates the potential for systemic delivery of a single CRISPR/Cas9 platform to restore dystrophin for a large percentage of DMD patients.

Introduction

Duchenne muscular dystrophy (DMD) is a severe muscle wasting disease caused by out-of-frame mutations in the *DMD* gene resulting in a lack of dystrophin protein. One therapeutic strategy is to restore the reading frame and turn a Duchenne mutation into a Becker muscular dystrophy (BMD) mutation. BMD is a milder form of the disease in which patients have in-frame mutations in *DMD*. We have developed a clustered regularly interspaced short palindromic repeats (CRISPR)/ CRISPR associated protein (Cas) 9 platform to permanently restore the reading frame by deleting *DMD* exons 45-55, which results in an internally deleted but in-frame dystrophin protein[57,137]. In Becker patients, an exon 45-55 deletion is associated with one of the mildest clinical phenotypes, where some patients are still asymptomatic into their 60s[22–26]. This region also encompasses a hotspot of DMD patient mutations[24,26]. We have previously demonstrated that our platform can restore dystrophin protein *in vitro*[57] and after local delivery to skeletal muscle using a humanized mouse model *in vivo*[137].

The CRISPR/Cas9 system for use in gene editing utilizes a guide RNA (gRNA) which targets the Cas9 endonuclease to a specific site in the genome and results in a double stranded DNA break (DSB). This DSB can be repaired through the DNA's endogenous repair machinery, non-homologous end joining (NHEJ), or through homology directed repair (HDR) using template DNA in cycling cells.

Effective systemic delivery of gene therapies, including CRISPR/Cas9, presents a significant challenge for muscle diseases. Some adeno-associated virus (AAV) serotypes have high tropism for muscle and AAV-micro-dystrophin trials have been initiated for DMD[33]. AAV has also previously been utilized for delivery of CRISPR/Cas9 in DMD mouse models. These studies have demonstrated the ability of AAV-CRISPR to restore mouse dystrophin protein after

local and systemic injection *in vivo*. Two forms of Cas (from either *Streptococcus pyogenes* (Sp) or *Staphylococcus aureus* (Sa) bacteria) have been used to edit the *Dmd* gene and some functional benefits were observed[60–63]. However, current AAVs may not be ideal for delivery of CRISPR/Cas9 to muscle. Since AAV results in an immune response to the capsid[138], it means that AAV can likely only be delivered one time without additional procedures. Since most gene editing strategies are relatively inefficient, the limitation of a single administration will likely not be clinically realistic. Furthermore, use of AAV as a delivery method could result in an enhanced immune response to the bacterial protein, Cas9. Previous work has demonstrated that both a cellular and a humoral immune response is induced against Cas9 following AAV-mediated delivery of CRISPR/Cas9 in muscle[74]. Because AAV is expected to stay episomal for many years in post-mitotic skeletal muscle cells, Cas9 will likely persist for an extended period of time, which could also enhance the immune response and/or potential for off-target effects. Lastly, currently available AAV serotypes do not efficiently target muscle stem cells[72,139], which would be required for a self-sustaining long-term therapy for DMD.

A component of this work is to develop non-viral means to deliver CRISPR *in vivo*. This effort has been primarily focused on developing nanoparticle carriers, which offer advantages over viral delivery. Nanoparticles can be easily modified, repeatedly administered, and can be biodegradable. There are currently over 75 clinical trials using nanoparticles composed of a variety of materials. Different formulations of nanoparticles carrying CRISPR have been utilized *in vitro* and in mice *in vivo*. These nanoparticles have been formed from lipids, DNA (called nanoclews), gold, or cationic polymers[77–89]. One published study used gold nanoparticles to deliver CRISPR/Cas9 to mdx muscle after local intramuscular injection[88]. However, this study is not likely to be translatable to DMD patients as it did not utilize systemic delivery. In addition,

the authors used an HDR approach, which is known to have low efficiency in post-mitotic muscle[43,63] and is thus likely not clinically realistic.

Here, we describe our work to develop polyrotaxane (PRX) nanoparticles to deliver a large CRISPR/Cas9 plasmid to muscle. Some examples of utilization of PRX molecules are as hydrogels, for iron chelation, or to deliver β-cyclodexrin[140–142]. PRXs have also been complexed with plasmid DNA, siRNA, or BMP2 to form nanoparticles[143–146]. PRXs are often composed of cyclodextrin (CD) rings threaded on a polymer chain capped with bulky stoppers. In this investigation we utilize formulations containing a polyethylene glycol (PEG) chain with CD rings that contain positively charged R groups which complex with negatively charged nucleic acids through an electrostatic interaction, thereby self-assembling into a nanoparticle.

To effectively use PRXs to deliver a CRISPR/Cas9 plasmid to muscle, multiple obstacles need to be overcome. First, the nanoparticles must home to muscle, exit the vasculature, traverse the extracellular matrix and basal lamina, cross the plasma membrane and release the cargo. Then the plasmid must escape the lysosome and traffic to the nucleus, Cas9 and the gRNAs be transcribed, Cas9 translated, assemble as a ribonucleoprotein (RNP) complex and enter the nucleus to cut the gene. Because of these many steps, we have systematically optimized our nanoparticles to overcome specific challenges as needed.

In this study we develop the first PRX platform for muscle by iteratively improving generations of PRXs that can deliver plasmid DNA to primary muscle cells *in vitro* and to skeletal muscle *in vivo*. We demonstrate that we can engineer the particles to achieve improved plasmid release by utilizing disulfide linkers and enhanced systemic biodistribution by using PRXs with increased PEGylation. Finally, we show low levels of restored dystrophin protein in our novel humanized mouse model of DMD, the hDMD del45 mdx mouse[137], after administering

our CRISPR/Cas9 platform complexed with PRXs via local intramuscular and systemic injections. Since AAV-mediated CRISPR delivery is the current standard in the field, we also utilized AAV as a comparison and demonstrated restored dystrophin after local and systemic AAV-CRISPR delivery.

Materials and Methods

Mice

All animal work was conducted under protocols approved by the UCLA Animal Research Committee in the Office of Animal Research Oversight. hDMD (Tg(DMD)72Thoen/J, 018900), C57BL/10 mdx (001801), and mdxD2 (D1.B10-Dmdmdx/J, 013141) mice were obtained from Jackson Laboratories. hDMD del45 mdx and hDMD del45 mdxD2 mice were generated as described[137]. Genotyping was performed as described[137].

Cell culture

Primary hDMD or hDMD del45 mdx myoblasts were obtained from 11-13 day old pups by dissociation of muscle tissue using a 1:1 mixture of 1.5mg/mL dispase (neutral protease, Worthington) and 1600U/mL collagenase II (Worthington) in PBS at 200µl per 100mg tissue. Muscles were minced, then incubated at 37°C with slow agitation for 30mins. Fibroblasts were removed by repeatedly pre-plating. Myoblasts were cultured on entactin-collagenIV-laminin cell attachment matrix (ECL, EMD Millipore) and maintained in F-10 HAM (Sigma) with 20% fetal bovine serum (FBS, Thermo Fisher), 5ng/mL basic fibroblast growth factor (bFGF, Promega) and 1% penicillin/streptomycin (P/S, Thermo Fisher). Myoblasts were differentiated to form myotubes (at >80% confluence) in DMEM (Thermo Fisher) with 2% horse serum (Thermo

Fisher), 1% insulin-transferrin-selenium (ITS, Thermo Fisher) and 1% P/S on Matrigel® basement membrane matrix (Corning).

CRISPR plasmid

gRNAs for the exon 45-55 deletion (44C4, 55C3) from [57] were cloned into px333 (Addgene 64073, Andrea Ventura [133]) in tandem using BbsI (New England BioLabs) and BsaI (New England BioLabs). Hereafter, px333 44C4+55C3 refers to the CRISPR plasmid encoding Cas9 and the two guide RNAs.

PRX synthesis

For G1 PRX, the following steps were completed. (i) PEG-diamine powder (Polysciences) was added to α-CDs to form a polyseudorotaxane inclusion complex. (ii) The polyseudorotaxane ends were blocked with a large blocking group, benzyloxycarbonyl tyrosine, by mixing the inclusion complex with Z-L-Tyr, BOP reagent, HOBt and DIEA in DMF. (iii) The α-CDs in the polyrotaxane were modified with positively charged amine groups by reaction with N,N-dimethylethylenediamine (DMAE).

For G2 PRX: (i) PEG di(OPSS) powder was mixed with 2-aminoethanethiol to generate a diamino-PEG with disulfide linkages at both ends (SS-PEG-diamine). (ii) The SS-PEG-diamine was added to α-CDs to form a SS-polyseudorotaxane inclusion complex. (iii) The polyseudorotaxane ends were blocked with a large blocking group, benzyloxycarbonyl tyrosine, as above. (iv) The α-CDs in the SS-polyrotaxane were modified with positively charged amine groups by reaction with DMAE.

For G3 PRX: (i) Two arms of a 4-arm-PEG amine polymer (10 kDa, Jenkem) were selectively blocked by a bulky group, NHS-Fluorescein (Thermo). (ii) The 4-arm-PEG was added to α-CDs to form a 2/4-arm-polyseudorotaxane inclusion complex. (iii) The polyseudorotaxane ends were blocked with a large blocking group, benzyloxycarbonyl tyrosine, as above. (iv) The α-CDs in the 2/4-arm-polyrotaxane were modified with positively charged amine groups by reaction with DMAE.

For G4 PRX: (i) Two arms of a 4-arm-PEG amine polymer were selectively blocked as above. (ii) The 4-arm-PEG was added to α-CDs to form a 2/4-arm-polyseudorotaxane inclusion complex. (iii) The polyseudorotaxane ends were blocked with a large blocking group, benzyloxycarbonyl tyrosine, as above. (iv) The α-CDs in the 2/4-arm-polyrotaxane were modified with pyridyldithiol groups by adding pyridyldithiol-cysteamine. (v) The α-CDs with cleavable positively charged amine groups were generated by reaction with DMAE.

For peptide conjugation to G3: Thiol groups from cysteine were introduced on the C-terminus of the peptides to facilitate the conjugation with 4-arm PEG molecules in G3 polyrotaxane (with end groups blocked with 4-succinimidyloxycarbonyl-alpha-methyl-α(2-pyridyldithio)toluene (SMPT) instead) via thiol-exchange chemistry. An oligo glycine spacer was included at both ends of the functional sequence so that conjugation wouldn't interfere with the binding efficiency. Sequences are as follows: NCAM ASKKPKRNIKAGGC[147], PipB RXRRBRRXRRBRXBGGC[148].

PRX delivery in vitro

Myoblasts were seeded at $1.2x10^5$ cells/cm^2 for growth conditions or $1.7x10^5$ cells/cm^2 for differentiation where the media was changed to differentiation media the following day. PRX

complexed with a pmax GFP reporter plasmid (Lonza), a pCSCMV:TdTomato reporter plasmid (Addgene 30530, Gerhart Ryffel, [149]), or px333 44C4+55C3 CRISPR plasmid (see above) was added to the cells at various PRX to plasmid ratios determined empirically and as follows: G1 PRX to plasmid: 10:1; G2 PRX to plasmid: 5:1; G3 and G4 PRX to plasmid: 3:1; peptide conjugated G3 PRX to plasmid: 5:1. For uptake studies, the particles were conjugated with FITC and the plasmid labeled with Cy3 using LabelIT® Tracker kit (Mirus Bio). Imaging for reporter expression was done at timepoints between 24hrs – 14 days using either a Leica TCS SP8 SMD or Axio Observer Z1 microscope (Zeiss). For CRISPR delivery, cells were harvested at day 7 or 14 and pelleted for genomic DNA extraction using the Quick gDNA mini prep kit (Zymo Research) and analyzed with the deletion PCR described below.

CRISPR exon 45-55 deletion PCR

To assay for the exon 45-55 deletion, individual PCR reactions containing primers flanking the deletion (purple arrows in Figure 4-1A) were performed on genomic DNA using AccuPrime Taq High Fidelity (Thermo Fisher) or Herculase II Fusion Polymerase (Agilent Genomics) as described[57]. PCR products were run on a 2% agarose gel and visualized with ethidium bromide staining.

NCAM peptide administration in vitro

A green fluorophore (5-FAM on N-terminus) labeled NCAM peptide (sequence ASKKPKRNIKAGGC[147]) was synthesized by Biomatik. 25µM peptide was incubated for 6hrs on C2C12 and B16 cells before imaging.

PRX delivery in vivo

For systemic biodistribution studies, 100µg px333 44C4+55C3 plasmid labeled with Cy3 LabelIT Tracker and complexed with PRX was injected into the tail vein of 8.5wk old mdx mice, which were sacrificed 24hrs later. Harvested muscles and organs were imaged with IVIS imaging for Cy3 signal. Muscles and organs were then flash frozen in isopentane.

For the circulation study, 300µg particles (100µg Cy3-labeled plasmid) were injected into the tail vein of C57/Bl6 mice and blood was harvested 5min, 1hr, 2hr, 4hr, 8hr and 24hr post-injection. The serum was separated and the fluorescence intensity of Cy3 was determined on a microplate reader (M5e, Molecular Device). The same injection dose diluted in the serum from untreated mice was also tested as total injection dose (ID), to which the fluorescence intensity of treated samples was normalized to give the percentage of ID.

Intramuscular injections of PRX were done into the tibialis anterior (TA) muscle using 2µg plasmid (either px333 44C4+55C3 or TdTomato reporter) complexed with PRX (at ratios given above) into hDMD del45 mdx mice (3rd backcross) at 5.5wks of age. HBSS was injected into the control mouse. Muscles were harvested and flash frozen in isopentane after 4wks.

For short term systemic efficacy studies, 50 or 100µg px333 44C4+55C3 plasmid complexed with PRX was injected into the tail vein of hDMD del45 mdxD2 mice (2nd backcross) at 11wks of age. Mice were dosed 4 times over 2.5wks. Muscles were harvested and flash frozen in isopentane after ~5wks (34 days).

Local PRX injections into the footpad were done as described for *in vivo* electroporation[134]. 1µg Cy3 labeled px333 44C4+55C3 plasmid complexed with PRX was injected subcutaneously into the footpad of mdx mice. The flexor digitorum brevis and

interosseous muscles were harvested and flash frozen at various timepoints between 24hrs-1wk post-injection.

AAV cloning and vector production

The original AAV-CRISPR plasmids were generated as described[63]. gRNAs 44C4 and 55C3 were cloned into the pAAV targeting plasmid in tandem from px333 into the original first targeting cassette and the original second targeting cassette was removed. pAAV plasmids were co-transfected with the pDG6 packaging plasmid in HEK293 cells to generate virus as described[63].

AAV delivery in vivo

Intramuscular delivery of $5x10^{10}$ v.g. of each vector was injected into the tibialis anterior (TA) of hDMD del45 mdx mice (3rd backcross) at 5.5wks of age. One mouse was only injected with the gRNA/mCherry reporter vector to look for the virus transduction efficiency. HBSS was injected into the control mouse. Muscles were harvested 4wks post-injection.

For systemic delivery, $2.85x10^{12}$ v.g. of each vector was injected retro-orbitally (r.o.) into hDMD del45 mdx mice (4th backcross) at p20. The control mouse was injected with PBS. Muscles were harvested ~5wks (33 days) later and half taken for mCherry and half for dystrophin analysis.

For analysis of mCherry expression, muscles were harvested, fixed in 1% PFA overnight, changed to 5% sucrose for at least 6hrs, then switched to 30% sucrose overnight before being flash frozen. For dystrophin staining, muscles were harvested and directly flash frozen in isopentane.

Immunostaining muscle sections

10µm cryosections were obtained from flash frozen or PFA fixed muscles and sampled at intervals that extended throughout the majority of the muscle body. For dystrophin staining, sections were fixed in cold acetone for 1-2mins, then TrueBlack (Biotium, 20-fold diluted in 70% ethanol) was added for 30s-1min, then blocking buffer (PBS with 5% horse serum and 10% goat serum) was added for at least 1hr, followed by the M.O.M. kit (Vector Labs) according to the manufacturer's protocol. Dystrophin (Abcam, ab15277, 1:200), MANEX48/50B (MDA Monoclonal Antibody Resource, [113], 1:10) and laminin (rat, R&D Systems, 1:25) primary antibodies were added overnight in TBS and 1% goat serum. Secondary AlexaFluor antibodies (Thermo Fisher) were added at 1:250 for 1.5hrs the following day.

For biodistribution and mCherry/TdTomato staining, TrueBlack was used in some cases. Blocking buffer of 0.25% gelatin, 0.1% tween and 3% BSA was applied for at least 1hr. Anti-laminin (rabbit, Sigma, 1:200) primary antibody was added overnight with the corresponding secondary antibody at 1:250 the following day. Slides were mounted with VECTASHIELD containing DAPI (Vector Laboratories). Control and treated slides were imaged at the same exposure using an Axio Observer Z1 microscope (Zeiss) and the contrast adjusted the same. The percent of mCherry or dystrophin positive cells were counted in ImageJ[111] and normalized by the total number of cells counted (revealed by laminin immunostaining).

Western blot analysis

Total protein was isolated from flash-frozen mouse muscles. Tissues were homogenized in 20x volume/g of lysis buffer: 50mM tris-HCl (pH 7.4), 7M urea, 2M thiourea, 4% CHAPS, 2% SDS, 50mM β-mercaptoethanol. Homogenized samples were incubated at 4°C for 45-60min

with gentle rotation. Then lysates were mixed with 6xRSB and passed several times through a syringe needle to shear the DNA and reduce viscosity. Afterwards samples were centrifuged for 5min at 5,000*g*. Clarified lysates were transferred to new tubes, protein concentration was measured, and samples were used as below.

To evaluate dystrophin content, cell lysates were subjected to 6% polyacrylamide gel electrophoresis (PAGE) for 3hrs at constant current (10mA per gel); followed by transfer to nitrocellulose membrane at constant voltage (100V) for 2.5hrs on ice. 0.05% sodium dodecyl sulfate (SDS) and 10mM dithiothreitol were added to the transfer buffer to facilitate blotting of high molecular proteins. Immunoblot assay was carried out with anti-dystrophin antibodies MANDYS106 (MDA Monoclonal Antibody Resource, [113], 1:120) or ab15277 (Abcam, 1:400), and α-actinin (Sigma, 1:1000), and stained with Ponceau S (Sigma). Secondary antibodies used were anti-mouse or anti-rabbit peroxidase conjugates from Sigma-Aldrich (1:10,000). Blots were developed using Radiance Plus HRP detection kit (Azure Biosystems). Signals were registered by the Azure c300 imaging system (Azure Biosystems).

For dystrophin quantification, serial dilutions of hDMD (wt)/mdxD2 TA lysates were run simultaneously with experimental samples. Optical density of each band in the dilution series was plotted against percentage to generate a standard curve. A linear fit to the data points was calculated and the corresponding % of hDMD (wt)/mdxD2 for the experimental samples was determined.

For Cas9 detection, 8% PAGE gels were run for 1.5hrs at 100V. Transfer was performed in Tris/Glycine with 20% MetOH for 1hr 15min at 100V. Immunoblotting was carried out as above with rabbit α-Cas9 ab204448 (Abcam, 1:2000), which was validated on cells transfected with a Cas9 plasmid.

Results

Design and synthesis of PRX nanoparticles and AAV

One goal of this work was to develop a non-viral nanoparticle carrier for delivery of our CRISPR/Cas9 platform, which permanently reframes the *DMD* gene by deleting exons 45-55 (**Figure 4-1A**). As this nanoparticle platform has been developed and tested, it has led to the systematic design and formulation of 4 generations of PRX nanoparticles (**Figure 4-1B**). Generations G1 and G2 are formed from a linear PRX with a single PEG chain and an average of 26-28 CD rings. The G3 and G4 PRXs are novel multi-arm formulations which have an additional PEG chain that lacks CD rings (containing an average of 26 CD rings per polymer), allowing for increased PEGylation and improved pharmacokinetics (PK) upon nanoparticle formulation. When PRX polymers are added to negatively charged nucleic acids they can self-assemble (**Figure 4-1C**). The G2 and G4 PRXs contain disulfide linkers which are expected to be cleaved in an intracellular reducing environment and lead to faster plasmid release. The G2 disulfide bond is between the PEG chain and the bulky end group and the G4 disulfide bond is between the R group and the CD ring. Both are expected to result in the positive charge diffusing away and the plasmid being released upon cleavage. We have also generated peptide-modified versions of the G3 particles, to aid with cell targeting and/or penetration.

In parallel, we synthesized AAV6 carrying our CRISPR platform in a dual-vector approach, with one vector containing SpCas9 driven by the muscle specific promoter CK8[150], and the other containing both gRNAs and an mCherry reporter (**Figure 4-1D**). Both delivery platforms, PRX-CRISPR and AAV-CRISPR, carry two gRNAs previously validated, one targeted to intron 44 (44C4) and one to intron 55 (55C3), and SpCas9, to cause an in-frame deletion of *DMD* exons 45-55[57,137].

All four PRX generations are taken up by and can deliver plasmids to hDMD and hDMD del45 primary murine muscle cells

Primary muscle cells obtained from hDMD and hDMD del45 mdx mice were exposed to labeled PRX nanoparticles *in vitro*. All particles demonstrated efficient uptake *in vitro* at multiple timepoints from 24hrs to 3 days post-administration (**Figures 4-2A** and **4-2D** and data not shown). However, analysis of G1 PRXs demonstrated high co-localization between the labeled particle and labeled plasmid cargo, even up to 1wk after administration, suggesting a failure to release the plasmid. PRX particles carrying a GFP reporter plasmid were then added to hDMD myotubes to assess their ability to deliver DNA. Only a few cells exposed to the G1 PRXs expressed GFP but addition of the disulfide redox sensitive bond in G2 PRX improved GFP expression at 1wk (**Figure 4-2B**). Delivery of the CRISPR/Cas9 plasmid *in vitro* demonstrated CRISPR-mediated deletion of exons 45-55 at 1wk using G2 PRX, whereas G1 PRX did not generate a deletion, even up to 2wks after administration (**Figure 4-2C**). Delivery of the G4 multi-arm PRX also led to more efficient CRISPR/Cas9-mediated deletion at 1wk compared to G3 (**Figure 4-2E**), likely due to an improved release mechanism, since less plasmid signal is seen co-localized with nanoparticle signal at 24hrs in G4 compared to G3 (**Figure 4-2D**).

Peptide conjugated PRXs show improved plasmid delivery to muscle cells in vitro

Two peptide conjugated versions of G3 PRX were tested *in vitro.* Since we ultimately want to target muscle stem cells, we used a neural cell adhesion molecule (NCAM) peptide, because NCAM is known to be expressed on both human muscle stem cells and activated mouse muscle stem cells[151–153]. Additionally, we used PipB, a cell penetrating peptide which was shown

to increase phosphorodiamidate morpholino oligonucleotide (PMO) uptake in muscle *in vivo*[148]. We validated that our NCAM peptide (taken from [147]) could bind to muscle cells *in vitro* by adding a FITC conjugated peptide to mouse C2C12 myotubes, which increase expression of NCAM right after fusion[154]. Peptide binding was shown by FITC signal on C2C12s but not on our negative control, B16 cancer cells (**Figure 4-3A**).

We then compared the ability of unmodified G3 and G4 PRXs with peptide-modified G3-PipB and G3-NCAM PRXs to deliver a TdTomato reporter plasmid in primary murine myoblasts. The peptide conjugation improved reporter expression by 67 or 71-fold at 48hrs for NCAM and PipB, respectively (**Figure 4-3B**). We also validated that these peptide-modified G3 particles could deliver TdTomato plasmid to primary myotubes (**Figure 4-3C**).

Systemic delivery of multi-arm PRX shows enhanced uptake in muscle

PRX nanoparticles were tested in dystrophic mice for systemic biodistribution to muscle. The linear G2 PRX was compared to the multi-arm G3 PRX after intravenous (i.v.) delivery in mdx mice. We observed enhanced passive muscle targeting of G3 PRX at 24hrs by *ex vivo* IVIS imaging (**Figure 4-4A**). We expect this improved muscle homing is due to the enhanced circulation half-life seen with the multi-arm compared to linear PRX in wild type mice (**Figure 4-4B** and Ji, Liu et al., in preparation). Thus, the multi-arm PRXs are more optimal for *in vivo* delivery.

Intramuscular delivery of AAV-CRISPR results in higher levels of restored dystrophin protein compared to PRX-CRISPR

We injected AAV and the two multi-arm PRX formulations into the TA muscle of hDMD del45 mdx mice *in vivo* and assessed their ability to deliver either reporter genes or our CRISPR/Cas9 platform 4 weeks later. Intramuscular (i.m.) injection of the AAV6 mCherry reporter vector in an hDMD del45 mdx mouse lead to ~50-60% transduction (quantified by percent mCherry positive cells); however, i.m. injection of G4-TdTomato reporter did not show any TdTomato positive fibers in the injected mouse (**Figure 4-5A**). AAV-CRISPR lead to ~25% dystrophin positive fibers by immunostaining, which do not express a dystrophin epitope internal to the CRISPR deletion, which was used to exclude revertant fibers. Both G3 and G4 PRX-CRISPR resulted in only a few (<1% fibers) expressing dystrophin (**Figure 4-5B**). The AAV-mediated dystrophin was also detectable by Western blotting (~11% of wild type) (**Figure 4-5C**), however we did not observe PRX-mediated dystrophin expression by Western blot (data not shown). Western blotting also demonstrated Cas9 expression in the AAV-CRISPR injected muscle (**Figure 4-5D**).

Systemic delivery in vivo of AAV-CRISPR results in higher levels of dystrophin compared to PRX-CRISPR

Systemic injection of AAV6-CRISPR in hDMD del45 mdx mice lead to mCherry expression and dystrophin restoration in many tissues including soleus (~34% mCherry positive fibers, ~23% dystrophin positive fibers), TA (~21% mCherry positive fibers, ~2% dystrophin positive fibers) and heart (~83% mCherry positive fibers, ~31% dystrophin positive fibers) 5 weeks post-injection (**Figure 4-6A** and **4-6B**). Dystrophin (~10% of wild type) and Cas9 in the

heart were detectable by Western blot (**Figure 4-6C** and **4-6D**). In contrast, i.v. injection of 4 doses of G3 PRX-CRISPR at either a low or high dose lead to few (<1%) dystrophin positive fibers in quadriceps (**Figure 4-6B**).

PRX nanoparticles do not efficiently enter muscle fibers in vivo

Due to the low efficiency of dystrophin restoration with our PRX nanoparticles, we assessed *in vivo* trafficking within muscle. Analysis of systemically or locally administered PRX particles in mdx mice showed PRX retention in the extracellular matrix (ECM) or basal lamina (**Figure 4-7**). After systemic injection, PRXs could be found both within blood vessels and within the muscle tissue, but often co-localized with laminin. After local delivery, most PRXs were observed in the interstitial space. In neither case did we see PRXs within muscle fibers, suggesting that the ECM and basal lamina present an *in vivo* trafficking barrier that will need to be overcome through nano-engineering.

Discussion

Here we describe the first development of a non-viral PRX carrier designed for delivery of a CRISPR/Cas9 plasmid to muscle. Stepwise optimization of PRX nanoparticles allowed us to create new generations of particles in which specific challenges were addressed. We show improved plasmid delivery *in vitro* using either redox sensitive linkers, to allow for faster cargo release, or NCAM or PipB peptides, to improve cellular penetration. We also demonstrate improved PRX homing to skeletal muscle after systemic injection using the novel multi-arm PRX. Direct delivery of our CRISPR/Cas9 platform *in vivo* through both viral (AAV6) and non-viral (PRX nanoparticles) strategies demonstrated restored dystrophin protein after local and

systemic injections. To date, AAV6 leads to higher levels of dystrophin protein, possibly due to the problem of PRX nanoparticles getting trapped in the ECM. This work offers the first demonstration of systemic nanoparticle-mediated delivery of CRISPR/Cas9 to skeletal muscle. Advancements on nanoparticle design will hopefully enable improved ECM trafficking and uptake in muscle fibers *in vivo.*

We have demonstrated that PRXs can passively home to dystrophic skeletal muscles; however, since they are not efficiently taken up by the muscle fibers, future studies will need to develop novel approaches to overcome the delivery barrier and improve the ability of the nanoparticles to enter muscle cells *in vivo*. We hypothesize that anionic proteins (such as heparin sulfate proteoglycans) within the ECM present a barrier for the positively charged PRXs[155,156], which have a zeta potential of 21-26mV. Potential reduction or masking of the positive charge may help prevent PRXs from getting stuck in the basement membrane or ECM. Additionally, testing other peptide conjugations or attempting to target endocytosis receptors may make *in vivo* uptake more efficient. Lastly, improved targeting of the PRXs to the heart and diaphragm will also need to be undertaken, since our current PRX formulations do not efficiently reach those muscles.

Successful delivery of CRISPR/Cas9 involves many considerations and the payload has unique challenges. Since SpCas9 is large (~4kb or 160kDa), its size may present an obstacle for payload packaging. Each form of the CRISPR platform, as DNA, RNA, or RNP, may require different delivery strategies and have different advantages. Plasmid or episomal DNA delivery may be less desirable since it is longer lasting, has potential for integration, and needs to be transcribed in the nucleus. In contrast, CRISPR RNA or RNPs are expected to be shorter lasting

and do not need to reach the nucleus for transcription. Thus, future work with PRXs should test their ability to deliver the CRISPR platform as RNA instead.

Although AAV-mediated delivery was more efficient than the PRX nanoparticles *in vivo*, AAV delivery of CRISPR/Cas9 presents other challenges. AAV delivery leads to long lasting expression of Cas9 in muscle that may lead to increased potential for off-target cutting or generation of an immune response against the muscle. Thus, methods to degrade the episomal Cas9 DNA, such as KamiCas9 or self-limiting CRISPR[157–159], are desirable and should be pursued. The elimination of the Cas9 expressing DNA would help prevent some of the safety concerns of Cas9 remaining in the cell for an extended period of time. Additionally, it would be desirable to be able to dose AAV-CRISPR in the same subject multiple times, which may be accomplished if high immunosuppression or plasmapheresis are used[160–163].

Ongoing work includes repeating a well-powered study in hDMD del45 mdx congenic mice so that functional testing can also be performed. Other future work aims to deliver CRISPR to muscle stem cells in order to obtain a long-lasting, sustainable therapy. Thus, testing and further modifications of PRXs or AAVs that can effectively target muscle stem cells is needed. Lastly, an unbiased assessment of off-target cutting should be completed after *in vivo* delivery of CRISPR/Cas9.

In summary, we have demonstrated non-viral carriers of CRISPR/Cas9 are able to restore low levels of dystrophin protein after deletion of *DMD* exons 45-55 in our novel humanized dystrophic mouse. This level of gene editing is currently inefficient compared to AAV-CRISPR, which generates higher levels of dystrophin protein. Importantly, this work assesses human dystrophin using a human sequence targeted CRISPR/Cas9 platform, which may allow for faster translation to patients.

Acknowledgments

We would like to thank Diana Becerra, Catherine Li, Jesus Perez, Marbella Quinonez, and Jane Wen for technical assistance. We are grateful for the Center for DMD at UCLA Muscle Phenotyping and Imaging Core. Schematic in Figure 4-1C was courtesy of Drs. Jinhong Jiang and Xiangsheng Liu. This material is based upon work supported by the National Science Foundation Graduate Research Fellowship Program under Grant No. DGE-1144087 (CSY), a UCLA Graduate Division Dissertation Year Fellowship (CSY), and a CMB T32 Ruth L. Kirschstein NRSA GM007185 (MRE). Additional funding was provided by the California Institute of Regenerative Medicine, the Eli & Edythe Broad Center of Regenerative Medicine and Stem Cell Research at UCLA, the Wellstone Cooperative Muscular Dystrophy Center (JSC), and NIAMS of the NIH (R01AR064327-ADP; P30 AR057230).

Author contributions

Conceptualization, Methodology, Visualization, Project Administration - CSY, MRE, YJ, XL, ADP, HM, MJS; Validation, Formal Analysis, Investigation- CSY, MRE, YJ, XL, EM; Writing-Original Draft- CSY; Writing- Review and Editing- CSY, ADP, MJS; Resources- NB, JSC, ADP, HM, MJS; Supervision- JSC, ADP, HM, MJS; Funding Acquisition- ADP, HM, MJS.

Figures

A

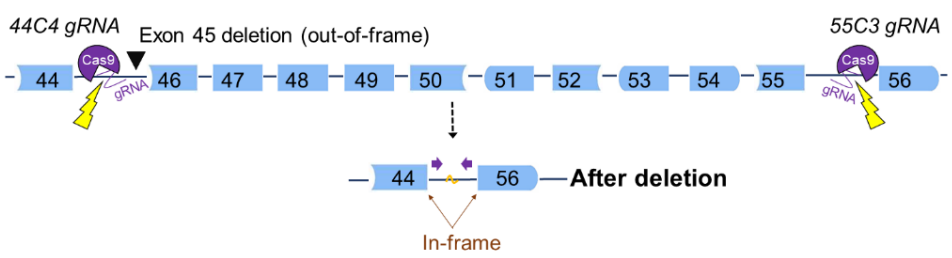

B

Generation of PRX	Design features	Description	Cartoon
Generation 1 (G1)	Linear PRX	Original design, self-assembly	
Generation 2 (G2)	Linear PRX with addition of cleavable linker	Faster cargo release	
Generation 3 (G3)	Multi-arm PRX Peptide conjugation	Increased PEGylation for improved PK, cell targeting	
Generation 4 (G4)	Multi-arm PRX with addition of cleavable linker	Increased PEGylation for improved PK plus faster cargo release	

C

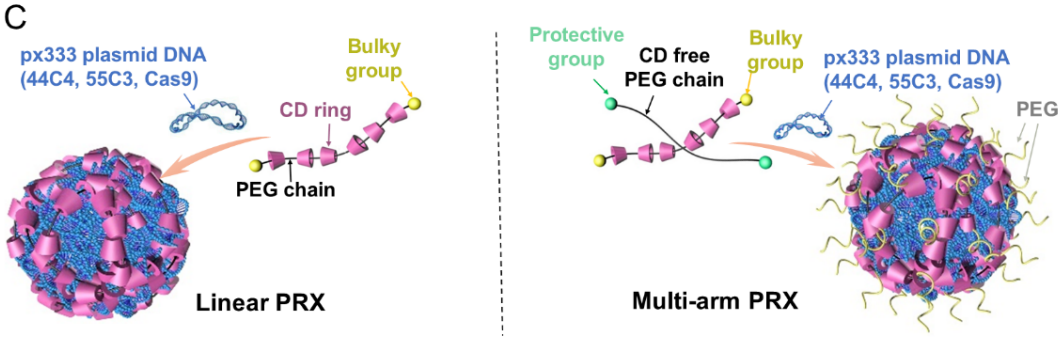

D

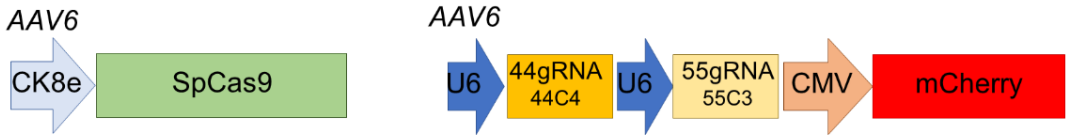

Figure 4-1: Overview of PRX and AAV delivery strategies.
A) Cartoon depicting the region of the *DMD* gene targeted for CRISPR/Cas9 deletion. One gRNA to intron 44 and one to intron 55 target Cas9, which generates double stranded breaks and results in removal of exons 45-55. This creates an in-frame deletion, thereby restoring the reading frame for out-of-frame DMD mutations in this region, such as an exon 45 deletion (black arrow head).

B) Table describing design features of the four different generations (G1-G4) of PRX nanoparticles. Cartoon shows simplified versions where black is the PEG chain, red is the CD ring, and green represents disulfide linkers.
C) Cartoon depicting the linear and multi-arm PRX design. Both contain PEG chains (in black) with positively charged CD rings (purple). When plasmid DNA is added (in blue) the positively charged PRX and negatively charged nucleic acids will self-assemble into a nanoparticle. The multi-arm PRX contains increased PEGylation on the surface of the particle.
D) Schematic of the dual-vector approach using AAV6. Due to the large size of Cas9, one entire vector is needed to contain Cas9 behind a muscle-specific promoter (CK8) and another vector contains the two gRNAs and an mCherry reporter.

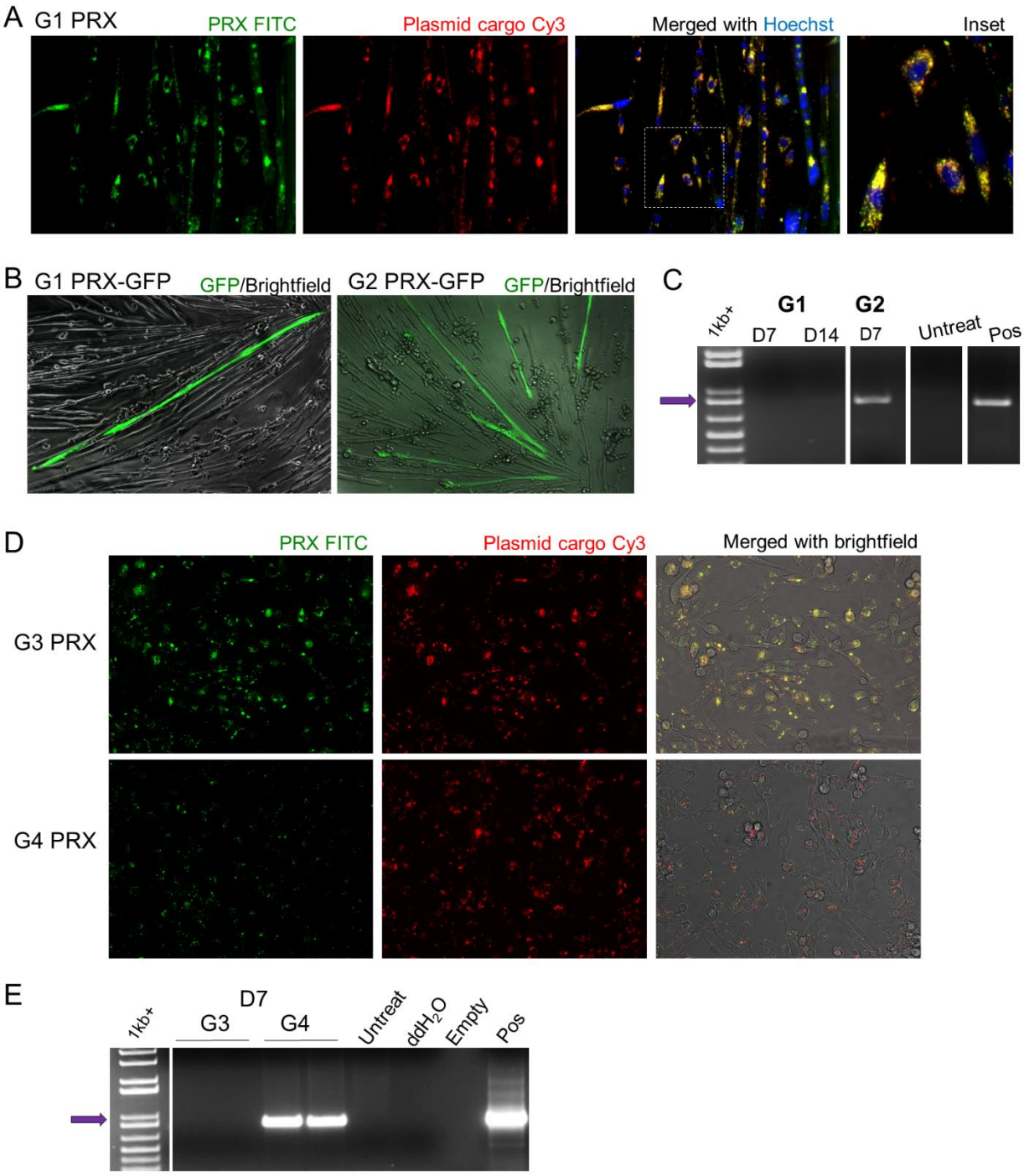

Figure 4-2: PRXs demonstrate successful uptake and plasmid delivery to muscle cells *in vitro*.

A) Imaging of G1 PRX nanoparticles labeled with FITC (green) and plasmid cargo (labeled with Cy3, red) in hDMD myotubes at day 3 after administration. There is a high colocalization of the particle and cargo signal in the cells demonstrating a lack of plasmid release.

B) Imaging of G1 and G2 PRX particles carrying a GFP plasmid in hDMD myotubes at day 7 after administration. G2, which contains the disulfide linker, results in more GFP positive cells.
C) Genomic DNA PCR for an exon 45-55 deletion (using primers that flank the deletion, shown in Fig 4-1A) 7 or 14 days after administration of G1 or G2 carrying the CRISPR/Cas9 plasmid to hDMD myotubes. G2 PRX-CRISPR results in deletion at day 7. Untreated (untreat) negative and positive (pos) controls are shown.
D) Imaging of G3 and G4 PRX nanoparticles labeled with FITC (green) and labeled plasmid cargo (red) in hDMD del45 myoblasts 24hrs after administration. There is less particle/plasmid colocalization in the cells seen with G4, which contains a disulfide linker.
E) Genomic DNA PCR for an exon 45-55 deletion at day 7 after administration of G3 or G4 carrying the CRISPR/Cas9 plasmid to hDMD del45 myoblasts. G4 PRX-CRISPR results in successful deletion. Untreated (untreat), water only (ddH_2O), and positive (pos) controls are shown.

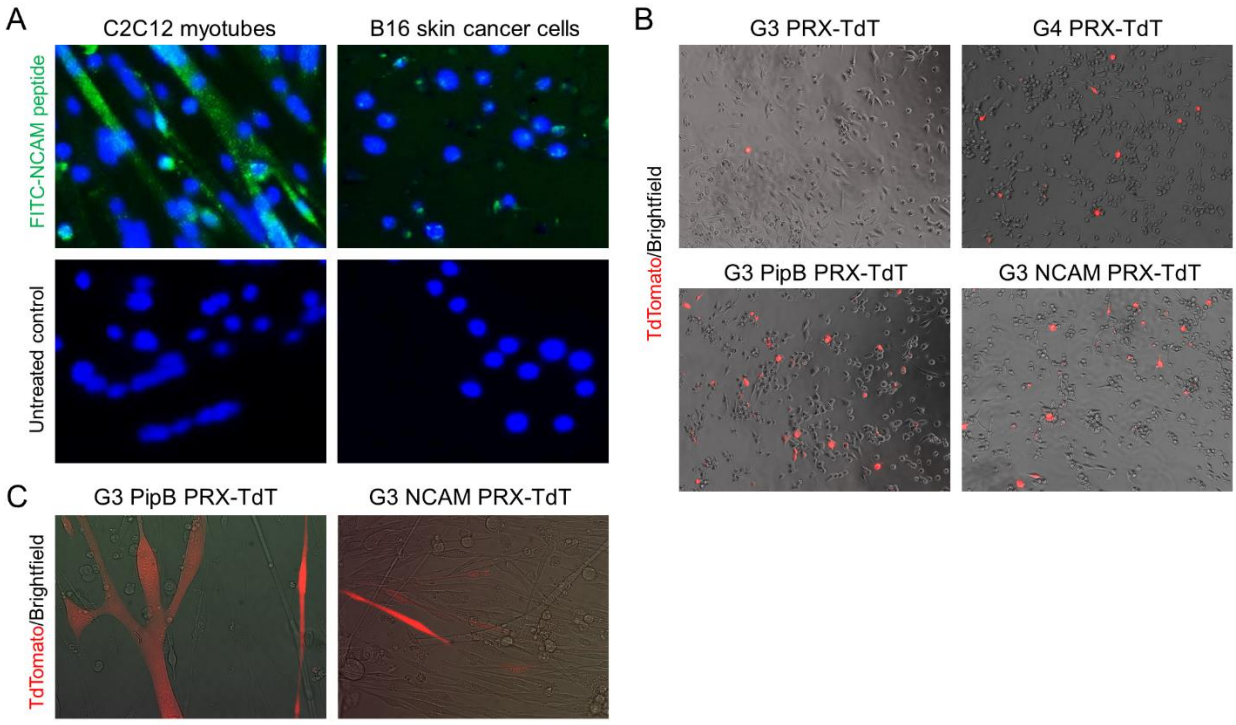

Figure 4-3: Peptide conjugated PRXs demonstrate improved delivery of a reporter plasmid in muscle cells *in vitro*.
A) Imaging of an NCAM peptide labeled with FITC added to C2C12 myotubes or B16 skin cancer cells for 6hrs. There is increased binding of the peptide on the C2C12 cells compared to the controls, demonstrating successful peptide binding to NCAM.
B) Imaging of G3, G4 and peptide conjugated G3 PRXs carrying a TdTomato (TdT, red) reporter plasmid in hDMD del45 myoblasts 48hrs after administration. Both peptide conjugated versions demonstrate a higher percentage of TdTomato+ cells (~70 fold higher than unconjugated).
C) Imaging of peptide conjugated G3 PRXs carrying a TdTomato reporter plasmid in hDMD del45 myotubes 24hrs after administration, demonstrating successful delivery.

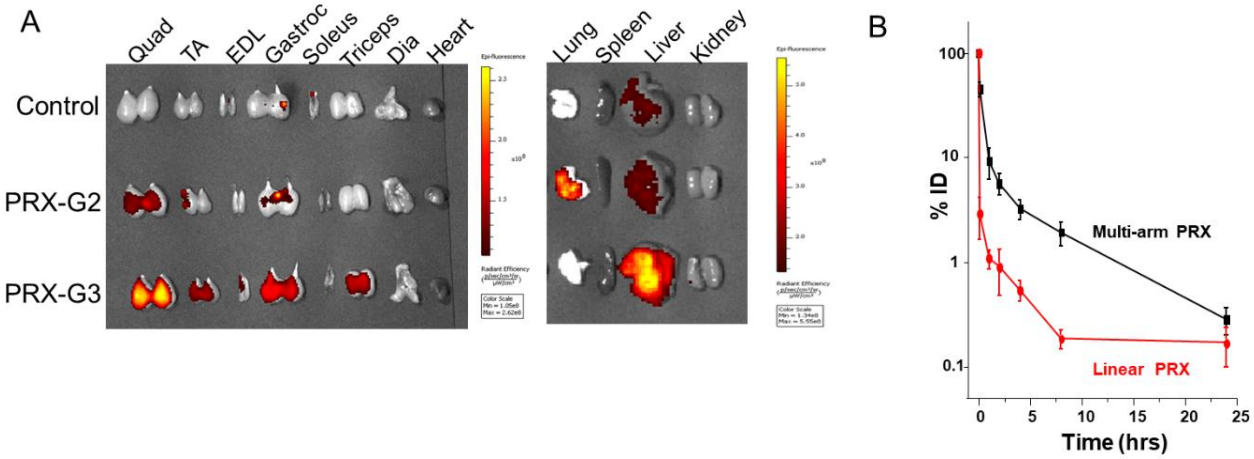

Figure 4-4: *In vivo* biodistribution of PRX nanoparticles.
A) *Ex vivo* IVIS imaging of harvested muscles and organs (quadriceps (quad), tibialis anterior (TA), extensor digitorum longus (EDL), gastrocnemius (gastroc), soleus, triceps, diaphragm (dia), heart, lungs, spleen, liver and kidneys) from non-injected control and i.v. injected PRX G2 and G3 (100µg plasmid) mdx mice at 24hrs. Imaging was performed for the Cy3 labeled plasmid cargo and demonstrated higher signal in the muscles of the G3 injected mice.
B) Plot of percent of injected dose (%ID) over time after i.v. injection of G1 (linear) and G3 (multi-arm) PRXs in C57 mice. The multi-arm PRX demonstrates enhanced circulation time.

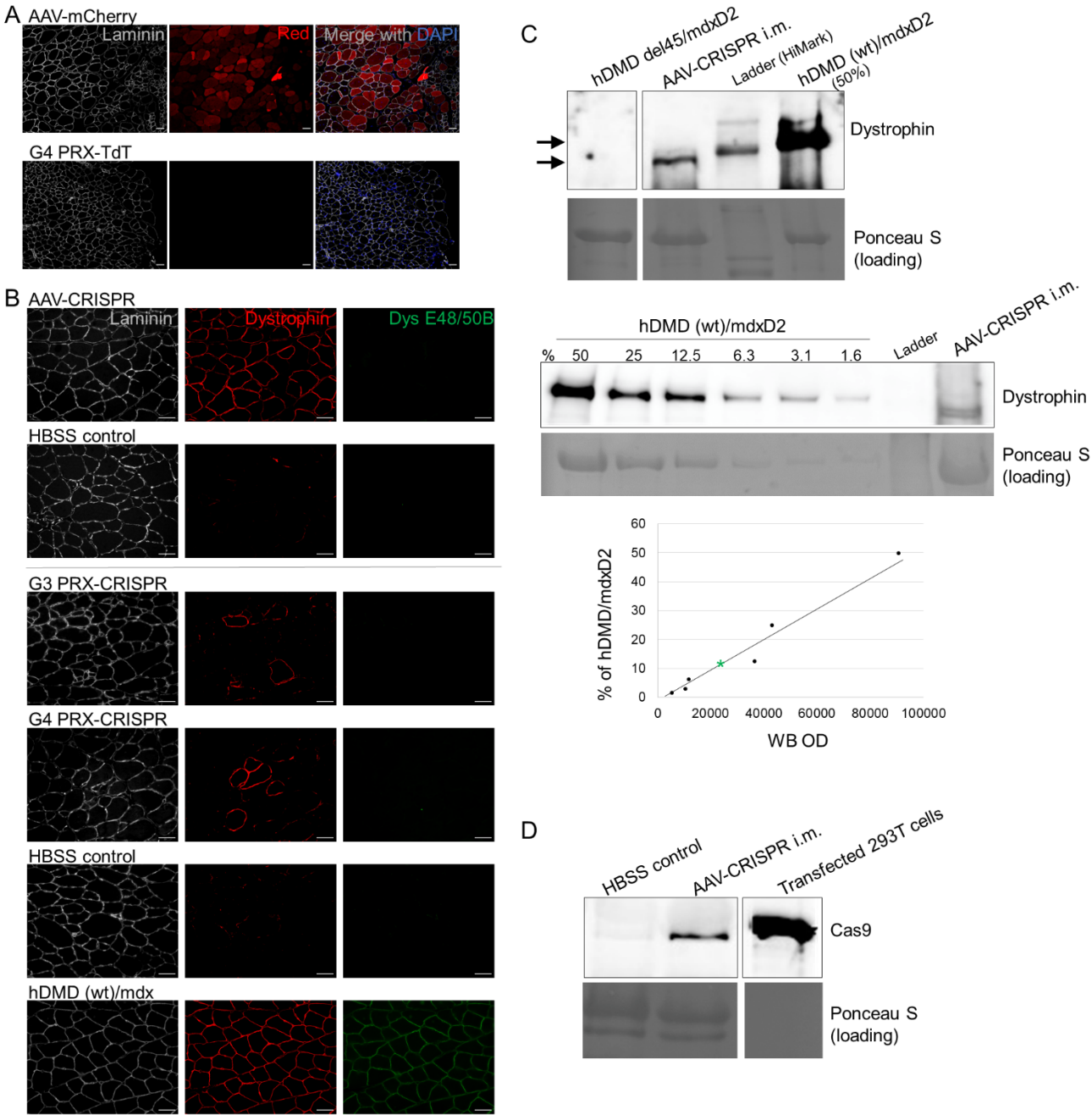

Figure 4-5: Dystrophin restoration after local delivery of AAV-CRISPR and PRX-CRISPR *in vivo*.

A) Imaging of reporter expression by mCherry or TdTomato (red) positive myofibers 4wks after i.m. injection into the TA of hDMD del45 mdx mice. AAV-mCherry results in robust transduction of 50-60% positive myofibers while G4 PRX-TdT does not effectively transfect myofibers *in vivo*. Laminin (gray) was used to outline the myofibers. Scale bar 50µm.
B) Immunostaining of laminin (gray), human/mouse dystrophin (red), and human/mouse dystrophin 48/50B (green) 4wks post i.m. injection into TA muscles from hDMD del45 mdx mice. $5x10^{10}$ v.g. of AAV and 2µg of plasmid in PRX were injected. Dystrophin 48/50B is used

to exclude revertant fibers since this epitope is internal to the CRISPR-generated exon 45-55 deletion. AAV-CRISPR injected muscles demonstrate ~25% dystrophin+ fibers whereas G3 and G4 PRX-CRISPR generates <1% dystrophin+ fibers. hDMD wild type (wt)/mdx mouse tissue was used as a positive control for the staining. Scale bar 50μm.
C) Western blot with anti-dystrophin (Abcam) on lysates from AAV-CRISPR and positive and negative control muscles showing restored dystrophin after i.m. injection. The molecular weight shift (66kDa) is seen in CRISPR generated dystrophin compared to wild type (arrows). Lower blot shows titration of wild type lysate from 1.6-50%, which was used to calculate the percent of dystrophin in the AAV-CRISPR sample. Graph depicts wild type standard curve and green asterisk demarks sample. Ponceau S is shown for loading.
D) Western blot with anti-Cas9 on lysates from AAV-CRISPR and positive and negative samples. CRISPR/Cas9 plasmid transfected HEK293T cells were used as a positive control. Ponceau S is shown for loading.

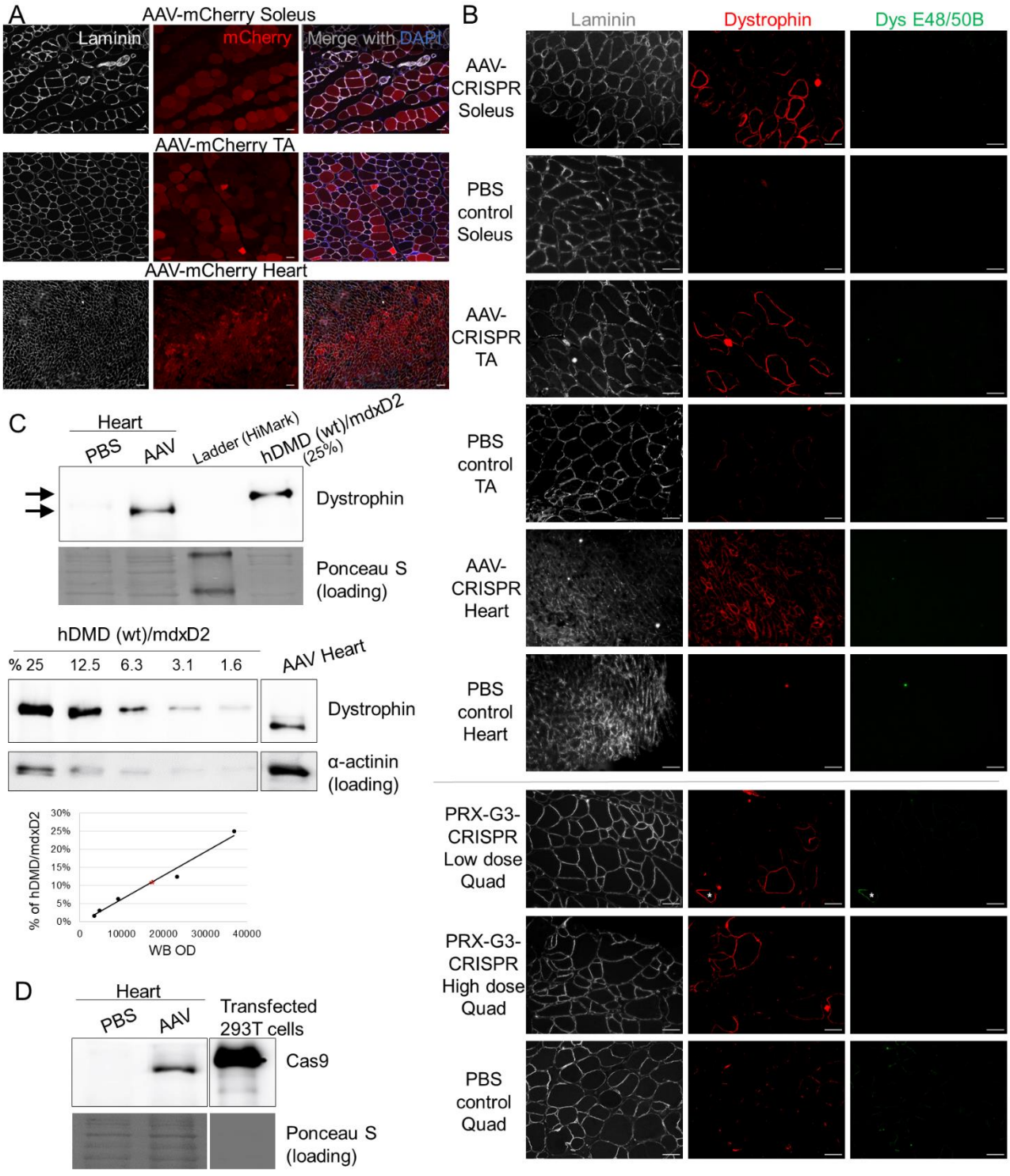

Figure 4-6: Dystrophin restoration after systemic delivery of AAV-CRISPR and PRX-CRISPR *in vivo*.

A) Imaging of AAV reporter expression by mCherry positive myofibers 5wks after r.o. injection in hDMD del45 mdx mice. Laminin (gray) was used to outline the myofibers. Scale bar 50μm.

B) Immunostaining of laminin (gray), human/mouse dystrophin (red), and human/mouse dystrophin 48/50B (green) on sections of hDMD del45 mdx mice given r.o. or i.v. injection of AAV-CRISPR or nano-CRISPR, respectively. $2.85x10^{12}$ v.g. of each AAV or four repeated doses of low (50µg plasmid) or high (100µg plasmid) PRXs were injected and the mice analyzed ~5wks post-injection. Dystrophin 48/50 is used to exclude revertant fibers since this epitope is internal to the CRISPR-generated exon 45-55 deletion, * demarks a revertant fiber. The soleus, tibialis anterior (TA), and heart tissues from the AAV injected mice and the quadriceps (quad) from the PRX injected mice are shown. Scale bar 50µm.
C) Western blot with anti-dystrophin (MANDYS106) on lysates from systemic AAV-CRISPR and positive and negative control muscles showing restored dystrophin in heart. The molecular weight shift (66kDa) is seen in CRISPR generated dystrophin compared to wild type. Lower blot shows titration of wild type lysate from 1.6-25%, which was used to calculate the percent of dystrophin in the AAV-CRISPR heart sample. Graph depicts wild type standard curve and red asterisk demarks sample. Ponceau S and α-actinin are shown for loading.
D) Western blot with anti-Cas9 on lysates from systemic AAV-CRISPR heart and positive and negative samples. CRISPR/Cas9 plasmid transfected HEK293T cells were used as a positive control. Ponceau S is shown for loading.

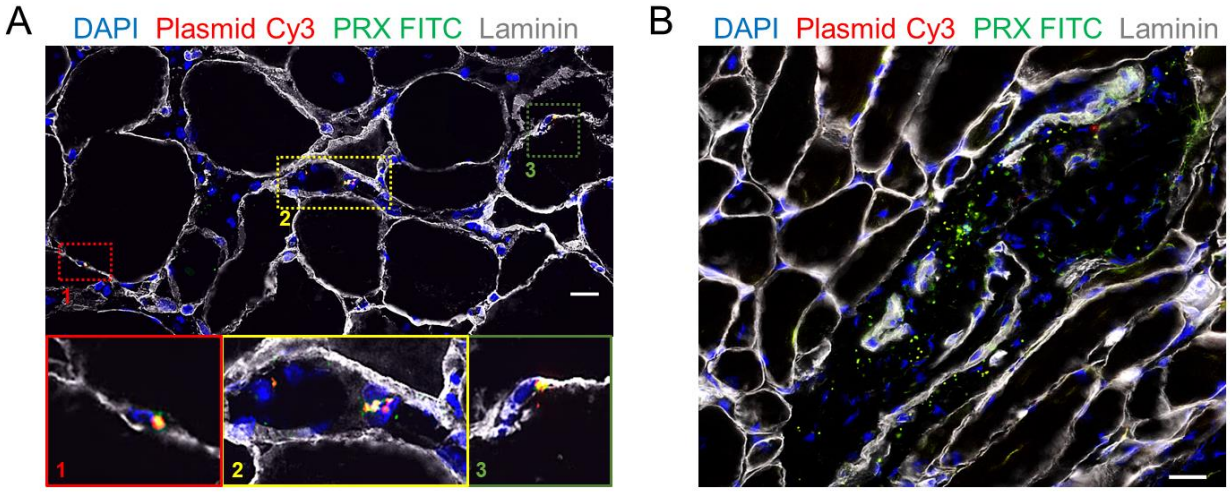

Figure 4-7: PRX nanoparticles appear trapped in the basal lamina or ECM after *in vivo* delivery.

A) Imaging of quadriceps muscle 24hrs after i.v. administration of G4 PRX where the nanoparticle is labeled with FITC (green), the cargo with Cy3 (red) and the fibers stained with laminin (grey). No particles are found within fibers and many appear to be trapped in the basement membrane, marked by laminin (insets 1 and 3). Inset 2 highlights PRXs found within a blood vessel. Scale bar 20µm.

B) Imaging of interosseous muscle 24hrs after footpad injection of G3 PRX where the nanoparticle is labeled with FITC (green), the cargo with Cy3 (red) and the fibers stained with laminin (grey). No particles are found within fibers and they appear to be trapped in the interstitial space. Scale bar 20µm.

Chapter 5 - Conclusions

Precise gene editing offers incredible promise for countless genetic diseases. The CRISPR/Cas system has advanced the gene editing field due to its wide applicability, high efficiency, and ease of use. Although the CRISPR field is rapidly progressing, concerns pertaining to off-target effects and the immune response to Cas9 still linger. Some important advances include new discoveries of various Cas enzymes which have different sizes, create different types of DSBs and require different PAMs, and some that can target RNA[164]. There has been progress on ways to make CRISPR safer, for example, through the use of truncated gRNAs[165], engineered Cas9s with less off-target activity[166–169], anti-CRISPR proteins to interfere with Cas9 activity[170,171], or a self-inactivating strategy by targeting a gRNA against the Cas9 sequence[157–159]. The bacterially-derived protein, Cas9, was shown to evoke a cellular and humoral response in murine muscle[74] but this issue has not been further studied in a systemic or long-term manner or in other animal models. Overall CRISPR/Cas gene editing is a revolutionary technology, and although the first human clinical trials have been initiated for *ex vivo* gene editing[45], there is still more work to be done before systemic direct delivery of CRISPR will be a safe option.

Additionally, the form in which CRISPR is delivered could impact its efficiency and safety. Plasmid or episomal DNA is likely to be the most long lasting and also has some potential for integration[172,173]. In addition, DNA requires trafficking to the nucleus for transcription, which can be a barrier for post-mitotic cells due to the lack of nuclear membrane breakdown during cell division. Strategies may be able to overcome these weaknesses by using self-inactivating gRNAs against the Cas9 sequence or conjugating nuclear penetrating peptides to the DNA. The alternative forms of CRISPR as RNA or ribonucleoprotein (RNP) complex offer some

advantages since they do not need to be transcribed in the nucleus and would likely have a shorter half-life, which could reduce off-target and immune effects.

Here we describe a CRISPR/Cas9 platform for Duchenne muscular dystrophy that can restore the reading frame for at least half of DMD patients and allow a Becker-like dystrophin protein to be produced. By targeting our gRNAs close to the flanking exons, we cover the largest number of patient mutations within this region and create a small chimeric intron. Although this is a large deletion, it is predicted to maintain correct spectrin-like repeat structure and is associated with one of the mildest BMD phenotypes seen in patients. We demonstrated successful deletion of exons 45-55 up to 725kb and generated clonal reframed DMD hiPSCs from two different patient lines. Upon differentiation of the reframed lines to skeletal and cardiac muscle cells we showed dystrophin and DGC expression *in vitro* and *in vivo* as well as restored membrane stability and miR31 levels *in vitro*[57].

Two potential routes of translation of this platform are through direct delivery of CRISPR to muscle *in vivo* or through delivery of corrected skeletal muscle progenitor cells derived from reframed hiPSCs (**Figure 5-1**). For the cell therapy approach, we demonstrated that locally engrafted CRISPR reframed cells could restore dystrophin and the DGC in an immunocompromised mdx mouse. However, for the direct delivery approach, we had to create a novel humanized dystrophic mouse model so the human *DMD* gene could be targeted *in vivo*. We used CRISPR/Cas9 to delete exon 45 in the hDMD mouse, thereby putting the human *DMD* gene out-of-frame. We crossed this hDMD del45 mouse to mdx and mdxD2 backgrounds, which lack murine dystrophin, and demonstrated these mice lack all dystrophin and present dystrophic histopathology in multiple muscles in the body. Upon electroporation of the CRISPR/Cas9

platform in the muscle *in vivo* we saw restoration of dystrophin a month later. This demonstrated proof-of-principle that we could apply our CRISPR platform in our novel mouse *in vivo*[137].

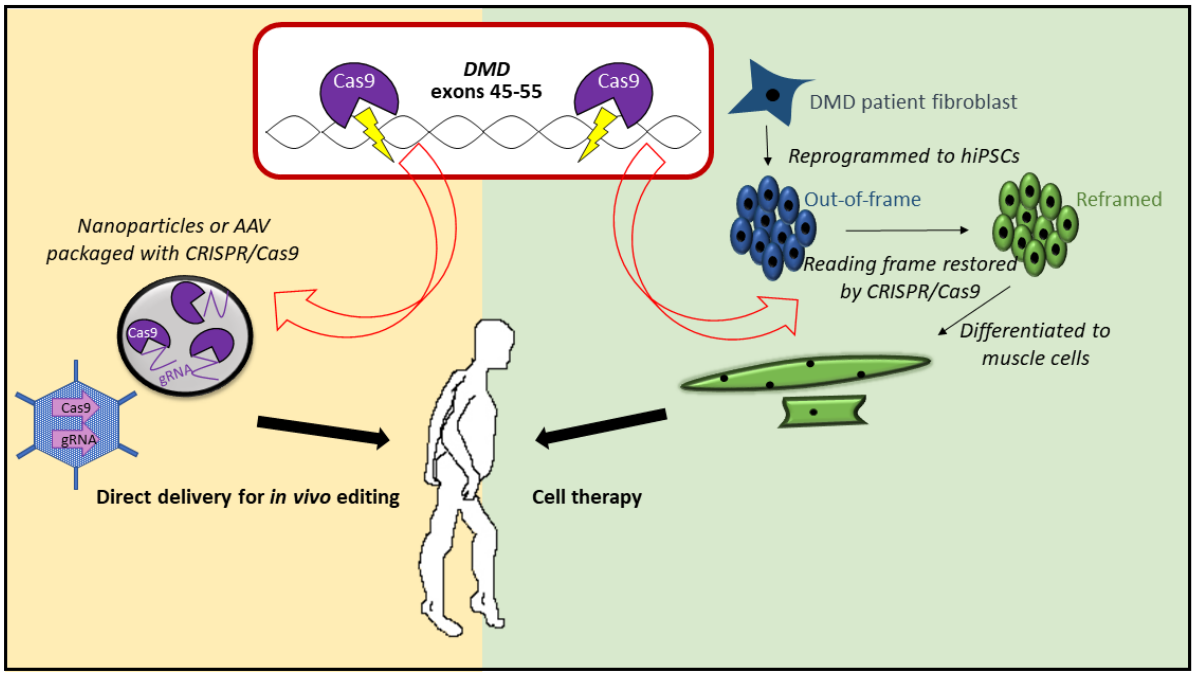

Figure 5-1: Therapeutic applications of CRISPR/Cas9 platform for DMD. Application of our CRISPR/Cas9 platform to reframe *DMD* by deletion of exons 45-55 could be done through either a cell therapy or direct delivery approach. For cell therapy, patient hiPSCs could be reframed, differentiated to muscle progenitor cells and delivered back to the patient (right). For direct delivery, the CRISPR platform could be packed in nanoparticles or AAV and directly injected into the patient (left).

The biggest challenge for direct delivery of CRISPR *in vivo* is how to target the CRISPR platform to all the muscles of the body. Some AAV serotypes have demonstrated high tropism for skeletal muscle, however AAV raises some concerns with how long Cas9 would be expressed, its failure to efficiently target muscle stem cells[72,139], and the inability to repeatedly administer it without other procedures. These could potentially be overcome with strategies to inactivate Cas9, new capsid generation and screening for muscle stem cell targeting, and plasmapheresis or high immunosuppression to remove/prevent anti-AAV antibodies[160–163]. However, since we were also interested in completely avoiding viral delivery we began

development of non-viral nanoparticle-mediated delivery platforms. We iteratively developed the first polyrotaxane (PRX) nanoparticles for muscle by creating four generations of particles, where some generations show improved delivery of reporter and CRISPR/Cas9 plasmids to muscle *in vitro* and can biodistribute to muscle *in vivo.* However, in comparison to AAV, the PRXs are not as efficient at restoring dystrophin after delivery of CRISPR/Cas9 through either local or systemic injection *in vivo.* We hypothesize there may be a trafficking or uptake problem with the muscle fibers *in vivo* and future work to overcome these obstacles through charge modulation or peptide targeting needs to be completed. Also, the PRXs are currently inefficient at targeting the heart and diaphragm after systemic injection and so specific iterations of PRXs should be developed to target these muscles.

Other important considerations for CRISPR-mediated dystrophin restoration is to understand the timing and efficiency needed to restore dystrophin to the threshold level necessary to protect each individual muscle fiber. Although studies have been done looking globally at what level of dystrophin is needed for improved function[29–32,174–176], the level needed on a per fiber basis is unclear. Also, the functional consequence of restoring a single exon skipped versus an exon 45-55 deletion versus a wild type dystrophin is unknown. Thus, future studies looking at if dystrophin positive fibers are lost over time and performing functional assessments could give some insight into the original efficiency and threshold needed. Additionally, understanding the long-term functionality of different internally deleted dystrophins could be done by generating Becker mouse models. Related, it is unclear what dystrophin level is needed for long-term functional benefit in humans. Sarepta's Exondys 51 exon skipping drug was approved based on a 1% induction of dystrophin by Western blot and

some improved function over 4 years[28], however the lifelong potential of this amount of dystrophin is unknown.

In future work, targeting of CRISPR/Cas to muscle stem cells would allow for the permanent correction to be propagated over time and result in long term dystrophin restoration. Furthermore, therapies to preserve heart function should be carried out in parallel to prevent cardiac failure. Lastly an unbiased assessment of off-target activity should be done to have an idea of any potential safety risks.

In sum, we have developed a therapeutically relevant CRISPR/Cas9 platform that restores the *DMD* reading frame for a large percentage of Duchenne patients using a single pair of gRNAs. We demonstrate potential utility of this platform through either a corrected cell therapy approach or through viral or non-viral delivery directly to muscle *in vivo* to restore dystrophin expression.

Bibliography

1. Ryder, S. *et al.* The burden, epidemiology, costs and treatment for Duchenne muscular dystrophy: An evidence review. *Orphanet J. Rare Dis.* **12,** 79 (2017).

2. Dumont, N. A. *et al.* Dystrophin expression in muscle stem cells regulates their polarity and asymmetric division. *Nat. Med.* **21,** 1455–1463 (2015).

3. Heslop, L., Morgan, J. E. & Partridge, T. A. Evidence for a myogenic stem cell that is exhausted in dystrophic muscle. *J. Cell Sci.* **113,** 2299–2308 (2000).

4. Jiang, C. *et al.* Notch signaling deficiency underlies age-dependent depletion of satellite cells in muscular dystrophy. *Dis. Model. Mech.* **7,** 997–1004 (2014).

5. Tichy, E. D. *et al.* Single Stem Cell Imaging and Analysis Reveals Telomere Length Differences in Diseased Human and Mouse Skeletal Muscles. *Stem Cell Reports* **9,** 1328–1341 (2017).

6. Bushby, K. *et al.* Diagnosis and management of Duchenne muscular dystrophy, part 2: implementation of multidisciplinary care. *Lancet Neurol.* **9,** 177–189 (2010).

7. Bushby, K. *et al.* Diagnosis and management of Duchenne muscular dystrophy, part 1: diagnosis, and pharmacological and psychosocial management. *Lancet Neurol.* **9,** 77–93 (2010).

8. Emery, A. E. H. & Skinner, R. Clinical studies in benign (Becker type) X-linked muscular dystrophy. *Clin. Genet.* **10,** 189–201 (1976).

9. Koenig, M. *et al.* The molecular basis for Duchenne versus Becker muscular dystrophy: Correlation of severity with type of deletion. *Am J Hum Genet* **45,** 498–506 (1989).

10. Gumerson, J. D. & Michele, D. E. The dystrophin-glycoprotein complex in the prevention of muscle damage. *J. Biomed. Biotechnol.* **2011,** 210797 (2011).

11. Batchelor, C. & Winder, S. Sparks, signals and shock absorbers: how dystrophin loss causes muscular dystrophy. *Trends Cell Biol.* **16,** 198–204 (2006).

12. Gao, Q. & McNally, E. M. The Dystrophin Complex: structure, function and implications for therapy. *Compr Physiol.* **5,** 1223–1239 (2015).

13. England, S. *et al.* Very mild muscular dystrophy associated with the deletion of 46% of dystrophin. *Nature* **343,** 180–182 (1990).

14. Crawford, G. E. *et al.* Assembly of the dystrophin-associated protein complex does not require the dystrophin COOH-terminal domain. *J. Cell Biol.* **150,** 1399–410 (2000).

15. Harper, S. Q. *et al.* Modular flexibility of dystrophin: implications for gene therapy of Duchenne muscular dystrophy. *Nat. Med.* **8,** 253–61 (2002).

16. Wang, B., Li, J. & Xiao, X. Adeno-associated virus vector carrying human minidystrophin genes effectively ameliorates muscular dystrophy in mdx mouse model. *PNAS* **97,** 13714–13719 (2000).

17. Yoshimura, M. *et al.* AAV vector-mediated microdystrophin expression in a relatively small percentage of mdx myofibers improved the mdx phenotype. *Mol. Ther.* **10,** 821–828 (2004).

18. Yue, Y. *et al.* Microdystrophin gene therapy of cardiomyopathy restores dystrophin-glycoprotein complex and improves sarcolemma integrity in the mdx mouse heart. *Circulation* **108,** 1626–1632 (2003).

19. Hakim, C. H. *et al.* A Five-Repeat Micro-Dystrophin Gene Ameliorated Dystrophic Phenotype in the Severe DBA/2J-mdx Model of Duchenne Muscular Dystrophy. *Mol. Ther. - Methods Clin. Dev.* **6,** 216–230 (2017).

20. Le Guiner, C. *et al.* Long-term microdystrophin gene therapy is effective in a canine model of Duchenne muscular dystrophy. *Nat. Commun.* **8,** 16105 (2017).

21. Nicolas, A. *et al.* Assessment of the structural and functional impact of in-frame mutations of the DMD gene, using the tools included in the eDystrophin online database. *Orphanet J. Rare Dis.* **7,** 45 (2012).

22. Taglia, A. *et al.* Clinical features of patients with dystrophinopathy sharing the 45-55 exon deletion of DMD gene. *Acta Myol.* **34,** 9–13 (2015).

23. Nakamura, A. *et al.* Follow-up of three patients with a large in-frame deletion of exons 45-55 in the Duchenne muscular dystrophy (DMD) gene. *J. Clin. Neurosci.* **15,** 757–63 (2008).

24. Beroud, C. *et al.* Multiexon skipping leading to an artificial DMD protein lacking amino acids from exons 45 through 55 could rescue up to 63% of patients with Duchenne muscular dystrophy. *Hum. Mutat.* **28,** 196–202 (2007).

25. Yazaki, M. *et al.* Clinical Characteristics of Aged Becker Muscular Dystrophy Patients with Onset after 30 Years. *Eur. Neurol.* **42,** 145–149 (1999).

26. Nakamura, A. *et al.* Comparison of the phenotypes of patients harboring in-frame deletions starting at exon 45 in the Duchenne muscular dystrophy gene indicates potential for the development of exon skipping therapy. *J. Hum. Genet.* **62,** 459–463 (2017).

27. Niks, E. H. & Aartsma-Rus, A. Exon skipping: a first in class strategy for Duchenne muscular dystrophy. *Expert Opin. Biol. Ther.* **17,** 225–236 (2017).

28. Sarepta Therapeutics, I. *Eteplirsen briefing document*. (2016).

29. van Putten, M. *et al.* The effects of low levels of dystrophin on mouse muscle function and pathology. *PLoS One* **7,** e31937 (2012).

30. van Putten, M. *et al.* Low dystrophin levels increase survival and improve muscle pathology and function in dystrophin/utrophin double-knockout mice. *FASEB J* **27,** 2484–95 (2013).

31. Godfrey, C. *et al.* How much dystrophin is enough: the physiological consequences of different levels of dystrophin in the mdx mouse. *Hum. Mol. Genet.* **24,** 4225–4237 (2015).

32. Sharp, P. S., Bye-A-Jee, H. & Wells, D. J. Physiological characterization of muscle strength with variable levels of dystrophin restoration in mdx mice following local antisense therapy. *Mol. Ther.* **19,** 165–171 (2011).

33. Duan, D. Micro-dystrophin gene therapy goes systemic in Duchenne muscular dystrophy patients. *Hum. Gene Ther.* hum.2018.012 (2018).

34. Finkel, R. S. Readthrough Strategies for Suppression of Nonsense Mutations in Duchenne/Becker Muscular Dystrophy: Aminoglycosides and Ataluren (PTC124). *J Child Neurol* **25,** 1158–64 (2010).

35. Miura, P. & Jasmin, B. J. Utrophin upregulation for treating Duchenne or Becker muscular dystrophy: How close are we? *TRENDS Mol. Med.* **12,** 122–129 (2006).

36. Barrangou, R. *et al.* CRISPR Provides Acquired Resistance Against Viruses in Prokaryotes. *Science.* **315,** 1709–1712 (2007).

37. Brouns, S. *et al.* Small CRISPR RNAs Guide Antiviral Defense in Prokaryotes. *Science.* **321,** 960–3 (2012).

38. Deltcheva, E. *et al.* CRISPR RNA maturation by trans-encoded small RNA and host factor RNase III. *Nature* **471,** 602–607 (2011).

39. Jinek, M. *et al.* A Programmable Dual-RNA-Guided DNA Endonuclease in Adaptive Bacterial Immunity. *Science.* **337,** 816–822 (2012).

40. Cong, L. *et al.* Multiplex genome engineering using CRISPR/Cas systems. *Science.* **339,** 819–823 (2013).

41. Mali, P. *et al.* RNA-guided human genome engineering via Cas9. *Science.* **339,** 823–826 (2013).

42. Garneau, J. E. *et al.* The CRISPR/cas bacterial immune system cleaves bacteriophage and plasmid DNA. *Nature* **468,** 67–71 (2010).

43. Kakarougkas, A. & Jeggo, P. A. DNA DSB repair pathway choice: An orchestrated handover mechanism. *Br. J. Radiol.* **87,** 20130685 (2014).

44. Barrangou, R. & Doudna, J. A. Applications of CRISPR technologies in research and beyond. *Nat. Biotechnol.* **34,** 933–941 (2016).

45. Cyranoski, D. CRISPR gene-editing tested in a person for the first time. *Nat. News* **539,** 479 (2016).

46. Reardon, S. First CRISPR clinical trial gets green light from US panel. *Nat. News* (2016).

47. Fehse, B. & Abramowski-Mock, U. The Time Is Ripe for Somatic Genome Editing: NIH Program to Strengthen Translation. *Mol. Ther.* **26,** 671–4 (2018).

48. Le Page, M. Boom in human gene editing as 20 CRISPR trials gear up. *New Scientist* (2017). Available at: https://www.newscientist.com/article/2133095-boom-in-human-gene-editing-as-20-crispr-trials-gear-up/.

49. Ousterout, D. G. *et al.* Multiplex CRISPR/Cas9-based genome editing for correction of dystrophin mutations that cause Duchenne muscular dystrophy. *Nat. Commun.* **6,** 6244 (2015).

50. Xue, H., Wu, J., Li, S., Rao, M. S. & Liu, Y. Genetic Modification in Human Pluripotent Stem Cells by Homologous Recombination and CRISPR/Cas9 System. *Methods Mol. Biol.* **1307,** 173–90 (2014).

51. Li, H. L. *et al.* Precise correction of the dystrophin gene in duchenne muscular dystrophy patient induced pluripotent stem cells by TALEN and CRISPR-Cas9. *Stem Cell Reports* **4,** 143–154 (2015).

52. Wojtal, D. *et al.* Spell Checking Nature: Versatility of CRISPR/Cas9 for Developing Treatments for Inherited Disorders. *Am. J. Hum. Genet.* **98,** 1–12 (2016).

53. Maggio, I., Liu, J., Janssen, J. M., Chen, X. & Gonçalves, M. A. F. V. Adenoviral vectors encoding CRISPR/Cas9 multiplexes rescue dystrophin synthesis in unselected populations of DMD muscle cells. *Sci. Rep.* **6,** 1–12 (2016).

54. Iyombe-Engembe, J. P. *et al.* Efficient Restoration of the Dystrophin Gene Reading Frame and Protein Structure in DMD Myoblasts Using the CinDel Method. *Mol. Ther. - Nucleic Acids* **5,** e283 (2016).

55. Zhang, Y. *et al.* CRISPR-Cpf1 correction of muscular dystrophy mutations in human cardiomyocytes and mice. *Sci. Adv.* **3,** (2017).

56. Kyrychenko, V. *et al.* Functional correction of dystrophin actin binding domain mutations by genome editing. *JCI Insight* **2,** 1–16 (2017).

57. Young, C. S. *et al.* A Single CRISPR-Cas9 Deletion Strategy that Targets the Majority of DMD Patients Restores Dystrophin Function in hiPSC-Derived Muscle Cells. *Cell Stem Cell* **18,** 533–40 (2016).

58. Lattanzi, A. *et al.* Correction of the Exon 2 Duplication in DMD Myoblasts by a Single CRISPR/Cas9 System. *Mol. Ther. - Nucleic Acids* **7,** 11–19 (2017).

59. Long, C. *et al.* Prevention of muscular dystrophy in mice by CRISPR/Cas9-mediated editing of germline DNA. *Science.* **345,** 1184–1188 (2014).

60. Long, C. *et al.* Postnatal genome editing partially restores dystrophin expression in a mouse model of muscular dystrophy. *Science.* **351,** 400–3 (2016).

61. Nelson, C. E. *et al.* In vivo genome editing improves muscle function in a mouse model of Duchenne muscular dystrophy. *Science.* **351,** 403–407 (2016).

62. Tabebordbar, M. *et al.* In vivo gene editing in dystrophic mouse muscle and muscle stem cells. *Science.* **351,** 407–411 (2016).

63. Bengtsson, N. E. *et al.* Muscle-specific CRISPR/Cas9 dystrophin gene editing ameliorates pathophysiology in a mouse model for Duchenne muscular dystrophy. *Nat. Commun.* **8,** 14454 (2017).

64. Xu, L. *et al.* CRISPR-mediated genome editing restores dystrophin expression and function in mdx mice. *Mol. Ther.* **24,** 564–9 (2016).

65. El Refaey, M. *et al.* In vivo genome editing restores dystrophin expression and cardiac function in dystrophic mice. *Circ. Res.* **121,** 923–929 (2017).

66. Amoasii, L. *et al.* Single-cut genome editing restores dystrophin expression in a new mouse model of muscular dystrophy. *Sci. Transl. Med.* **9,** (2017).

67. Hicks, M. R. *et al.* ERBB3 and NGFR mark a distinct skeletal muscle progenitor cell in human development and hPSCs. *Nat. Cell Biol.* **20,** 46–57 (2017).

68. Xi, H. *et al.* In Vivo Human Somitogenesis Guides Somite Development from hPSCs. *Cell Rep.* **18,** 1573–1585 (2017).

69. Shelton, M. *et al.* Derivation and expansion of PAX7-positive muscle progenitors from human and mouse embryonic stem cells. *Stem Cell Reports* **3,** 516–29 (2014).

70. Chal, J. *et al.* Differentiation of pluripotent stem cells to muscle fiber to model Duchenne muscular dystrophy. *Nat. Biotechnol.* **33,** 962–9 (2015).

71. McGreevy, J. W., Hakim, C. H., McIntosh, M. A. & Duan, D. Animal models of Duchenne muscular dystrophy: from basic mechanisms to gene therapy. *Dis. Model. Mech.* **8,** 195–213 (2015).

72. Arnett, A. L. *et al.* Adeno-associated viral vectors do not efficiently target muscle satellite cells. *Mol. Ther. Methods Clin. Dev.* **1,** 14038 (2014).

73. Louis Jeune, V., Joergensen, J. A., Hajjar, R. J. & Weber, T. Pre-existing Anti–Adeno-Associated Virus Antibodies as a Challenge in AAV Gene Therapy. *Hum. Gene Ther. Methods* **24,** 59–67 (2013).

74. Chew, W. L. *et al.* A multifunctional AAV-CRISPR-Cas9 and its host response. *Nat. Methods* **13,** 868–874 (2016).

75. Singh, R. & Lillard Jr, J. W. Nanoparticle-based targeted drug delivery. *Exp. Mol. Pathol.* **86,** 215–223 (2009).

76. Bobo, D., Robinson, K. J., Islam, J., Thurecht, K. J. & Corrie, S. R. Nanoparticle-Based Medicines: A Review of FDA-Approved Materials and Clinical Trials to Date. *Pharm. Res.* **33,** 2373–2387 (2016).

77. Yin, H. *et al.* Therapeutic genome editing by combined viral and non-viral delivery of CRISPR system components in vivo. *Nat. Biotechnol.* **34,** 328–333 (2016).

78. Sun, W. *et al.* Self-Assembled DNA Nanoclews for the Efficient Delivery of CRISPR-Cas9 for Genome Editing. *Angew. Chem. Int. Ed.* **54,** 12029–12033 (2015).

79. Miller, J. B. *et al.* Non-Viral CRISPR/Cas Gene Editing In Vitro and In Vivo Enabled by Synthetic Nanoparticle Co-Delivery of Cas9 mRNA and sgRNA. *Angew. Chem. Int. Ed.* **56,** 1059–1063 (2017).

80. Wang, M. *et al.* Efficient delivery of genome-editing proteins using bioreducible lipid nanoparticles. *PNAS* **113,** 2868–2873 (2016).

81. Mout, R. *et al.* Direct Cytosolic Delivery of CRISPR/Cas9-Ribonucleoprotein for Efficient Gene Editing. *ACS Nano* **11,** 2452–2458 (2017).

82. Lee, K. *et al.* Synthetically modified guide RNA and donor DNA are a versatile platform for CRISPR-Cas9 engineering. *Elife* **6,** 1–17 (2017).

83. Ha, J. S. *et al.* Poly-sgRNA/siRNA ribonucleoprotein nanoparticles for targeted gene disruption. *J. Control. Release* **250,** 27–35 (2017).

84. Jiang, C. *et al.* A non-viral CRISPR/Cas9 delivery system for therapeutically targeting HBV DNA and pcsk9 in vivo. *Cell Res.* **27,** 440–443 (2017).

85. Zuris, J. A. *et al.* Cationic lipid-mediated delivery of proteins enables efficient protein-based genome editing in vitro and in vivo. *Nat. Biotechnol.* **33,** 73–80 (2015).

86. Timin, A. S. *et al.* Efficient gene editing via non-viral delivery of CRISPR–Cas9 system using polymeric and hybrid microcarriers. *Nanomedicine Nanotechnology, Biol. Med.* **14,** 97–108 (2018).

87. Yin, H. *et al.* Structure-guided chemical modification of guide RNA enables potent non-viral in vivo genome editing. *Nat. Biotechnol.* **35,** 1179–1187 (2017).

88. Lee, K. *et al.* Nanoparticle delivery of Cas9 ribonucleoprotein and donor DNA in vivo induces homology-directed DNA repair. *Nat. Biomed. Eng.* **1,** 889–901 (2017).

89. Finn, J. D. *et al.* A Single Administration of CRISPR/Cas9 Lipid Nanoparticles Achieves Robust and Persistent In Vivo Genome Editing. *Cell Rep.* **22,** 2227–2235 (2018).

90. Wang, P. *et al.* Thermo-triggered Release of CRISPR-Cas9 System by Lipid-Encapsulated Gold Nanoparticles for Tumor Therapy. *Angew. Chem. Int. Ed.* **57,** 1491–1496 (2018).

91. Afzal, E. *et al.* Nanolipodendrosome-loaded glatiramer acetate and myogenic differentiation I as augmentation therapeutic strategy approaches in muscular dystrophy. *Int. J. Nanomedicine* **8,** 2943–2960 (2013).

92. Bassi, E. *et al.* Persistent dystrophin protein restoration 90 days after a course of intraperitoneally administered naked 2'OMePS AON and ZM2 NP-AON complexes in mdx mice. *J Biomed Biotechnol* **2012,** 897076 (2012).

93. Bibee, K. P. *et al.* Rapamycin nanoparticles target defective autophagy in muscular dystrophy to enhance both strength and cardiac function. *FASEB J* **28,** 2047–2061 (2014).

94. Falzarano, M. S., Bassi, E., Passarelli, C., Braghetta, P. & Ferlini, A. Biodistribution Studies of Polymeric Nanoparticles for Drug Delivery in Mice. *Hum. Gene Ther.* **25,** 927–928 (2014).

95. Falzarano, M. S. *et al.* Biodistribution and molecular studies on orally administered nanoparticle-AON complexes encapsulated with alginate aiming at inducing dystrophin rescue in mdx mice. *Biomed Res. Int.* **2013,** 527418 (2013).

96. Kinouchi, N. *et al.* Atelocollagen-mediated local and systemic applications of myostatin-targeting siRNA increase skeletal muscle mass. *Gene Ther.* **15,** 1126–1130 (2008).

97. Ochiya, T. *et al.* New delivery system for plasmid DNA in vivo using atelocollagen as a carrier material: The Minipellet. *Nat. Med.* **5,** 707–710 (1999).

98. Rimessi, P. *et al.* Cationic PMMA nanoparticles bind and deliver antisense oligoribonucleotides allowing restoration of dystrophin expression in the mdx mouse. *Mol. Ther.* **17,** 820–827 (2009).

99. Kim, J., Cao, L., Shvartsman, D., Silva, E. A. & Mooney, D. J. Targeted Delivery of Nanoparticles to Ischemic Muscle for Imaging and Therapeutic Angiogenesis. *Nano Lett* **11,** 694–700 (2011).

100. Negishi, Y. *et al.* Bubble liposomes and ultrasound exposure improve localized morpholino oligomer delivery into the skeletal muscles of dystrophic mdx mice. *Mol. Pharm.* **11,** 1053–1061 (2014).

101. Pearce, J. M. S., Pennington, R. J. T. & Walton, J. N. Serum enzyme studies in muscle disease: Part III Serum creatine kinase activity in relatives of patients with the Duchenne type of muscular dystrophy. *J. Neurol. Neurosurg. Psychiatry* **27,** 181–185 (1964).

102. Echigoya, Y. *et al.* Long-term efficacy of systemic multiexon skipping targeting

dystrophin exons 45-55 with a cocktail of vivo-morpholinos in mdx52 mice. *Mol. Ther. Nucleic Acids* **4,** e225 (2015).

103. Cacchiarelli, D. *et al.* miR-31 modulates dystrophin expression: new implications for Duchenne muscular dystrophy therapy. *EMBO Rep.* **12,** 136–141 (2011).

104. Ran, F. A. *et al.* Genome engineering using the CRISPR-Cas9 system. *Nat. Protoc.* **8,** 2281–308 (2013).

105. Karumbayaram, S. *et al.* From skin biopsy to neurons through a pluripotent intermediate under good manufacturing practice protocols. *Stem Cells Transl. Med.* **1,** 36–43 (2012).

106. Alva, J. A., Lee, G. E., Escobar, E. E. & Pyle, A. D. Phosphatase and tensin homolog regulates the pluripotent state and lineage fate choice in human embryonic stem cells. *Stem Cells* **29,** 1952–1962 (2011).

107. Abujarour, R. *et al.* Myogenic differentiation of muscular dystrophy-specific induced pluripotent stem cells for use in drug discovery. *Stem Cells Trans Med* **3,** 149–60 (2014).

108. Kimura, E. *et al.* Cell-lineage regulated myogenesis for dystrophin replacement: a novel therapeutic approach for treatment of muscular dystrophy. *Hum. Mol. Genet.* **17,** 2507–17 (2008).

109. Arshi, A. *et al.* Rigid microenvironments promote cardiac differentiation of mouse and human embryonic stem cells. *Sci Technol Adv Mater* **14,** 1–14 (2013).

110. Minami, I. *et al.* A small molecule that promotes cardiac differentiation of human pluripotent stem cells under defined, cytokine- and xeno-free conditions. *Cell Rep.* **2,** 1448–60 (2012).

111. Rasband, W. ImageJ. *U. S. National Institutes of Health* (1997).

112. Muir, L. A., Nguyen, Q. G., Hauschka, S. D. & Chamberlain, J. S. Engraftment potential of dermal fibroblasts following in vivo myogenic conversion in immunocompetent dystrophic skeletal muscle. *Mol. Ther. Methods Clin. Dev.* **1,** 14025 (2014).

113. Man, N. & Morris, G. E. Use of epitope libraries to identify exon-specific monoclonal antibodies for characterization of altered dystrophins in muscular dystrophy. *Am J Hum Genet* **52,** 1057–1066 (1993).

114. Woo, J. S., Cho, C.-H., Kim, D. H. & Lee, E. H. TRPC3 cation channel plays an important role in proliferation and differentiation of skeletal muscle myoblasts. *Exp. Mol. Med.* **42,** 614–27 (2010).

115. Cradick, T. J., Qiu, P., Lee, C. M., Fine, E. J. & Bao, G. COSMID: A web-based tool for identifying and validating CRISPR/Cas off-target sites. *Mol. Ther. Nucleic Acids* **3,** e214 (2014).

116. Dekel-Naftali, M. *et al.* Screening of human pluripotent stem cells using CGH and FISH reveals low-grade mosaic aneuploidy and a recurrent amplification of chromosome 1q. *Eur. J. Hum. Genet.* **20,** 1248–55 (2012).

117. Guan, X. *et al.* Dystrophin-deficient cardiomyocytes derived from human urine: new biologic reagents for drug discovery. *Stem Cell Res.* **12,** 467–80 (2014).

118. Menke, A. & Jockusch, H. Extent of shock-induced membrane leakage in human and mouse myotubes depends on dystrophin. *J. Cell Sci.* **108,** 727–733 (1995).

119. Arechavala-Gomeza, V., Anthony, K., Morgan, J. & Muntoni, F. Antisense Oligonucleotide-Mediated Exon Skipping for Duchenne Muscular Dystrophy: Progress and Challenges. *Curr. Gene Ther.* **12,** 152–160 (2012).

120. Partridge, T. Myoblast transplantation. *Neuromuscul. Disord.* **12,** S3-6 (2002).

121. Bladen, C. L. *et al.* The TREAT-NMD DMD Global Database: analysis of more than 7,000 Duchenne muscular dystrophy mutations. *Hum. Mutat.* **36,** 395–402 (2015).

122. Carsana, A. *et al.* Analysis of dystrophin gene deletions indicates that the hinge III region of the protein correlates with disease severity. *Ann. Hum. Genet.* **69,** 253–9 (2005).

123. Nelson, C. E. *et al.* In vivo genome editing improves muscle function in a mouse model of Duchenne muscular dystrophy. *Science.* **351,** 403–7 (2016).

124. Tabebordbar, M. *et al.* In vivo gene editing in dystrophic mouse muscle and muscle stem cells. *Science.* **351,** 407–11 (2016).

125. Long, C. *et al.* Postnatal genome editing partially restores dystrophin expression in a mouse model of muscular dystrophy. *Science.* **351,** 400–3 (2016).

126. Mendell, J. R. *et al.* Evidence-based path to newborn screening for Duchenne muscular dystrophy. *Ann. Neurol.* **71,** 304–13 (2012).

127. Monaco, A. P., Bertelson, C. J., Liechti-Gallati, S., Moser, H. & Kunkel, L. M. An explanation for the phenotypic differences between patients bearing partial deletions of the DMD locus. *Genomics* **2,** 90–95 (1988).

128. Aartsma-Rus, A. & van Ommen, G.-J. B. Antisense-mediated exon skipping: a versatile tool with therapeutic and research applications. *RNA* **13,** 1609–24 (2007).

129. ’t Hoen, P. A. C. *et al.* Generation and characterization of transgenic mice with the full-length human DMD gene. *J. Biol. Chem.* **283,** 5899–907 (2008).

130. Heydemann, A. *et al.* Latent TGF-β – binding protein 4 modifies muscular dystrophy in mice. *JCI* **119,** 3703–12 (2009).

131. Coley, W. D. *et al.* Effect of genetic background on the dystrophic phenotype in mdx

mice. *Hum Mol Genet* **25,** 130–145 (2016).

132. Swaggart, K. a *et al.* Annexin A6 modifies muscular dystrophy by mediating sarcolemmal repair. *PNAS* **111,** 6004–9 (2014).

133. Maddalo, D. *et al.* In vivo engineering of oncogenic chromosomal rearrangements with the CRISPR/Cas9 system. *Nature* **516,** 423–7 (2014).

134. DiFranco, M., Quinonez, M., Capote, J. & Vergara, J. DNA transfection of mammalian skeletal muscles using in vivo electroporation. *JoVE* 1–7 (2009).

135. Kendall, G. C. *et al.* Dantrolene enhances antisense-mediated exon skipping in human and mouse models of Duchenne muscular dystrophy. *Sci. Transl. Med.* **4,** 164ra160 (2012).

136. Thanh, L. T., Nguyen, T. M., Helliwell, T. R. & Morris, G. E. Characterization of revertant muscle fibers in Duchenne muscular dystrophy, using exon-specific monoclonal antibodies against dystrophin. *Am J Hum Genet* **56,** 725–731 (1995).

137. Young, C. S., Mokhonova, E., Quinonez, M., Pyle, A. D. & Spencer, M. J. Creation of a Novel Humanized Dystrophic Mouse Model of Duchenne Muscular Dystrophy and Application of a CRISPR/Cas9 Gene Editing Therapy. *J. Neuromuscul. Dis.* **4,** 139–145 (2017).

138. Bowles, D. E. *et al.* Phase 1 gene therapy for duchenne muscular dystrophy using a translational optimized AAV vector. *Mol. Ther.* **20,** 443–455 (2012).

139. Ellis, B. L. *et al.* A survey of ex vivo/in vitro transduction efficiency of mammalian primary cells and cell lines with Nine natural adeno-associated virus (AAV1-9) and one engineered adeno-associated virus serotype. *Virol. J.* **10,** 74 (2013).

140. Watanabe, J., Ooya, T., Park, K., Kim, Y. & Yui, N. Preparation and characterization of poly(ethylene glycol) hydrogels cross-linked by hydrolyzable polyrotaxane. *J Biomater Sci Polm Ed* **11,** 1333–45 (2000).

141. Liu, Z., Lin, T. M., Purro, M. & Xiong, M. P. Enzymatically Biodegradable Polyrotaxane-Deferoxamine Conjugates for Iron Chelation. *ACS Appl. Mater. Interfaces* **8,** 25788–25797 (2016).

142. Tamura, A. & Yui, N. Polyrotaxane-based systemic delivery of β-cyclodextrins for potentiating therapeutic efficacy in a mouse model of Niemann-Pick type C disease. *J. Control. Release* **269,** 148–158 (2018).

143. Terauchi, M. *et al.* Supramolecular Polyelectrolyte Complexes of Bone Morphogenetic Protein-2 with Sulfonated Polyrotaxanes to Induce Enhanced Osteogenic Differentiation. *Macromol. Biosci.* **15,** 953–964 (2015).

144. Dandekar, P. *et al.* Cellular delivery of polynucleotides by cationic cyclodextrin polyrotaxanes. *J. Control. Release* **164,** 387–393 (2012).

145. Ooya, T. *et al.* Biocleavable polyrotaxane-plasmid DNA polyplex for enhanced gene delivery. *J Am Chem Soc* **128,** 3852–3853 (2006).

146. Yamashita, A. *et al.* Synthesis of a biocleavable polyrotaxane-plasmid DNA (pDNA) polyplex and its use for the rapid nonviral delivery of pDNA to cell nuclei. *Nat Protoc* **1,** 2861–2869 (2006).

147. Ronn, L. C. *et al.* Identification of a neuritogenic ligand of the neural cell adhesion molecule using a combinatorial library of synthetic peptides. *Nat Biotechnol* **17,** 1000–1005 (1999).

148. Yin, H. *et al.* Pip5 transduction peptides direct high efficiency oligonucleotide-mediated dystrophin exon skipping in heart and phenotypic correction in mdx mice. *Mol. Ther.* **19,** 1295–1303 (2011).

149. Waldner, C., Roose, M. & Ryffel, G. U. Red fluorescent Xenopus laevis: A new tool for grafting analysis. *BMC Dev. Biol.* **9,** 37 (2009).

150. Himeda, C. L., Chen, X. & Hauschka, S. D. Design and Testing of Regulatory Cassettes for Optimal Activity in Skeletal and Cardiac Muscles. in *Muscle Gene Therapy: Methods and Protocols* 3–19 (Humana Press, 2011).

151. Snijders, T. *et al.* Satellite cells in human skeletal muscle plasticity. *Front. Physiol.* **6,** 283 (2015).

152. Fidziańska, A. & Kamińska, A. Neural cell adhesion molecule (N-CAM) as a marker of muscle tissue alternations. Review of the literature and own observations. *Folia Neuropathol.* **33,** 125–8 (1995).

153. Capkovic, K. L., Stevenson, S., Johnson, M. C., Thelen, J. J. & Cornelison, D. D. W. Neural cell adhesion molecule (NCAM) marks adult myogenic cells committed to differentiation. *Exp. Cell Res.* **314,** 1553–1565 (2008).

154. Moore, S. E., Thompson, J., Kirkness, V., Dickson, J. G. & Walsh, F. S. Skeletal muscle neural cell adhesion molecule (N-CAM): changes in protein and mRNA species during myogenesis of muscle cell lines. *J. Cell Biol.* **105,** 1377–86 (1987).

155. Lieleg, O., Baumgärtel, R. M. & Bausch, A. R. Selective filtering of particles by the extracellular matrix: An electrostatic bandpass. *Biophys. J.* **97,** 1569–1577 (2009).

156. Velleman, S. G., Shin, J., Li, X. & Song, Y. Review: The skeletal muscle extracellular matrix: Possible roles in the regulation of muscle development and growth. *Can. J. Anim. Sci.* **92,** 1–10 (2012).

157. Ruan, G. X. *et al.* CRISPR/Cas9-Mediated Genome Editing as a Therapeutic Approach for Leber Congenital Amaurosis 10. *Mol. Ther.* **25,** 331–341 (2017).

158. Petris, G. *et al.* Hit and go CAS9 delivered through a lentiviral based self-limiting circuit.

Nat. Commun. **8,** 15334 (2017).

159. Merienne, N. *et al.* The Self-Inactivating KamiCas9 System for the Editing of CNS Disease Genes. *Cell Rep.* **20,** 2980–2991 (2017).

160. Halbert, C. L., Standaert, T. A., Wilson, C. B. & Miller, A. D. Successful readministration of adeno-associated virus vectors to the mouse lung requires transient immunosuppression during the initial exposure. *J. Virol.* **72,** 9795–805 (1998).

161. Manning, W. C., Zhou, S., Bland, M. P., Escobedo, J. A. & Dwarki, V. Transient Immunosuppression Allows Transgene Expression Following Readministration of Adeno-Associated Viral Vectors. *Hum. Gene Ther.* **9,** 477–85 (1998).

162. Corti, M. *et al.* Evaluation of Readministration of a Recombinant Adeno-Associated Virus Vector Expressing Acid Alpha-Glucosidase in Pompe Disease: Preclinical to Clinical Planning. *Hum. Gene Ther. Clin. Dev.* **26,** 185–193 (2015).

163. Chicoine, L. G. *et al.* Plasmapheresis eliminates the negative impact of AAV antibodies on microdystrophin gene expression following vascular delivery. *Mol. Ther.* **22,** 338–347 (2014).

164. Cebrian-Serrano, A. & Davies, B. CRISPR-Cas orthologues and variants: optimizing the repertoire, specificity and delivery of genome engineering tools. *Mamm. Genome* **28,** 247–261 (2017).

165. Fu, Y., Sander, J. D., Reyon, D., Cascio, V. M. & Joung, J. K. Improving CRISPR-Cas nuclease specificity using truncated guide RNAs. *Nat. Biotechnol.* **32,** 279–84 (2014).

166. Slaymaker, I. M. *et al.* Rationally engineered Cas9 nucleases with improved specificity. *Science.* **351,** 84–8 (2016).

167. Chen, J. S. *et al.* Enhanced proofreading governs CRISPR-Cas9 targeting accuracy. *Nature* **550,** 407–410 (2017).

168. Kleinstiver, B. P. *et al.* High-fidelity CRISPR-Cas9 nucleases with no detectable genome-wide off-target effects. *Nature* **529,** 490–495 (2016).

169. Yin, H. *et al.* Partial DNA-guided Cas9 enables genome editing with reduced off-target activity. *Nat. Chem. Biol.* **14,** 311–316 (2018).

170. Bondy-Denomy, J. *et al.* Multiple mechanisms for CRISPR-Cas inhibition by anti-CRISPR proteins. *Nature* **526,** 136–139 (2015).

171. Shin, J. *et al.* Disabling Cas9 by an anti-CRISPR DNA mimic. *Sci. Adv.* **3,** e1701620 (2017).

172. Wang, Z. *et al.* Detection of integration of plasmid DNA into host genomic DNA following intramuscular injection and electroporation. *Gene Ther.* **11,** 711–721 (2004).

173. Deyle, D. R. & Russell, D. W. Adeno-associated virus vector integration. *Curr Opin Mol Ther* **11,** 442–7 (2009).

174. Gentil, C. *et al.* Dystrophin Threshold Level Necessary for Normalization of Neuronal Nitric Oxide Synthase, Inducible Nitric Oxide Synthase, and Ryanodine Receptor-Calcium Release Channel Type 1 Nitrosylation in Golden Retriever Muscular Dystrophy Dystrophinopathy. *Hum. Gene Ther.* **27,** 712–726 (2016).

175. Neri, M. *et al.* Dystrophin levels as low as 30% are sufficient to avoid muscular dystrophy in the human. *Neuromuscul. Disord.* **17,** 913–918 (2007).

176. Waldrop, M. A. *et al.* Low-level dystrophin expression attenuating the dystrophinopathy phenotype. *Neuromuscul. Disord.* **28,** 116–21 (2018).